376

CLOUD-TO-GROUND LIGHTNING PARAMETERS DERIVED FROM LIGHTNING LOCATION SYSTEMS

The Effects of System Performance

Working Group
C4.404

April 2009

Working Group C4.404

CLOUD-TO-GROUND LIGHTNING PARAMETERS DERIVED FROM LIGHTNING LOCATION SYSTEMS

The Effects of System Performance

Members

Gerhard Diendorfer – Austria (Convenor)
Marina Bernardi - Italy
Kenneth Cummins - USA
Francisco De La Rosa - USA
Blas Hermoso - Spain
Ali Hussein - Canada
Tatsuo Kawamura - Japan
Farhad Rachidi - Switzerland
Vladimir Rakov - USA
Wolfgang Schulz - Austria
Horracio Torres – Columbia

ISBN: 978-2-85873-063-6

TABLE OF CONTENTS

1 Executive Summary

Introduction

This report has been developed in the framework of TF C4.404 “Lightning Location System Data” and is a logical continuation of CIGRE Report 94, (1995) and Report 172, (2000). Lightning parameters are essential input variables to procedures for estimating the lightning performance of transmission lines.

This document begins with a detailed overview of lightning flash properties and parameters. A few of these lightning parameters, particularly those of main importance for power engineering, can be derived from data recorded by Lightning Location System (LLS). LLS data have the enormous advantage of covering extended areas up to continental scale on a continuous basis and can therefore observe the related exposure of technical services to the lightning threat. Parameters that are typically derived from LLS observations are the ground flash density (GFD), ground stroke density (GSD), peak current distribution, flash multiplicity, and polarity. These lightning parameters can vary significantly from storm to storm or between seasons.

This report is intended to provide a comprehensive overview about the effect of LLS performance on Cloud-to-Ground (CG) lightning parameters derived from such systems. An understanding of the ranges of uncertainties and errors of any derived lightning parameter is essential in order to avoid misinterpretation of results.

The available technology for detecting and locating lightning to ground has significantly improved over the last decade. LLS upgrades and/or LLS extensions are causing changes in the network performance that result in changes in LLS-inferred lightning parameters. These effects must be considered in order to allow data from different LLS to contribute to our understanding of true regional and climatological differences in lightning parameters.

Various techniques and sensor types are employed to detect and then locate lightning events. Lightning radiated electromagnetic fields are acquired by electric or magnetic field sensors in the VLF, LF and VHF frequency ranges. Methods and effects discussed in this report are generally applicable for any network technology that is based on surface-propagating EM-field measurements in the VLF/LF frequency range.

Effects of Network Detection Efficiency

The fraction of flashes or strokes that are detected by an LLS, referred to as the detection efficiency (DE), has a direct impact on virtually all LLS-inferred lightning parameters. Undetected flashes will result in low measures of lightning incidence and since DE is determined by the fraction of low peak current events that are missed by a network, imperfect DE also results in peak current distributions that are biased to larger mean and median values, and flash multiplicity distributions that are biased to

smaller mean and median values. Given the importance of understanding LLS DE, this document discusses the effect of using different location methods in terms of required number of sensors to obtain a location. Model-based calculations of DE range from about 60% to 90% for the same network design, depending on location method and geometry. Model based calculations result in DE reductions ranging from about 5% to 20% when one sensor is removed from an assumed 6-sensor reference network, representing e.g. the effect of temporary outage of a sensor.

Reprocessing of lightning data from an operational network for different parameter settings demonstrates the validity of the DE model simulations, at least regarding relative DE. The median peak current increased by +24% from -9.7 kA to -12.0 kA when data from combined MDF/TOA sensors were reprocessed to use only the time information and requiring 4 sensors to compute a location. Clearly, it is important to keep these effects in mind when comparing mean peak current values of LLS systems employing different sensor types (TOA versus MDF/TOA) and operated in different regions. Observations of regional differences in mean peak current values may reflect LLS performance differences rather then true regional effects. Differences can also result from different network geometries, from improper calibration of E-field sensors, or from different propagation models and field-to-current conversions.

Performance Validation with Ground Truth Data

Ground truth data are essential to validate the performance of operational LLS and to compare results with the model calculations. Direct measurements of lightning striking instrumented towers or from triggered lightning allow estimation of all three major performance parameters of a LLS - detection efficiency (for strokes and flashes), location accuracy, and peak current estimates. Evaluation of lightning to the Gaisberg tower in Austria using the ALDIS LLS shows a flash DE of 98% and a stroke DE of 85% for stoke peak currents greater than 2 kA.

For similar analysis of triggered lightning in Florida (I_{median} of stroke amplitudes 15.3 kA) a triggered-flash DE (no first stroke) of 84% and stroke DE of 60% is reported by Jerauld et al. (2005). The main reason for the lower DE of triggered lightning flashes in Florida compared to tower lightning in Austria is the significantly larger sensor baseline in Florida and employment of a mixture of TOA and MDF/TOA sensors, requiring 3-4 sensors to compute a location.

LLS Inferred Peak Current Distribution

Peak current estimates given by LLS are on average in reasonable good agreement with the directly measured peak currents for (electrically short) towers strikes and in triggered lightning, although significant differences are possible in individual events (typically ~20% but can be larger), likely caused by the natural variation in return stroke speed. This uncertainty of the peak current should be taken into account when LLS data of a specific event are applied in the case study of a lightning-related failure. Discrepancies between directly measured peak currents and LLS inferred

peaks at the CN Tower appear to be the result of an enhancement of the radiated electromagnetic fields that occurs when lightning strikes a very tall object.

Modern LLS have improved ability to detect lower amplitude sources, and thereby increased the potential for misclassified cloud discharges. Combined video/EM-field observations suggest that most (~90%) of the positive small events (< 10 kA) are actually cloud discharges and that most (~90%) larger positive events (> 20 kA) are likely to be CG strokes. The (small) population of positive discharges in the range 10-20 kA is actually a mix of CG and cloud discharges. Misclassification is less likely with negative events, even for amplitudes < 10 kA. Improvement of the CG:IC classification method of LLS is needed before e.g. CG:IC ratios or percentage of positive events can by used as a reliable thunderstorm index. Misclassified events also corrupt peak current distributions.

Significant differences exist between median peak currents of -30 kA for first strokes and -12 kA for subsequent strokes based on tower measurements some decades ago and the median peak currents inferred by LLS. In Austria a median current of first strokes of -10 kA is inferred by the EUCLID network. On the other hand, the median values obtained using U.S. NLDN video-validated first strokes in the western U.S. ranged from -13.3 to -18.1 kA. The lower value in Austria is probably a combination of higher DE of small peak currents due to shorter baselines of the LLS (compared to the U.S. NLDN), and true regional differences in lightning characteristics. Median peak current of subsequent strokes for the tower measurements is -10 kA in Austria and equal to the LLS inferred median peak current of subsequent strokes in Austria. The median values for subsequent strokes in preexisting channels in the western U.S. ranged from -11.9 and -14.0 kA. These U.S. NLDN values are known (Biagi et al., 2007) to be artificially higher due to poor detection of low-current strokes. We also have to note that the field-to-current conversion procedure used by LLS for all types of strokes has been validated (using rocket-triggered lightning and tower lightning) only for negative subsequent strokes and peak currents lower than 60 kA, and is not necessarily applicable to negative and positive first strokes and positive subsequent strokes.

Conclusions

The ground truth references (tower measurements and triggered lightning) confirmed the general validity of inferred peak currents. As almost all these ground truth data represent subsequent strokes we can conclude that LLS with “ideal” DE can provide accurate subsequent-stroke peak current distributions. The very limited number of first stroke data at the Gaisberg tower also indicates that LLS inferred peaks for first strokes may also be accurate. Unfortunately, this leaves us with unexplained differences in the median peak current values between the early tower measurements and modern LLS measurements.

The effect of tall object “attraction” on the lightning peak current frequency distribution was first investigated by Sargent (1972). As the elevated tower is more attractive

for flashes of large peak currents, the measured distribution is biased to higher values. This issue is separate from the impact of tall towers in the LLS-inferred peak current due to changes in near-ground return stroke velocity. Depending on the expression used to calculate the attractive radius of the tower, Borghetti et al. (2004) calculated distributions of the peaks to ground level with median values 20% to 40% lower than those of the original distribution - relevant to instrumented tower data. Their results show further that for all but one of the considered attractive radius models it is the presence of the tower, more than its height, to have the major impact on the peak current distributions. Interestingly, CIGRE concluded that experimental data from Europe and South Africa show that first-stroke peak currents are not greatly influenced by the height of the structure on which they were measured (CIGRE Document 118, 1997, page 16). Clearly, additional experimental data would be very useful in order to validate these theoretical findings.

2 The Lightning Flash

2.1 Terminology and definitions

Lightning or the lightning discharge in its entirety, whether it strikes ground or not, is usually termed a "lightning flash" or just a "flash". A lightning discharge that involves an object on ground or in the atmosphere is sometimes referred to as a "lightning strike." A commonly used non-technical term for a lightning discharge is a "lightning bolt". The terms "stroke" or "component stroke" apply only to components of cloud-to-ground discharges. Each stroke involves a downward leader, an upward return stroke, and may involve a relatively low level "continuing current" that immediately follows the return stroke. Transient processes occurring in a lightning channel while it carries continuing current are termed M components. First strokes are initiated by "stepped" leaders while subsequent strokes (all strokes other than the first stroke) following previously-formed channels are initiated by "dart" or "dart-stepped" leaders.

From the observed polarity of the charge "effectively" lowered to ground and the direction of propagation of the initial leader, four different types of lightning discharges between cloud and Earth have been identified. The term "effectively" is used to indicate that individual charges are not transported all the way from the cloud to ground during the lightning processes. Rather the flow of electrons (the primary charge carriers) in one part of the lightning channel results in the flow of other electrons in other parts of the channel. For example, individual electrons in the lightning channel move only a few meters during a return stroke which transfers a coulomb or more of charge to ground. The four types of lightning, illustrated in Fig. 2.1, are (a) downward negative lightning (b) upward negative lightning (c) downward positive lightning, and (d) upward positive lightning. Discharges of all four types can be viewed as effectively transporting cloud charge to the ground and therefore are usually termed cloud-to-ground discharges (sometimes referred to as CGs). It is believed that downward negative lightning flashes (type (a)) account for about 90% or more of global cloud-to-ground lightning, and that 10% or less of cloud-to-ground discharges are downward positive lightning flashes (type (c)). Some lightning flashes transfer both negative and positive charges to ground. These are referred to as bipolar lightning discharges. Upward lightning discharges (types (b) and (d)) are thought to occur only from tall objects (higher than 100 m or so) or from objects of moderate height located on mountain tops. Rocket-triggered lightning is similar in its phenomenology to the upward lightning initiated from tall objects. Statistical distributions of subsequent-return-stroke peak currents in natural downward, natural upward, and rocket-triggered lightning are similar (Rakov, 2001). The majority of lightning discharges, two-thirds to three-quarters, do not involve ground. These are termed cloud discharges and sometimes are referred to as ICs or CCs. Cloud discharges include intracloud, intercloud, and cloud-to-air discharges.

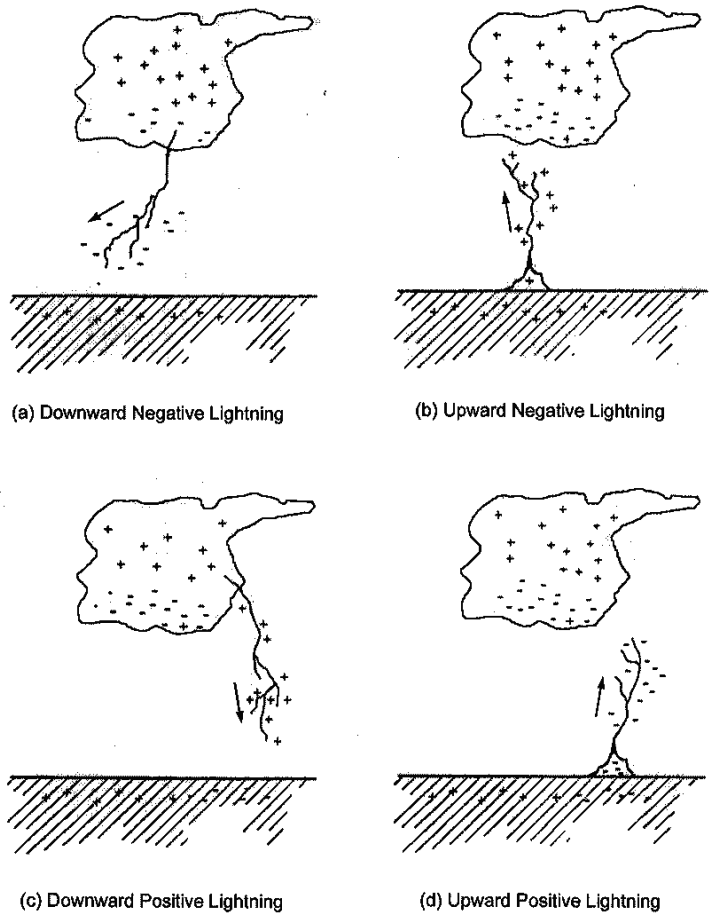

Fig. 2.1 Four types of lightning effectively lowering cloud charge to ground. Only the initial leader is shown for each type. For each lightning type name given below the sketch, direction indicates the direction of propagation of the initial leader and polarity refers to the polarity of the cloud charge effectively lowered to ground. Some lightning flashes (not illustrated in this Figure) transfer both negative and positive charges to ground.

2.2 General characterization of negative CGs

The salient properties of downward negative lightning discharges, the most common type of cloud-to-ground (CG) lightning, are summarized in Table 2.1. In the right most column of Table 2.1 we have indicated those lightning parameters that can be inferred from data reported by presently operating LLS are signaled by a “YES”. Lightning parameters in Table 2.1 are based on research that was conducted on specific locations and often involved a relatively small number of events. LLS, on the other hand, can provide lightning information covering large geographical areas and a number of continuous years including all seasons.

Table 2.1: Characterization of negative cloud-to-ground lightning (Rakov and Uman 2003)

Parameter	Typical Value [a)]	Parameter derivable from LLS data
Stepped leader		
Step length, m	50	
Time interval between steps, μs	20-50	
Step current, kA	>1	
Step charge, mC	>1	
Average propagation speed, m/s	2×10^5	
Overall duration, ms	35	
Average current, A	100-200	
Total charge, C	5	
Electric potential, MV	~ 50	
Channel temperature, K	~ 10,000	
First return stroke [b)]		
Peak current, kA	**30**	**YES**
Maximum current rate of rise, kA/μs	10-20	
Current risetime (10-90%), μs	5	
Current duration to half-peak value, μs	70-80	
Charge transfer, C	5	
Propagation speed, m/s	$(1\text{-}2) \times 10^8$	
Channel radius, cm	~ 1-2	
Channel temperature, K	~ 30,000	
Dart leader		
Speed, m/s	$(1\text{-}2) \times 10^7$	
Duration, ms	1-2	
Charge, C	1	
Current, kA	1	
Electric potential, MV	~ 15	
Channel temperature, K	~ 20,000	
Dart-stepped leader		
Step length, m	10	
Time interval between steps, μs	5-10	
Average propagation speed, m/s	$(1\text{-}2) \times 10^6$	
Subsequent return stroke [b)]		
Peak current, kA	**10-15**	**YES**
Maximum current rate of rise, kA/μs	100	
10-90% current rate of rise, kA/μs	30-50	
Current risetime (10-90%), μs	0.3-0.6	
Current duration to half-peak value, μs	30-40	
Charge transfer, C	1	
Propagation speed, m/s	$(1\text{-}2) \times 10^8$	
Channel radius, cm	~ 1-2	
Channel temperature, K	~ 30,000	
Continuing current (longer than 40 ms or so) [c)]		
Magnitude, A	100-200	
Duration, ms	~ 100	
Charge transfer, C	10-20	

Parameter	Typical Value [a)]	Parameter derivable from LLS data
M component [b)]		
Peak current, A	100-200	
Current risetime (10-90%), μs	300-500	
Charge transfer, C	0.1-0.2	
Overall flash		
Duration, ms	**200-300**	**YES** [d)]
Number of strokes per flash	**3-5**	**YES**
Interstroke interval, ms	**60**	**YES**
Charge transfer, C	20	
Energy, J	10^9-10^{10}	

a) Typical values are based on a comprehensive literature search and unpublished experimental data acquired by the University of Florida Lightning Research Group.
b) All current characteristics for return strokes and M components are based on measurements at the lightning channel base.
c) About 30 to 50% of lightning flashes contain continuing currents longer than 40 ms or so.
d) LLS allow to determine the time from the first stroke to the start of the last stroke in a flash - duration of last stroke is not included in flash duration.

2.3 Number of strokes per flash (Multiplicity)

A typical negative cloud-to-ground flash is composed of 3 to 5 strokes (leader/return stroke sequences). The observed percentage of single-stroke flashes in Florida is 17%, similar to the 14% reported for New Mexico thunderstorms (e.g., Rakov et al., 1994), the 21% observed in Sri Lanka (Cooray and Jayaratne, 1994), and the 18% in Sweden (Cooray and Perez, 1994). Thus, the overwhelming majority (about 80% or more) of negative CG flashes contain more than one stroke.

2.4 Multiple ground strike points

One-third to one-half of all lightning discharges to earth, both single- and multiple-stroke flashes, strike ground at more than one point with the spatial separation between the channel terminations being up to many kilometers. Histogram of the distances between the multiple terminations of 22 individual cloud-to-ground flashes in Florida is shown in Fig. 2.2. The average number of ground terminations per flash in New Mexico and Florida thunderstorms is 1.7 (Kitagawa et al., 1962; Rakov and Uman 1990b) and 1.5 in Arizona and France (Valine and Krider, 2002). Thus, when the total number of ground strike points is needed, a correction factor of 1.5 to 1.7 has to be applied to LLS flash density values in order to take into account multiple channel terminations on ground.

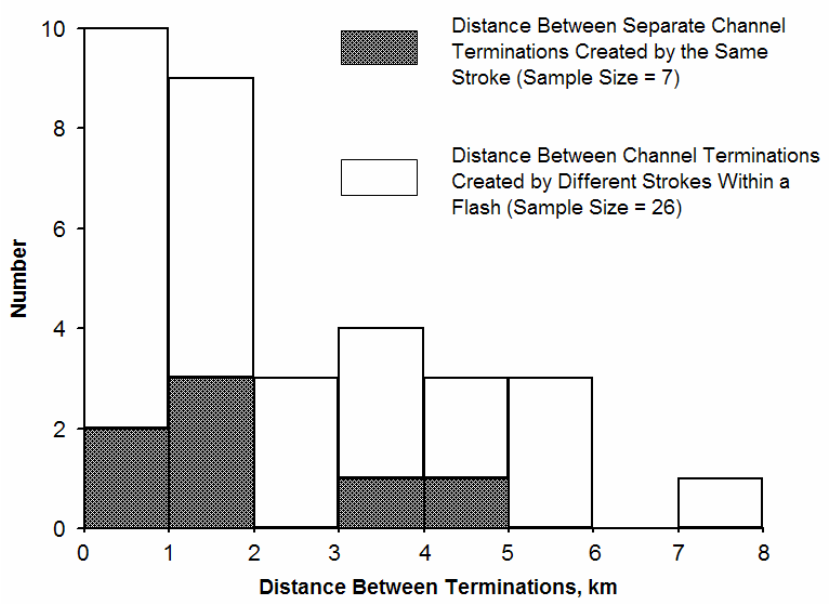

Fig. 2.2 Histogram of the distance between the multiple terminations of 22 individual ground flashes in Florida. Adapted from Thottappillil et al. (1992)

2.5 Continuing current and M components

The impulsive component of the current in a subsequent return stroke is often followed by a continuing current which has a magnitude of tens to hundreds of amperes and a duration up to hundreds of milliseconds. Continuing currents with a duration in excess of 40 ms are traditionally termed long continuing currents. Between 30 and 50% of all negative cloud-to-ground flashes contain long continuing currents. The source for continuing current is the cloud charge, as opposed to the charge distributed along the leader channel, the latter charge contributing to at least the initial few hundred microseconds of the return-stroke current observed at ground. Continuing current typically exhibits a number of superimposed surges that rise to peak and fall off to the background current level in some hundreds of microseconds, with the peak being generally in the hundreds of amperes range but occasionally in the kiloamperes range. These current surges are associated with enhancements in the relatively faint luminosity of the continuing-current channel and are called M components.

2.6 Interstroke interval and flash duration

The time interval between successive return strokes in a flash is usually several tens of milliseconds (see Fig. 2.3), although it can be as large as many hundreds of milliseconds if a long continuing current is involved and as small as one millisecond or less. About 20% of flashes contain return strokes separated by relatively short time intervals of some tens to some hundreds of microseconds (Rakov and Uman 1994). The total duration of a flash is typically some hundreds of milliseconds.

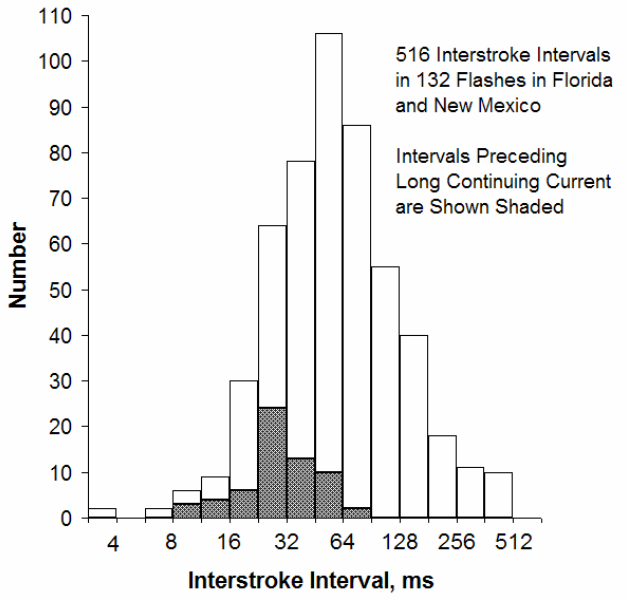

Fig. 2.3 Histogram of 516 interstroke intervals in 132 flashes in Florida and New Mexico. Intervals preceding strokes initiating long continuing current are shown shaded. Adapted from Rakov and Uman (1990a)

2.7 Parameters of negative CGs derived from channel base current measurements

The most complete characterization of the return stroke in negative downward flashes, the type that normally strikes flat terrain and structures of moderate height, that is, shorter than 100 m or so, is due to Karl Berger and co-workers (e.g., Berger 1955a,b 1962, 1967a,b, 1972, 1980; Berger and Vogelsanger 1965, 1969; Berger and Garbagnati 1984; Berger et al., 1975). The data of Berger were derived from oscillograms of current measured using resistive shunts installed at the tops of two 70-m high towers on the summit of Monte San Salvatore in Lugano, Switzerland. The summit of the mountain is 915 m above sea level and 640 m above the level of Lake Lugano, located at the base of the mountain. The towers are of moderate height, but because the mountain contributed to the electric field enhancement near the tower tops, the effective height of each tower was estimated by Eriksson (1978) to be 350 m. As a result, the majority of lightning strikes to the towers were of the upward type. In this section we only consider return strokes in negative downward flashes. A total of 101 are included in the summary by Berger et al. (1975). Berger's data were additionally analyzed by Anderson and Eriksson (1980). Fisher et al. (1993) compared the return-stroke parameters published by both Berger et al. (1975) and Anderson and Eriksson (1980) with their counterparts in triggered lightning.

The results of Berger et al. (1975) are still used to a large extent as the primary reference source for both lightning protection and lightning research. These results are presented in Fig. 2.4 and Fig. 2.5 and in Table 2.2. Fig. 2.4 shows, on two time scales, A and B, the average current waveshapes for negative first and subsequent strokes. The averaging procedure involved the normalization of waveforms from many strokes to their respective peak currents (so that all have peaks equal to unity) and subsequent alignment using the 0.5 peak point on the initial rising portion of the waveforms. The overall duration of the current waveforms is some hundreds of microseconds. The rising portion of the first-stroke waveform has a characteristic concave shape, the initial slower part generally thought to be due to the upward connecting leader. The averaging procedure masked secondary maxima typically observed in first-stroke waveforms and generally attributed to major branches. Fig. 2.5 shows the cumulative statistical distributions (solid-line curves) of return-stroke peak currents for (1) negative first strokes, (2) negative subsequent strokes, and (3) positive strokes (each was the only stroke in a flash), the latter being considered further in Section 2.8 below. These empirical distributions are approximated by log-normal distributions (dashed lines) and shown on cumulative probability distribution graph paper, on which a Gaussian (normal) cumulative distribution appears as a slanted straight line, with the horizontal (peak current) scale being logarithmic (base 10). The vertical scale gives the percentage of peak currents exceeding a given value on the horizontal axis. The vertical scale is symmetrical with respect to the 50-% value and does not include the 0 and 100-% values; it only asymptotically approaches those. For a log normal distribution the 50-% (median) value is equal to the geometric mean value. The lightning peak current distributions for negative first and subsequent strokes shown in Fig. 2.5 are also characterized by their 95-, 50-, and 5-% values based on the log normal approximations in Table 2.2, which contains a number of

other parameters derived from the current oscillograms. The minimum peak current value included in the distributions is 2 kA. Clearly, the parameters of statistical distributions can be affected by the lower and upper measurement limits. Rakov (1985) showed that, for a log-normal distribution, the parameters of a measured, “truncated” distribution and a knowledge of the lower measurement limit can be used to recover the parameters of the actual, “untruncated” distribution. He applied the recovery procedure to the various lightning peak current distributions found in the literature and concluded that the peak current distributions published by Berger et al. (1975) can be viewed as practically unaffected by the lower measurement limit of 2 kA. Note from Fig. 2.5 and Table 2.2 that the median return-stroke current peak for first strokes is 2 to 3 times higher than that for subsequent strokes.

Further, Rakov (2003a) showed that tower-top current measurements of Berger et al. (1975) are not significantly affected by the transient response of the 70-m high towers on which their measurements were made.

About one third of multiple-stroke flashes have at least one subsequent stroke that is larger (in terms of its initial field peak and by inference current peak) than the first stroke in the flash (Thottappillil et al., 1992). This does not necessarily mean that the relevant peak current is larger, as the two return stroke velocities are different (higher for subsequent strokes) which means a higher radiated peak field starting from the same peak current (Rachidi et al., 2004).

Also, on the one hand negative first strokes transfer about a factor of four larger total charge than do negative subsequent strokes. On the other hand, subsequent return strokes are characterized by 3 to 4 times higher current maximum steepness (current maximum rate of rise). Note that the current maximum rate of rise reported by Berger et al. (1975) and given in Table 2.2 is an underestimate of the actual value due to the limited time resolution of oscillographic data, as discussed later in this section. Only a few percent of negative first strokes are expected to exceed 100 kA, while about 20% of positive strokes have been observed to do so. On the other hand, the 50-% (median) values of the current distributions for negative and positive strokes are similar. It is worth noting that directly measured current waveforms of either polarity found in the literature do not exhibit peaks exceeding 300 kA or so, although less reliable peak current estimates from the residual magnetization of ferromagnetic detectors (magnetic links) and inferences from remotely measured electric and magnetic fields (considered later in this section) suggest the existence of currents up to 500 kA and even higher (e.g., Le Boulch and Plantier 1990). Lyons et al. (1998), using U.S.NLDN (U.S. National Lightning Detection Network ®) data for 14 selected summer months from 1991-1995, reported that the largest current peaks were 957 and 580 kA for negative and positive flashes, respectively. It is important to note that peak currents reported by the U.S. NLDN and by other similar systems are estimated from measured magnetic radiation field peaks using an empirical formula, the validity of which has only been tested for negative subsequent strokes with peak currents not exceeding 60 kA. On the other hand some of these extremely high peak currents reported by LLS could be the result of completely misplaced stroke locations and detailed analysis of correlated sensor reports is required to confirm the peak current values.

The action integral (also referred to as specific energy) in Table 2.2 represents the energy that would be dissipated in a 1-Ω resistor if the lightning current were to flow through it. It is thought that the heating of electrically conducting materials and the explosion of nonconducting materials is, to a first approximation, determined by the value of the action integral.

Note that the interstroke interval in Table 2.2 is likely mislabeled by Berger et al. (1975) and is actually the no-current interval, that is, the interstroke interval excluding any continuing current, as discussed by Fisher et al. (1993).

Essentially no correlation was found between the current peak and maximum current rate of rise (correlation coefficients reported by Berger et al. (1975) for negative first and subsequent strokes are 0.36 and 0.11, respectively). On the other hand, similar data for triggered-lightning strokes suggest that a moderate correlation does exist between the current peak and either the 10-90 or the 30-90% rate of rise (Fisher et al., 1993), and that a relatively strong correlation exists between the current peak and the maximum rate of rise (Leteinturier et al., 1990, 1991). Anderson and Eriksson (1980), using Berger's data, found a weak correlation between the logarithms of peak current and either the 10-90% rate of rise or the 30-90% risetime.

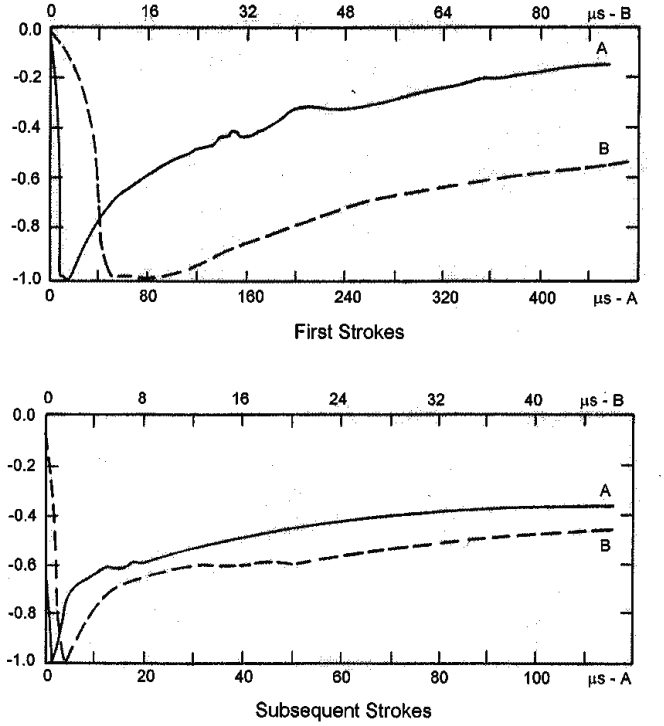

Fig. 2.4 Average negative first and subsequent stroke waveshapes each shown on two time scales, A and B. The lower time scales (A) correspond to solid-line curves, while the upper time scales (B) correspond to dashed-line curves. The vertical (amplitude) scale is in relative units with the peak values being equal to negative unity. Adapted from Berger et al. (1975).

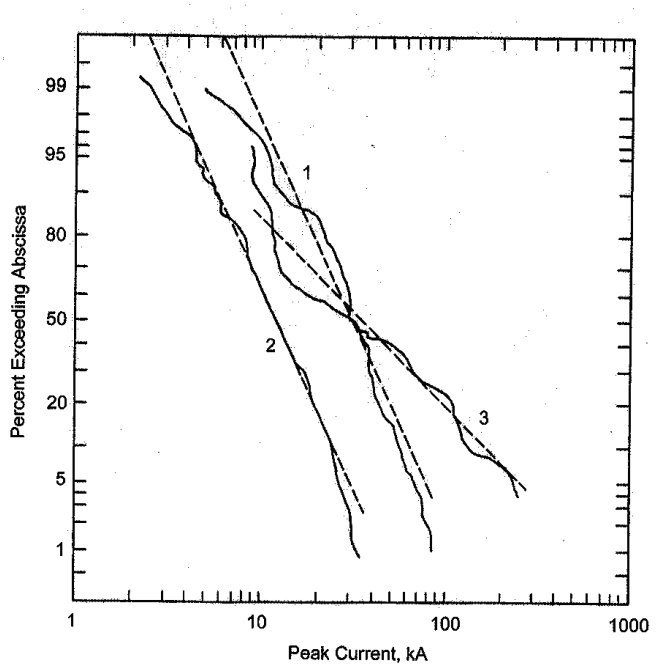

Fig. 2.5 Cumulative statistical distributions of return-stroke peak current from measurements at the tower top (solid-line curves) and their log-normal approximations (slanted dashed lines) for (1) negative first strokes, (2) negative subsequent strokes, and (3) positive first (and the only) strokes, as reported by Berger et al. (1975)

Table 2.2: Parameters of downward negative lightning derived from channel-base current measurements. Adapted from Berger et al. (1975).

Parameters	Units	Sample Size	% Exceeding Tabulated Value		
			95%	50%	5%
Peak current (minimum 2 kA)	kA				
First strokes		101	14	30	80
Subsequent strokes		135	4.6	12	30
Charge (total charge)	C				
First strokes		93	1.1	5.2	24
Subsequent strokes		122	0.2	1.4	11
Complete flash		94	1.3	7.5	40
Impulse charge (excluding continuing current)	C				
First strokes		90	1.1	4.5	20
Subsequent strokes		117	0.22	0.95	4
Front duration (2 kA to peak)	μs				
First strokes		89	1.8	5.5	18
Subsequent strokes		118	0.22	1.1	4.5
Maximum di/dt	kA/μs				
First strokes		92	5.5	12	32
Subsequent strokes		122	12	40	120

Parameters	Units	Sample Size	% Exceeding Tabulated Value		
			95%	50%	5%
Stroke duration (2 kA to half peak value on the tail) First strokes Subsequent strokes	μs	 90 115	 30 6.5	 75 32	 200 140
Action integral ($\int i^2dt$) First strokes Subsequent strokes	A^2s	 91 88	 6.0×10^3 5.5×10^2	 5.5×10^4 6.0×10^3	 5.5×10^5 5.2×10^4
Time interval between strokes	ms	133	7	33	150
Flash duration All flashes Excluding single-stroke flashes	ms	 94 39	 0.15 31	 13 180	 1100 900

Direct measurements of natural lightning return stroke currents on instrumented towers have also been made by researchers in the United States (McCann, 1944), in Italy (Garbagnati et al., 1978; Garbagnati and Lo Piparo, 1982), in Russia (Gorin et al., 1977; Gorin and Shkilev, 1984), in South Africa (Eriksson, 1978), in Canada (Hussein et al., 1995; Janischewskyj et al., 1997), in Germany (Beierl, 1992; Fuchs et al., 1998), in Japan (Miyake et al., 1992; Goto and Narita 1992, 1995; Asakawa et al., 1997), in Switzerland (Montandon, 1992), in Austria (Diendorfer et al., 2000a, 2000b, 2002), and in Brazil (Lacerda et al., 1999; Visacro et al., 2004). In most studies, the towers experienced predominantly upward discharges. The measurements for negative downward flashes in Italy yielded results similar to those of Berger et al. (1975), although the downward and upward flashes were separated solely on the basis of the early part of the first-stroke current waveshapes.

The measurements in South Africa were made on a 60-m high tower (CSIR research mast) located on a hill some 80 m above the surrounding relatively flat terrain (Eriksson, 1978). The tower was insulated from ground via a short spark gap that operated during the lightning discharge, and the current was measured at the bottom of the tower using a current transformer (Rogowski coil). A similar instrumented tower has been used in Brazil (e.g., Visacro et al., 2004). Most of the other published tower measurements have been made at the top of the tower. All flashes recorded at the South African tower lowered negative charge to ground. The 50-% peak current for 22 first return strokes was 40 kA, about 30% higher than in Switzerland (Anderson et al., 1984).

In one downward flash composed of three strokes, a maximum current steepness of 180 kA/μs was measured for the second stroke, appreciably higher than the 5-% value of 120 kA/μs (Table 2.2) reported for subsequent strokes by Berger et al. (1975). The corresponding peak current was also unusually large, over 70 kA.

As reported by Berger and Garbagnati (1984), the smallest measurable time in Berger et al.'s (1975) oscillograms was 0.5 μs (0.5 mm on the 30-μs oscilloscopic sweep). Note that the 95-% value of front duration of 0.22 μs for subsequent strokes in Table 2.2 is a prediction of the log normal approximation, not an experimental value. It follows from the above that the risetimes reported by Berger et al. (1975) are likely biased toward larger values and rates of rise toward lower values. The median 10-90% risetime estimated for subsequent strokes by Anderson and Eriksson (1980) from Berger et al.'s (1975) oscillogram is 0.6 μs, comparable to the median values ranging from 0.3 to 0.6 μs for triggered lightning strokes (Leteinturier et al., 1991; Fisher et al., 1993). The median 10-90% current rate of rise reported for natural subsequent strokes by Anderson and Eriksson (1980) is 15 kA/μs, almost three times lower than the corresponding value of 44 kA/μs in the data of Leteinturier et al. (1991) and more than twice lower than the value of 34 kA/μs found by Fisher et al. (1993). The largest value of the maximum rate of rise, 411 kA/μs, was measured by Leteinturier et al. (1991, Fig. 4) for a triggered lightning stroke terminating on a launcher grounded to salt water. The corresponding directly measured current was greater than 60 kA, the largest reported for summer triggered lightning. The mean value of the current derivative reported by Leteinturier et al. (1991) is 110 kA/μs. The higher observed values of current rate of rise for triggered-lightning return strokes than for natural return strokes are likely due to the use of better instrumentation (digital oscilloscopes with better upper frequency response), although the influence of lightning triggering conditions has not yet been ruled out.

2.8 Parameters of negative CGs derived from remote measurements

A variety of indirect in-situ methods have been used to obtain crude estimates of lightning currents, typically peak value and maximum rate of rise, particularly in the 1930s to 1950s in the USSR (e.g., Stekolnikov and Lamdon, 1942), United States (e.g., Lewis and Foust, 1945), and Germany (e.g., Baatz, 1951). These methods, including those using magnetizable materials placed near the current carrying conductor, are summarized by Uman (1969, 1984). Additionally, there have been many attempts to infer lightning currents from remotely measured electric and magnetic fields (e.g., Norinder and Dahle, 1945; Uman and McLain, 1970; Uman et al., 1973a, b; Dulzon and Rakov 1980; Krider et al., 1996; Cummins et al., 1998a). For example, Krider et al. (1996), using measured electric field derivatives and the simple Transmission Line return stroke model (Uman and McLain, 1970), inferred that average values of the peak of the di/dt waveform and its duration at half-peak value for first return strokes were 115 kA/μs and 75 ns, respectively. Such "remote" measurements are model dependent and, therefore, inferior to direct measurements. However, recent triggered-lightning studies indicate that a reasonable estimate of the subsequent return-stroke peak current I_p can be obtained from the electric field E_p measured at a distance D using the following regression equation (Rakov et al. 1992).

$$I_p = 1.5 - 0.037 \cdot E_p \cdot D \qquad \textbf{(2.1)}$$

where I_p is in kA and taken as negative, E_p is positive and in V/m, and D is in km. The triggered-lightning data (28 events) used to derive Eq. (2.1) were obtained by Willett et al. (1989), and the range of peak field values was from 1.9 to 11 V/m (normalized to 100 km). For 18 out of 28 strokes used to derive Eq. (2.1) the two-dimensional return-stroke speed, averaged over 457-625 m, was measured and found to vary from 1.2×10^8 to 1.9×10^8 m/s with a mean value about 1.5×10^8 m/s. The field to current conversion equation used in LLS is discussed in section 3.6 and section 6.2 of this document.

2.9 Parameters of positive CGs derived from channel base current measurements

The median charge transfer by positive flashes is about an order of magnitude greater than that by negative flashes. The difference between the median peak currents for positive discharges and negative first strokes is small (35 kA vs. 30 kA), however, the 5-% peak current for positive discharges is 250 kA (Table 2.3), more than a factor of three greater than the 80 kA 5-% peak current for negative first strokes (Table 2.2). All current waveforms observed by Berger et al. (1975) for positive lightning can be divided into two categories. The first category includes "microsecond-scale" waveforms that are similar to those for negative lightning, and the second category includes "millisecond-scale" waveforms with risetimes up to hundreds of microseconds. Examples of the two types of current waveforms along with the sketches illustrating the processes presumably leading to the formation of these waveforms are given in Fig. 2.6. While the "microsecond-scale" waveforms are probably formed in a manner similar to that in downward negative lightning, the "millisecond-scale" waveforms are likely to be a result of the M-component mode of charge transfer to ground (Rakov 2003b).

Table 2.3: Lightning current parameters for positive flashes. Adapted from Berger et al. (1975).

Parameters	Units	Sample Size	% Exceeding Tabulated Value		
			95%	50%	5%
Peak current (minimum 2 kA)	kA	26	4.6	35	250
Charge (total charge)	C	26	20	80	250
Impulse charge (excluding continuing current)	C	25	2.0	16	150
Front duration (2 kA to peak)	μs	19	3.5	22	200
Maximum di/dt	kA/μs	21	0.20	2.4	32
Stroke duration (2 kA to half peak value on the tail)	μs	16	25	230	2000
Action integral ($\int i^2 dt$)	A^2s	26	2.5×10^4	6.5×10^5	1.5×10^7
Flash duration	ms	24	14	85	500

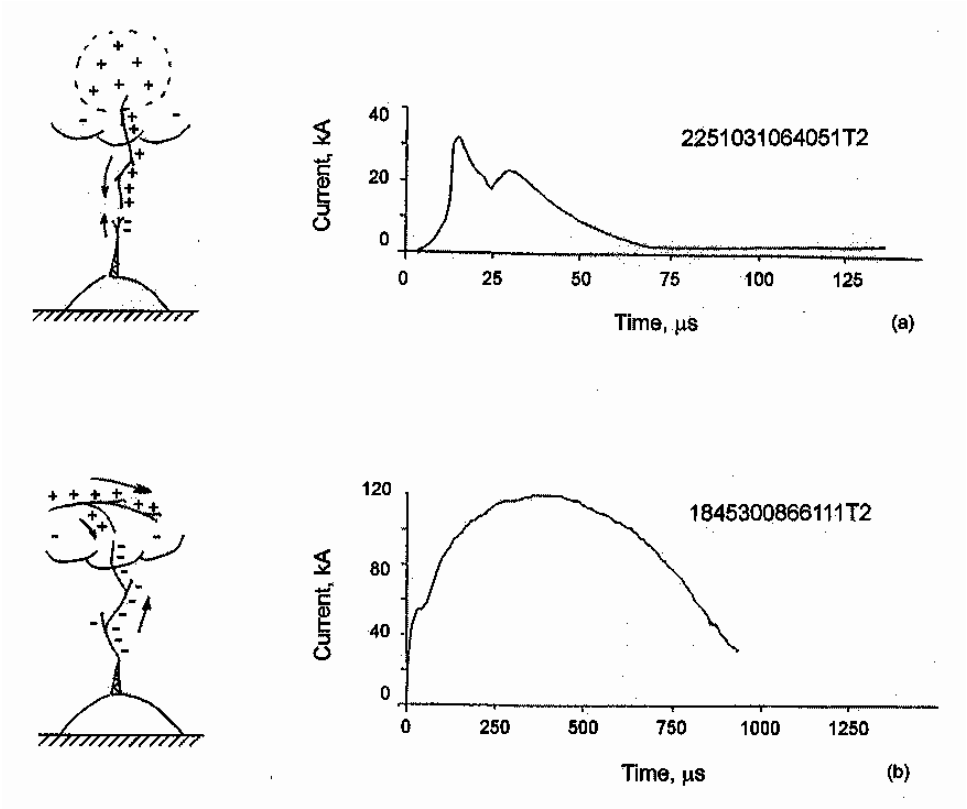

Fig. 2.6 Examples of two types of positive lightning current waveforms observed by K. Berger: (a) "microsecond-scale" waveform (right panel) and a sketch (left panel) illustrating the type of lightning that might have led to the production of this waveform; (b) "millisecond-scale" waveform (right panel) and a sketch (left panel) illustrating the type of lightning that might have led to the production of this current waveform.

The following is a list of five observed properties that are thought to be characteristic of positive lightning discharges:

(1) Positive flashes are usually composed of a single stroke, whereas about 80% of negative flashes contain two or more strokes. Multiple-stroke positive flashes do occur, but they are relatively rare. Ishii et al. (1998) observed that subsequent strokes in multiple-stroke positive flashes in winter storms in Japan always create a new termination on ground.

(2) Positive return strokes tend to be followed by continuing currents that typically last for tens to hundreds of milliseconds. Brook et al. (1982), from multiple-station electric field measurements, inferred continuing currents in positive flashes in excess of 10 kA, an order of magnitude larger than for negative flashes, for periods up to 10 ms. Due assessment of the impact of such large currents on surges arresters should be sought.

(3) From electric field records, positive return strokes often appear to be preceded by significant in-cloud discharge activity lasting, on average, in excess of 100 ms. Several researchers (e.g., Fuquay 1982; Rust 1986) have reported

that positive lightning discharges often involve long horizontal channels, up to tens of kilometers in extent.

Our knowledge of the physics of positive lightning remains much poorer than that of negative lightning. Positive lightning can be the dominant type of CG lightning during the cold season, during the dissipating stage of a thunderstorm, and in some other situations including severe storms and thunderclouds formed over forest fires or contaminated by smoke (see e.g. Murray et al., 2000).

2.10 Bipolar lightning

A review of bipolar lightning is given by Rakov (2005). It appears that bipolar lightning flashes occur not less often than positive flashes, at least when tall strike objects are involved. The occurrence of bipolar lightning suggests that the cloud charge structure cannot always be described by a simple, vertically stacked charge model. It is likely that positively and negatively charged regions can exist at about the same height in the cloud.

2.11 Lightning return stroke speed

Lightning return stroke speed is an important parameter in lightning protection studies and in computing lightning electric and magnetic fields. An explicit or implicit assumption of the return-stroke speed is involved in inferring lightning currents from remotely measured electric and magnetic fields (see later in paragraph 3.6). A review of the available experimental data on return-stroke speed for both natural and rocket-triggered lightning is given by Rakov (2004).

The average propagation speed of a negative return stroke (first or subsequent) below the lower cloud boundary is typically between one-third and one-half of the speed of light. For positive return strokes, the speed is of the order of 10^8 m/s, although data are very limited. The negative return-stroke speed within the bottom 100 m or so, that is, at early times when the peaks of the channel-base current and of remote electric and magnetic fields are formed, is expected to be between one-third and two-thirds of the speed of light. The negative return stroke speed usually decreases with height for both first and subsequent strokes. There exists some experimental evidence that the negative return stroke speed may vary non-monotonically along the lightning channel, initially increasing and then decreasing with increasing height. There are contradicting views regarding the variation of positive return stroke speed with height. The often assumed relationship between the return-stroke speed and peak current is generally not supported by experimental data, as illustrated in Fig. .

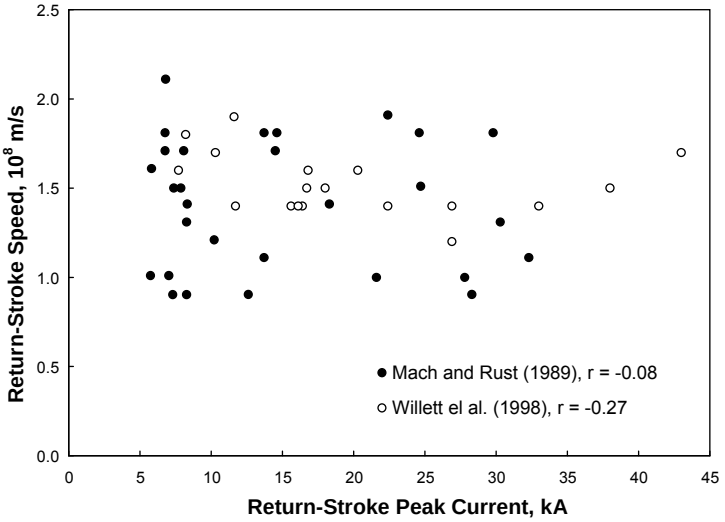

Fig. 2.7 Return-stroke speed vs. peak current for 29 triggered-lightning strokes observed at the Kennedy Space Center (KSC), Florida, in 1986 and reported by Mach and Rust (1989) and 18 triggered-lightning strokes from the 1987 KSC experiments reported by Willett et al. (1989). Peak current shown in the scatter plot as 38 kA may be an underestimate. Note that the linear correlation coefficients (r) for both data sets are low and negative, not in support of the often assumed relationship between these two lightning parameters

2.12 Characteristics of lightning as a function of season, location, and storm type

Many results in this section are given without attempting to speculate on the physical processes possibly responsible for the various observed features. We refrain from such speculations here because of the complexity and variability of lightning generation mechanisms, with some of the reported results being potentially deficient in the identification of all significant factors involved and in the statistical significance of these results. Additionally, the interpretation of data is often complicated by the inherent limitations of lightning detection techniques. Further information on the lightning activity versus meteorological, geographical, and other factors can be found in Rakov (1992) and Holle and Lopez (1993).

2.12.1 Season

Orville and Songster (1987) and Orville et al. (1987), using the U.S. East Coast DF lightning detection network in 1984-1985, found that the percentage of positive lightning during the summer is less than 5%, but in October it begins to increase, reaching a maximum of slightly over 80% in February and then decreasing to less than 10% in April. In the winter, most of the storms were dominated by positive flashes and occurred over the ocean. Orville and Huffines (1999), using 1995-1997 U.S. NLDN data for the contiguous United States, reported that the minimum percentage of positive flashes occurred in the July-August period and the maximum occurred in January-February. Further, Orville and Songster (1987) and Orville et al. (1987) inferred that the median return-stroke peak current increases by approximately 50% in the winter season for both positive and negative flashes. On the other

hand, Orville and Huffines (1999) reported, from 1995-1997 U.S. NLDN data, that the median return-stroke peak current for first strokes in negative flashes remained approximately constant from January through November at about 20 kA, increasing to 24 kA in December. The median positive current peak was 25 kA in February, 15 kA in July, and 24 kA in December. Note that the peak current values reported by Orville and Huffines (1999) are averages over the contiguous United States, and that the seasonal dependence of peak current may vary from one region to another. Finally, Orville et al. (1987) observed that the percentage of single-stroke negative flashes increased from 40% in the summer to over 80% in the winter (along the U.S. east coast from North Carolina to Maine), although both figures are likely to be overestimates due to the fact that the locating system fails to detect small subsequent strokes (Rakov et al., 1994; Cummins et al., 1998a; Rakov and Huffines 2003).

Moore and Orville (1990), using ground-flash data from the State University of New York at Albany (SUNYA) DF lightning detection network in conjunction with satellite, surface, upper air, and lake temperature data, studied the characteristics of Great Lakes-induced storms. These storms occurred in the fall and winter and typically produced only a few cloud-to-ground flashes, mostly positive (except for one storm). Both positive and negative flashes were associated with higher peak currents than in the summer. Also in winter, relatively high lightning activity has been found in the rainbands over the warm Gulf Stream off the east coast of the U.S. near North Carolina during northwesterly offshore flow (e.g., Biswas and Hobbs 1990; Orville 1990b; Dodge and Burpee 1993).

Brook (1992), using an electric field measuring system with a bandwidth from 0.1 Hz to about 1 MHz, observed that for negative lightning in winter (1) the initial breakdown pulses have larger amplitudes and (2) the stepped leader durations are shorter than in summer lightning. No seasonal differences were found for positive lightning. On the basis of the observations for negative lightning, Brook (1992) concluded that winter discharges may be considerably more energetic than summer ones.

Hojo et al. (1989), using an LLP (Lightning Locating and Protection) DF lightning locating network, studied the seasonal variations of ground flash density, the distribution of peak magnetic field for first strokes, and the polarity of ground flashes in the coastal area of the Sea of Japan. Ground flash density maps for summer and winter were reported to be markedly different. In winter, ground strikes occurred primarily to the sea surface, and those to the land were no more than 30 km from the coast. For positive lightning, the peak magnetic field was larger in winter. However, for negative lightning no such seasonal variation was observed, the latter finding being in contrast to the results of Orville et al. (1987). The seasonal variation of the polarity of ground flashes in Japan is similar to that reported by Orville et al. (1987) for the northeastern part of the United States. The seasonal variations of the time characteristics of return-stroke field waveforms were analyzed by Ishii and Hojo (1989). They found that at distances of 100-300 km the zero-crossing time for both polarities is shorter in winter.

Cummins et al. (1998a) attributed an increase in the detection of small positive discharges to misclassified ICs and therefore probably some of the above reported conclusions based on CG/IC ratios and peak current distribution of positive strokes need to be revised.

2.12.2 Region

We discuss here the dependence of lightning characteristics on location in general. Dependencies on latitude and topography are discussed separately in Sections 2.11.3 and 2.11.4, respectively and are subject of a separate CIGRE report under development. Cooray and Jayaratne (1994) compared lightning characteristics determined from their electric field measurements in Sri Lanka with similar characteristics observed in Sweden (Cooray and Perez 1994) and in Florida (Rakov and Uman 1990a, b; Thottappillil et al., 1992). The geometric mean interstroke intervals in Sri Lanka, Sweden, and Florida are 57, 48, and 57 ms, respectively. The mean number of strokes per flash and percentage of single-stroke flashes are 4.5 and 21% in Sri Lanka, 3.4 and 18% in Sweden, and 4.6 and 17% in Florida. The similarity of the lightning characteristics given above for the three different geographical regions is rather remarkable.

The literature on the height and magnitude of the negative cloud charge and the electric dipole moment change per flash has been reviewed by Jacobson and Krider (1976), and the literature on the flash duration and the frequency of occurrence of continuing current has been reviewed by Livingston and Krider (1978). The locations of negative charge centers apparently always occur at about the same cloud temperature level, typically -10 to -34°C, although these temperatures occur at different heights above the local terrain in different locations.

Changnon (1988), using thunderstorm records at 152 first-order weather stations distributed across the contiguous United States for a 30-year period (1948-1977), studied "thunder events" which were defined as periods of discrete thunder activity heard at a given weather station. In fact, a thunder event is the thunderstorm, the end of which usually being defined as the time after which thunder is not heard for at least 15 minutes. The sum of the durations of all thunder events during a year is the annual number of thunderstorm hours, T_H. Since a thunderstorm day T_D is composed of one or more thunder events (thunderstorms), the two characteristics are closely related with the correlation coefficients ranging, according to Changnon (1988), from +0.84 to +0.98. Annual averages of thunder events are high along the Gulf Coast (>100) in the central U.S. (Kansas, Missouri, Illinois with >75 events) and in the southwest (Arizona with 60 events). Thunder events are least along the west coast (<20) and in the northeast (<30). A peak in thunder events is present in the central U.S. in all months, and its position is always closely related to the major center of cold frontal activity. The peak in the southwest is related to the summer monsoon intrusion of moist tropical Pacific air and related frontal activity. The peak along the Gulf Coast of Florida is a result of sea breeze induced convergence, localized heating, and occasional tropical disturbances in summer and fall. Maps of ground flash density for the contiguous Unites States, based on data from the U.S. NLDN show more than two orders of magnitude variability in this parameter.

Boccippio et al. (2000) analyzed lightning data from the OTD and LIS instruments based on satellites for variability between land and ocean, various geographic regions, and different convective "regimes." They found that ocean storms produce lightning at rates that are not dissimilar from those of continental storms. According to Boccippio et al. (2000), the bulk of the observed differences in regional flash rate between land and ocean is accounted for by differences is storm spacing (density) and/or frequency of occurrence.

Westcott (1995), using U.S. NLDN data in and around 16 cities for June, July, and August of 1989-1992, found an enhancement of 40 to 85% in the cloud-to-ground lightning activity over and downwind of many of these cities. Further, Orville et al. (2001), from a similar study for the period from 1989 through 2000, reported elevated ground flash densities, in both summer and winter, centered over and downwind of the metropolitan area of Houston, Texas. They suggested that the observed enhancement of lightning activity could be caused by enhanced convergence associated with the urban heat island and altered microphysical processes associated with antropogenic pollution.

2.12.3 Latitude

Thomson (1980) has reviewed the literature on interstroke time interval and number of strokes per flash and finds no statistically significant correlation with latitude. This does not, however, preclude a latitude dependence which some investigators (Pierce 1970; Takeuti et al., 1975) have inferred should exist, while others (Harris and Salman 1972) have found not to exist. Rather, Thomson (1980) concludes that "the distributions of both interstroke intervals and the number of strokes per flash are more sensitive to local influences, including measurement and sampling techniques, than they are to latitude effects."

Orville and Huffines (1999) reported that the mean number of strokes per negative flash (also called the "multiplicity" when it is reported by the U.S. NLDN) appeared to increase with decreasing latitude in the eastern half of the United States, from 1-1.5 in Maine to over 3 in Florida. These multiplicity values are probably underestimates due to the fact that the U.S. NLDN fails to detect small strokes. Thus, the observed latitudinal trend could in part be due to both first and subsequent strokes in Florida being, on average, larger than those in higher latitudes, as indicated for first strokes below.

Rakov and Dulzon (1984, 1988) and Pinto et al. (1997), on the basis of their reviews of the literature on lightning current measurements in different countries, and Orville (1990a), on the basis of the analysis of current estimates provided by an LLP DF lightning locating network in the U.S., argued that lightning peak currents for first strokes tend to increase as the latitude decreases. Some of the variation in peak current reported by Orville (1990a), however, might be due to instrumental or propagation effects, Schulz et al. (2005).

A discussion of the possible latitudinal dependence of the ratio of cloud to cloud-to-ground flashes is found in Prentice and Mackerras (1977), Livingston and Krider

(1978), Rakov and Dulzon (1984), Mackerras and Darveniza (1994), and Mackerras et al. (1998).

2.12.4 Topography

Rakov et al. (1989) used a single-station lightning locating system "Ochag" (Russian for source location) in the North Caucasus region of Russia to estimate the spatial variation in N_g with topography. In this system, azimuth is determined via magnetic direction finding, and distance is roughly estimated via the so-called EH ranging algorithm (Kononov et al., 1986; Kononov and Petrenko 1996). The EH ranging algorithm utilizes the expected difference between the electric and magnetic field waveforms in the distance interval from 15 to 100 km. Rakov et al. (1989) found a factor of 1.7 higher average value of N_g for a mountainous area than for a plain terrain area, the two areas being about equally covered by the lightning locating system. Orville (1994), on the other hand, reported lower values of N_g for the Appalachian Mountains than in the neighboring areas to the east and west, from the U.S. NLDN data for 1989-1991. Kitagawa (1989) reported that the number of thunderstorm days per month (averaged over July and August) in Japan was the highest over the inland Kanto Plain, lowest over the open sea coasts, and intermediate over the mountainous regions.

Reap (1986) analyzed cloud-to-ground lightning location data for the summers of 1983 and 1984 from the BLM network in the 11 western states of the continental United States. The lightning locations and occurrence rates were examined in relation to the topographic features of the generally mountainous western U.S. terrain. Reap (1986) found a high correlation between terrain elevation, which ranged from sea level to near 3 km, and the time of maximum lightning activity: at the higher elevations, maximum lightning activity occurred in the early afternoon to midafternoon whereas at lower elevations it occurred later. The cloud-to-ground lightning activity was also found to increase with increasing terrain elevation, consistent with observations of Rakov et al. (1989) but in contrast with the results of Orville (1994) for the Appalachian Mountains. Schulz and Diendorfer (1999) found in Austria an increase in flash density for altitudes ranging from 500 m to 2000 m and for altitudes above 2000 m they observed a rapid decrease of lightning density.

King and Balling (1994), using 1989 and 1990 data from the BLM network, analyzed the diurnal variations of lightning flashes in Arizona during the summer monsoon season. In much of the state, the maximum occurred in the mid-to-late afternoon period, but it occurred closer to midnight in the large valley of central Arizona, a finding consistent with that of Reap (1986) discussed above.

Lopez and Holle (1986) used networks of LLP DFs in northeastern Colorado and in central Florida to study the diurnal and the spatial variation of the lightning ground flash density and to relate those results to the geographic and climatic characteristics of the two regions. The geographic feature of primary importance in Colorado is the mountains and in Florida is the interface between the waters of the Gulf of Mexico or the Atlantic Ocean and the land of the peninsula. For the summer of 1983, detailed maps of the ground flash density as a function of the time of day are given for both

locations. Lopez and Holle (1986) showed from these maps that the temporal and spatial distributions of lightning are clearly related to the local topographic features. Reap (1994), using 1987-1990 data from the SUNYA DF lightning locating network for Florida, observed organized coastal maxima in lightning activity related to land-sea-breeze convergence zones that form in direct response to the low-level wind flow, the two primary maxima in lightning activity being near Tampa and west of Cape Canaveral, and a minimum over Lake Okeechobee.

Lucas and Orville (1996), using lightning data from one LLP DF installed at Kavieng, Papua New Guinea, examined the frequency of cloud-to-ground lightning over the ocean as well as its diurnal variation. The data, acquired during 57 days in January and February of 1993, indicated that flash counts over the land sector were approximately nine times higher than flash counts over the ocean sector. The highest lightning activity occurred around local midnight for both land and ocean sectors. Hidayat and Ishii (1998), using data from a four-station LLP MDF/TOA network on the island of Java, Indonesia, reported the average annual ground flash density over the entire island to be more than an order of magnitude greater than over the Indian Ocean, about 100 km south of the island. Further, Hidayat and Ishii (1999) estimated that the median current peak for lightning over the ocean was at least 20% higher than for lightning over the land.

Orville and Huffines (1999) reported, from 1995-1997 U.S. NLDN data, that median current peaks for first strokes in negative flashes were relatively high, typically exceeding 26 kA, along U.S. continental coastal areas, particularly along the West Coast. Mountainous regions appeared to have lower median negative current peaks of about 15 to 20 kA. Median positive current peaks exceeded 40 kA in the upper Midwest but were less than 10 kA in Louisiana and Florida, although the latter value is an underestimate due to misidentification and hence inclusion of some small amplitude cloud flashes in the ground-flash data.

Takeuti et al. (1975) and Takeuti (1976), using a video camera and an electric field meter, found that cloud-to-sea lightning and cloud-to-ground lightning were similar in the number of strokes per flash and the interstroke interval distribution.

2.12.5 Storm type

For frontal and for air-mass storms, Rakov and Dulzon (1986) have compared the statistical distributions of (1) the ratio of cloud to cloud-to-ground discharges z, (2) the return-stroke peak current I, (3) the number of strokes per flash n averaged over the storm, and (4) the time interval between strokes Δt. Distributions of z, I, and n were estimated from electric field measurements in the Tomsk region of Russia, while distributions of Δt were those previously analyzed for latitudinal dependence by Thomson (1980). Rakov and Dulzon (1986) found that frontal storms are characterized by a larger mean value of z, 4.5 (13 storms) versus 1.8 (22 storms) for air-mass storms, a larger mean value of n, 2.7 (11 storms) versus 1.8 (14 storms), and a smaller geometric mean value of Δt, 51 ms versus 69 ms. The difference between the distributions of I was found to be statistically insignificant, with the geometric mean values of I being 15 and 17 kA for frontal and air-mass storms, respectively.

Holzer (1953), working in New Mexico, found that at all stages of the development of an individual thunderstorm cell, ground flashes in frontal storms constituted a larger fraction of the total than in nonfrontal storms. In both classes of storms the cloud flashes became relatively more frequent in the latter stages of the life-cycle of the cell. The average number of "repeated elements" (strokes) in cloud-to-ground flashes for air-mass storms was found to be about 2, while for the frontal storms the average number was nearly 5. The average intervals between strokes were similar, about 50 ms. Schonland (1956) also reported that in South Africa there was a greater number of strokes per flash in frontal storms than in air-mass storms. Kitterman (1980), using a streak camera observed a greater percentage of "high-order multiple stroke ground flashes" in frontal storms than in air-mass storms, while flash durations in these two types of storms were similar.

3 Overview on Lightning Detection Methods

Before the development of weather radars, a variety of sferics detection systems were the primary means of identifying and mapping thunderstorms at medium and long ranges. In the 1920s, Watson-Watt and Herd (1926) developed a cathode-ray direction finder (CRDF) that utilized a pair of orthogonal loop antennas tuned to a frequency near 10 kHz, where propagation in the earth-ionosphere waveguide is relatively efficient, to detect the horizontal magnetic field produced by lightning. Two or more CRDFs at known positions were sufficient to determine the location of a discharge from the intersection of simultaneous direction vectors. Since that time, a variety of other detection methods have been developed, exploiting lightning-produced signals in frequency ranges from near-DC up through the very-high-frequency (VHF/UHF) range. It has become clear that the best frequency range for detecting and precisely locating cloud-to-ground (CG) discharges, particularly when trying to derive CG lightning parameters, is the VLF/LF range (Cummins and Murphy, 2000; Rakov and Uman, 2003). Since an analysis of CG parameters is the primary objective of this document, we limit this discussion of lightning detection methods to modern approaches that operate on surface-propagated VLF/LF signals produced by CG discharges. The sensors in these systems are typically separated by 50-400 km, employing measurements of the radiation magnetic and/or electric field. CG discharges are located in terms of their ground strike points using various forms of magnetic direction finding (MDF), time-of-arrival (TOA), and combinations thereof. More comprehensive discussions including other detection methods and frequency ranges can be found in Cummins and Murphy (2000) and Rakov and Uman (2003).

In this section we also discuss the general methods used by VLF/LF LLS's to derive key lightning parameters. This includes classification of lightning type (CG vs. cloud discharges) and combining CG strokes into flashes. The method for estimating peak current from recorded electric and magnetic fields is described in Section 6.

3.1 Gated, Wideband Magnetic Direction-Finders (MDFs)

In 1976, an improved magnetic DF system was developed for locating CG lightning within a range of about 500 km (Krider et al., 1976, 1980). This system operated in the time-domain (i.e., covering the LF and VLF bands from about 1 to 500 kHz) and was designed to respond to field waveforms that were characteristic of the return strokes in CG flashes (Krider et al., 1980). When such a field was detected, the magnetic direction was sampled (in both a north-south loop and an east-west loop) just at the time of the initial field peak. Initial field peak occurs at a time, when the upward propagating return stroke has reached a height of a few hundred meters and therefore the resulting direction vector pointed as closely as possible to the location where the stroke attached to ground. The electric field is also sampled at this time to determine the stroke polarity. When employed in a network of MDFs, the location of the stroke can be determined by triangulation using two sensors, and the peak current can be estimated from the measured peak field and distance. When three or more sensors report a discharge, an optimization which minimizes the "angle disagreement" between the reporting sensors can be employed. This process is illustrated in Figure 3.1. The three points (L12, L13, and L23) show the possible "triangulated" lo-

cations that would be computed if only two sensors were to report the discharge. The use of gated field measurements and multi-sensors optimization results in significant improvements in location accuracy for CG lightning, when compared to early MDF techniques employing triangulation.

.

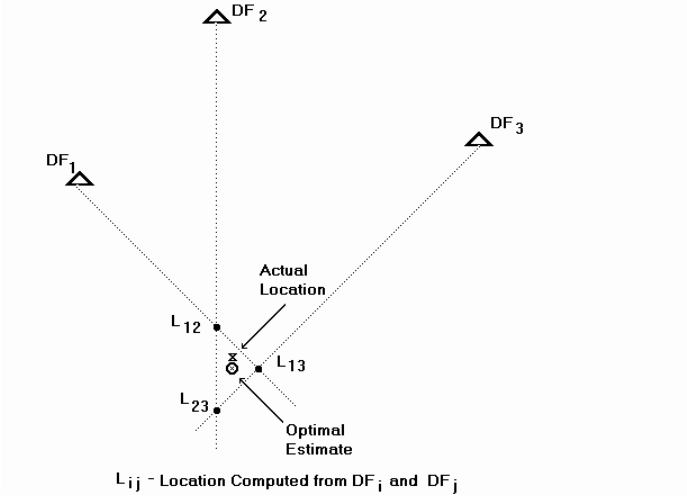

Fig. 3.1 Optimal location algorithm for direction finding (Cummins and Murphy, 2000)

There are certain conditions where the geometrical relationship between direction-finding sensors and the lightning discharge produce poor results. Specifically, if the discharge occurs along a line between two sensors, and these sensors are the only ones to see the discharge, then errors in azimuth measurement can result in significant errors in location. In some circumstances, the measurements may not produce an intersection at all. Because of this baseline problem, practical networks have at least three sensors.

3.2 Time-of-Arrival (TOA) Systems

Lewis et al. (1960) described a method for locating lightning that is based on measurements of the time-of-arrival of a radio pulse at several stations that are precisely synchronized. A constant difference in the arrival time at two stations defines a hyperbola, and multiple stations provide multiple hyperbolas whose intersections define a source location. This technique is illustrated in Fig. 3.2. Under some geometrical conditions, curves produced from only three sensors will result in two intersections, leading to an ambiguous location as shown in Fig. 3.3. This problem is generally avoided if four sensors detect the discharge. A detailed theoretical analysis of this early methodology, collectively referred to as location by hyperbolic intersections, was performed by Lewis (1960). Time-of-arrival (TOA) methods can provide accurate locations at long ranges (Lee, 1989), and if the antennas are properly sited, the systematic errors are minimal. Casper and Bent (1992) developed a wideband TOA receiver (termed the Lightning Position and Tracking System or LPATS) that is suitable for locating lightning sources at medium and long ranges using the hyperbolic method (Bent and Lyons, 1984).

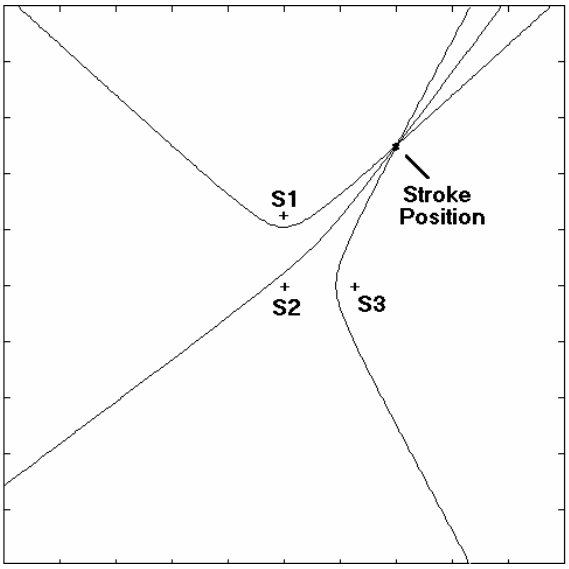

Fig.3.2 Hyperbolic intersection method for locating lightning using three sensors. (Cummins and Murphy, 2000)

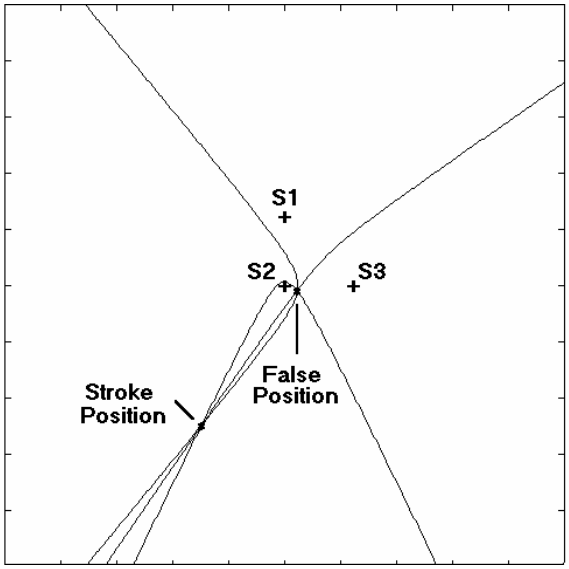

Fig3.3 Example of an ambiguous location for a three-sensor hyperbolic intersection. (Cummins and Murphy, 2000)

3.3 Combined Direction Finding and Time-of-Arrival (MDF+TOA)

In the early 1990's, a procedure for combining direction-finding and time-of-arrival to produce yet another lightning location method was intoduced which is generally referred to in the literature on the subject as IMPACT (**IMP**roved **A**ccuracy using **C**ombined **T**echnology) method. In this approach, direction finding provides azimuth information and absolute arrival time provides range information. These measurements produce three estimated parameters -- latitude, longitude, and discharge time. Thus the MDF+TOA method has redundant information which allows for an optimized estimate of location even when only two sensors provide both timing and angle information. The combined MDF+TOA location algorithm offers advantages over either a MDF or TOA method taken alone. For example, a discharge that occurs along the baseline between two MDF+TOA sensors will be more accurately located by the intersection of two direction vectors and two "TOA range circles" than by the direction intersection alone (Cummins et al., 1993)

The MDF+TOA algorithm can utilize information from any combination of direction finding, TOA, or combined (MDF+TOA) sensors. Fig. 3.4 shows a typical lightning stroke in Florida that was detected by five sensors in the U.S. NLDN – three MDF+TOA and two TOA sensors. The direction measurements are shown as straight-line vectors, and range circles centered on each sensor represent the TOA measurements.

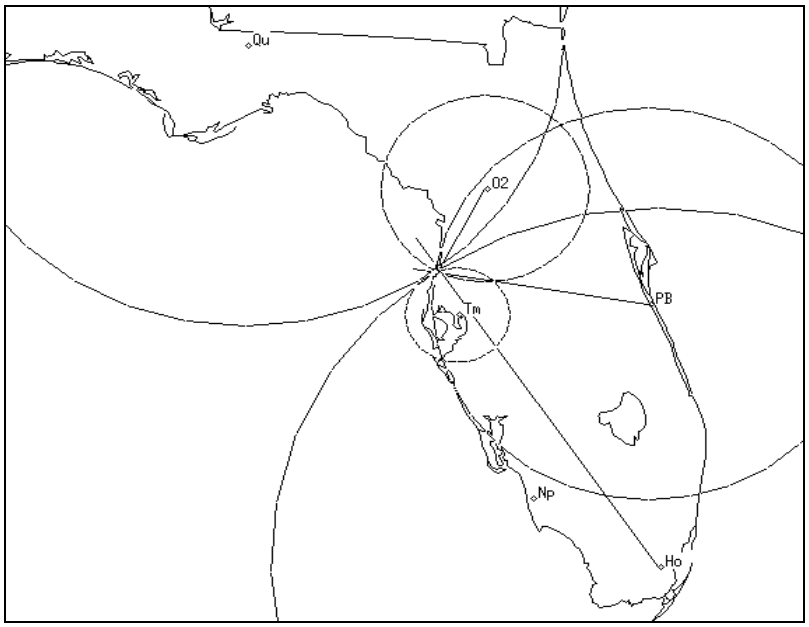

Fig. 3.4 Example of the MDF+TOA location algorithm using two TOA (time-of-arrival) and three MDF+TOA sensors (Cummins et al., 1998b)

3.4 Classification of Lightning Type

Although the electric and magnetic fields produced by return strokes in CG flashes are by far the largest VLF/LF lightning "signal", various components of in-cloud and intra-cloud flashes can also be detected in this frequency range. Some LLS sensors include a large set of "waveform criteria" that reject events that differ from usual strokes of CG flashes (Krider et al, 1980), whereas others report waveform parameters that are subsequently used by the central processing system to classify the discharges as "cloud" or CG. The trend over the last decade has been to "loosen" or eliminate the waveform criteria, in order to improve detection of small and/or unusual CG strokes and to allow detection and reporting of some cloud discharges. This has led to an increasing fraction of misclassified events, primarily resulting from cloud discharges being called small positive CG strokes. A specific subset of cloud discharges known as "narrow bipolar pulses" has peak fields that are in the range of the values produced by low- to moderate-current CG strokes (Smith et al., 1999), and are thought to be the primary source of misclassified discharges.

Recent studies employing GPS-synchronized video cameras (Biagi et al., 2007) using U.S. NLDN data from 2003-2004 have shown that most positive discharges with peak current below 10 kA in the southern U.S. are cloud discharges, whereas nearly all positive discharges above 20 kA are CG. Findings for negative discharges suggest that there is very little misclassification, at least in this area. Video studies on the U.S. central plains showed that there may be a higher percentage of misclassified negative discharges due to the nature of storms in that area. The U.S. NLDN currently employs several waveform criteria to exclude many non-lightning events, but the criteria used to exclude cloud discharges were relaxed somewhat in 1995 (Wacker and Orville, 1999) and eliminated during the 2002-2003 upgrade of the

U.S. NLDN. Discharges are currently classified using a Peak-to-zero (PTZ) duration criterion, which is the time from the initial peak in the waveform until the first zero-crossing after this peak. Discharges with small PTZ values are classified as cloud discharges. The specific PTZ values (separate for positive and negative discharges) can be set by the LLS operator at the central processor (e.g. LP2000), and has an effect on the amount of misclassification.

Ishii et al. (2005) compared data from the Japanese Lightning Detection Network (JLDN) with GPS synchronized lightning electromagnetic impulse (LEMP) records to evaluate JLDN's ability to discriminate between CG and IC discharges. During summer periode about 90% of the JLDN located positive CG strokes with peak currents of less than 10 kA were actually misclassified IC discharges.

The classification of lightning discharges has direct implications for lightning parameters derived from a LLS. Since the misclassified events are generally smaller than CG first strokes, they will alter the peak current distribution, producing smaller mean and median values (Orville et al., 2002), and increasing the width of the distributions. Ishii et al.(2005) applied a simple correction method to eliminate misclassified IC events from the CG peak current distribution and estimated an increase of the median positive peak current from +16 kA to +30 kA.

There is little effect on the multiplicity distribution of positive flashes (Orville and Huffines, 2001; Schulz et al., 2005) due to the low multiplicity for positive flashes and for the misclassified positive discharges. However, there is the potential for a significant change to the multiplicity distribution for negative flashes. The most likely problem would be that cloud discharges appear as small negative flashes with low multiplicity. Clearly, any comparisons of peak current or multiplicity distributions between regional networks, or within a network over time, needs to consider the accuracy of classification and any changes/differences in classification methods. The suppliers of commercial LLS systems should provide experimental results that document the accuracy of classification and show the dependence on operator-configurable parameters.

3.5 Grouping CG Strokes into Flashes

Various methods can be used to group strokes into flashes, and this will affect several derived lightning parameters. Systems manufactured by LLP and based on the "APA" central processor (prior to 1995) employed an angle-based algorithm where each DF sensor counted all strokes that occurred within $\pm$2.5 degrees of the first stroke for a period of one second after the first stroke, and the flash multiplicity was simply the largest number of strokes detected by any DF. This method will overestimate the multiplicity when concurrent flashes occurred at similar azimuths relative to any of the sensors (Cummins et al., 1998a). All other grouping algorithms group strokes into flashes using a spatial clustering algorithm illustrated in Fig. 3.5. Strokes are added to any active flash for a specified time period (usually 1 second) after the first stroke, as long as the additional strokes are within a specified clustering radius (usually 10 km) of the first stroke and the time interval from the previous stroke is less than a maximum interstroke interval (usually 500 ms). In the unlikely event that a

stroke is a candidate for more than one flash, it is assigned to the flash with the (spatially) closest first stroke. Additionally, in modern central processors (e.g. LP2000 or CP8000), if a stroke is located more than the clustering radius from the first stroke but is not clearly separated from that stroke because their location confidence regions overlap, then the stroke is included in the flash. The maximum multiplicity of a flash is usually a configurable parameter of the system; any strokes after that are considered to be members of a new flash. Depending on the system configuration, strokes may be counted in the multiplicity even if they have a polarity that is opposite that of the first stroke. Finally, the systems generally allow the user to determine if the assigned flash peak current is the value associated with the first return stroke or the largest stroke in the flash.

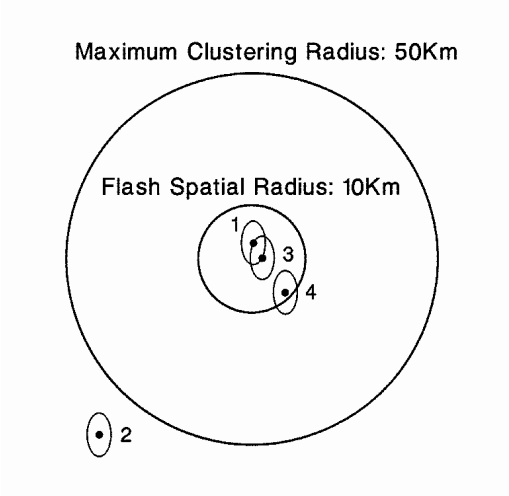

Fig. 3.5 Spatial clustering method for grouping strokes into flashes (Cummins et al., 1998b)

Clearly, the flash algorithm can have an affect on the measured flash multiplicity and peak current distribution. Since the spatial clustering algorithm implicitly requires that all counted strokes are located by the LLS, the estimated multiplicity for this algorithm will be very dependent on subsequent stroke detection efficiency (See Section 5.3). As part of a recent 10-year analysis of lightning data in Austria (Schulz et al., 2005), the authors found a 20% decrease in estimated negative flash multiplicity when changing from the angle-based flash algorithm to the spatial clustering algorithm, using the default parameters. Also, the flash peak current distribution will clearly change depending on the choice of “first stroke” or “largest stroke” as the flash peak current. Schulz et al. (2005) found a +14% increase in the median peak current for negative flashes and +4% increase for positive flashes when the largest stroke amplitude was assigned as the flash amplitude.

There is an interesting and important implication for lightning protection analysis associated with the meteorologically-based flash grouping algorithms discussed above. Lightning “flash” reports typically relate to the location of the first return stroke and a count of all strokes (multiplicity) associated with this meteorological event. Today “Flash counts” or GFD (ground flash density) are used as a quantitative replacement for the thunderday or thunderhour estimates of lightning exposure of an object. However, in order to assess fully the lightning threat to a specific asset or structure, one

must understand the nature of multiple ground contacts that are frequently associated with a single flash (See Section 2.4). On average, there appears to be about 1.5-1.7 strike points for each CG flash. Hence, for a complete evaluation of the threat from CG lightning, one should use the area density of ground strike points as GFD. At the moment, commercial LLS's are limited in that they can resolve only strike points that are separated by several hundred meters, but this is already much less than the 10 km radius used for clustering the strokes of the meteorological flash event (see also section 5.1).

3.6 Peak current estimate

According to the TL model (Uman et al., 1975) the current peak I_p is related to the far-field peak E_p and to the return-stroke speed (assuming that v=const, the ground is perfectly conducting, and the return-stroke front has not reached the top of the channel) through the following expression:

$$I_p = \frac{2.\pi.\varepsilon_0.c^2.D}{v}.E_p \qquad \textbf{(3.1)}$$

where D is the horizontal distance between the lightning channel and the observation point, v is the return stroke velocity, and c is the speed of light.

Assuming a typical return stroke velocity of 1.10^8 m/s and a distance D = 100 km, Eq.(3.1) becomes

$$I_p\,[kA] = 5.\ E_p\,[V/m]. \qquad \textbf{(3.2)}$$

This linear relation is used to infer lightning peak currents from measured peak fields. Often the peak current is inferred from the so called LLP-Units, which are directly proportional to the peak electric field in V/m. Given by one of the manufacturers the following relation exists between the LLP-Units (sensor output signal) and the electric field at the sensor site.

$$52\ V/m \triangleq 1158\ LLP\text{-}Units \qquad \textbf{(3.3)}$$

Combining Eq.() and Eq.() results in the often used direct conversion of the range normalized signal strength RNSS (normalized to 100 km) in LLP units to peak current in kA in the form of

$$I_p\,[kA] \simeq 0.23.RNSS\,[LLP\text{-}Units] \qquad \textbf{(3.4)}$$

Although, due to the high variability of key parameters such as the return stroke speed, it is impossible to determine the lightning current accurately from the remotely measured electric or magnetic field for a given event, it has been shown by Rachidi et al., 2004, that the statistical estimation (e.g. in terms of mean values and standard

deviations) is possible. In Rachidi et al., 2004, it is shown additionally that for the Transmission Line (TL) model, the equation permitting to infer the mean value of the return stroke current from the mean value of electric or magnetic field and the mean value of speed has the same functional form as the well-known TL current–far field relationship given in Eq.(3.1) above. This result gives, to a certain extent, a theoretical justification to the use of lightning location systems (LLS) to infer parameters of lightning current statistical distributions.

It is worth to note that the linear relationship used to infer the peak current from the peak field is not solely based on the TL model. Existence of a linear relationship has been validated by simultaneous measurements of currents and fields from triggered lightning and lightning to towers (see also chapter 8). In these studies the necessity to take into account the propagation effects was also realized and hence attenuation models are implemented in today's lightning locating software (see Section 6).

4 Model-Based Detection Efficiency of CG Lightning Strokes

There are a numerous factors that determine the detection efficiency (DE) of a lightning location system. The following brief treatment of this issue serves to summarize key issues, helping to explain the difficulty in estimating DE as well as providing useful background information for users of the data. The information is also used to provide the rationale for network DE correction methods covered in Section 9 of this document.

Throughout this document, DE is defined as the percentage (or fraction) of discharges (of any given type) that are reported by the LLS. Some specific examples are stroke DE_s (the fraction of all strokes, including first and subsequent) and subsequent stroke DE_{su} (excludes first strokes). Flash DE_f is unique in that a flash is reported (detected) if at least one stroke (first or subsequent) is detected. Therefore flash DE_f can be much higher than any form of stroke DE.

The task of lightning detection begins with the electromagnetic field produced by the lightning discharge. In the case of CG lightning being detected at VLF/LF frequencies, the peak field strength (electric and/or magnetic) is roughly proportional to the peak current of the return stroke, as summarized in Cummins et al., 1998b. The magnitude of the resulting field at a remote sensor location, which establishes the detectability of the signal by that sensor, is determined by the attenuation of this field strength that occurs due to normal propagation, and additional losses due to finite conductivity along the propagation path (see section 6.2). Once this attenuated signal reaches a remote sensor, it must exceed the detection threshold of the sensor, which is determined by sensor gain, threshold setting, and local noise. In order to obtain a location for the lightning discharge, then the signal must be seen by a sufficient number of sensors, which depends on strike point location (relative to the detecting sensors), and on the applied location method (MDF, TOA, or both – See Section 3).

A graphical depiction of the detection process that is amenable to direct modeling is shown in Fig. 4.1. The first step involves the occurrence of a CG stroke with peak current I_0, selected from the probability distribution P_I (the peak-current distribution). The peak electric and/or magnetic field produced by the stroke, having traveled a distance R_i, then reaches sensor S_i with incident signal SS_i as defined in Section 6.

The probability of the sensor S_i detecting this stroke is defined by the *sensor* DE function DE_i illustrated in Fig. 4.1. Note that there is a minimum signal strength (detection threshold) below which no events are detected, and that the maximum detectability is not reached until the signal is a bit larger than the detection threshold. Note also that as signal strength increases further, the DE_i decreases and eventually returns to zero when the sensor “over-ranges” and is no longer able to provide reliable information. Since each sensor that detects a specific stroke will be at a different distance, they may all have different sensor DE_i values for this stroke. Using the assumption that each sensor responds independently from all other sensors, these DE_i values are independent for each sensor S_i. For more information on how to get an estimate of the actual DE of a sensor see paragraph 7.5.

Based on this assumption, and by defining the probability of sensor S_i NOT detecting the event as $Q_i = 1\text{-}DE_i$, then the probability of a specific combination of sensors detecting the event is simply the product of the appropriate DE_i and Q_i values for all sensors. For example, the probability that a stroke with current I_0 is detected by a minimum of 2 sensors of a 3 sensor network, is

Prob(detection of a stroke in a three sensor network) =

$$[DE_1(I_0,r_1)*DE_2(I_0,r_2)*Q_3(I_0,r_3)] + [DE_1(I_0,r_1)*Q_2(I_0,r_2)*DE_3(I_0,r_3)] + [Q_1(I_0,r_1)*DE_2(I_0,r_2)*DE_3(I_0,r_3)] + [DE_1(I_0,r_1)*DE_2(I_0,r_2)*DE_3(I_0,r_3)] \quad \textbf{(4.1)}$$

as the signal strength at the sensor site is a function of I_0 and the distance r_i.

Using this construct, it is possible to determine the probability of detection for any specific number of sensors in a network of arbitrary size.

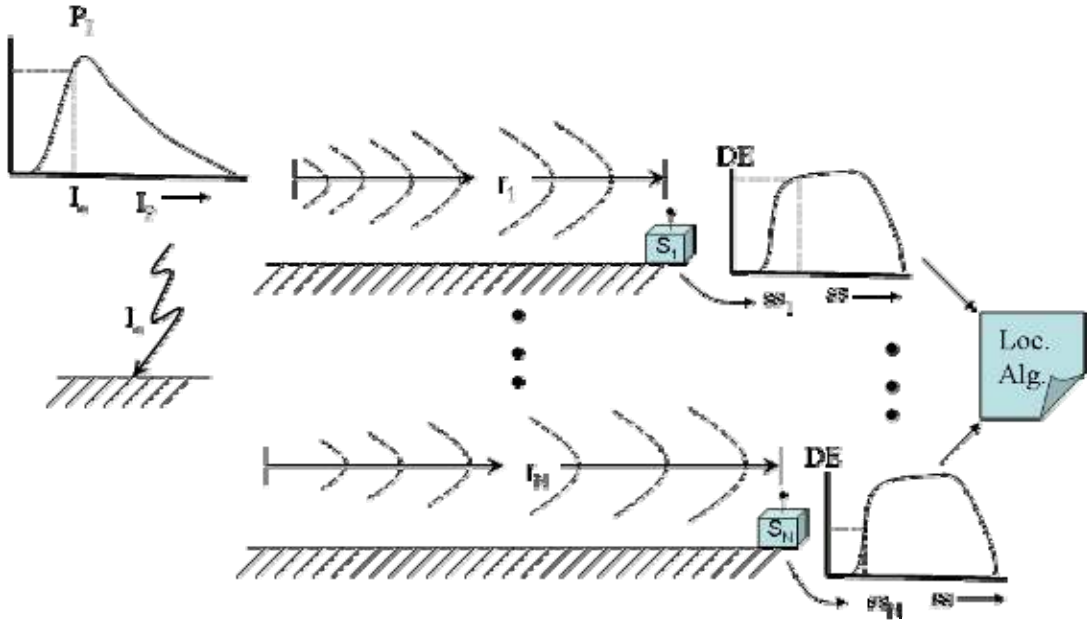

Fig. 4.1 Simplified model for LLS network detection efficiency based on given $DE_i(SS_i)$ function for each sensor in the network

In order to produce a modeled overall DE estimate for a region, the region of interest is typically broken up into a set of rectangular grid cells. For a point in the center of each cell, and for each possible peak current value, the model must determine the DE for each sensor. In order to determine the overall network detection efficiency for a specific peak current and grid point, one simply sums the probabilities for “N” or more sensors detecting a discharge, where N is the minimum number of sensors required by the network to locate a discharge. For networks that employ MDF in combination with TOA, N is two. For networks that employ direction finding by itself, N is 2-3, depending on the stroke location relative to the sensors locations. For networks that employ only the TOA method, N is 3-4. The overall DE is determined from the

sum of DE values for each current value (I_0), weighted by their probability of occurrence taken from the peak current distribution P_i.

To summarize, the fundamental information required to accurately model network DE is therefore the distribution of peak currents, the detection threshold characteristics of the sensors, the propagation conditions (regional conductivity), and knowledge of the location method (2,3, or 4 sensors required to get a location). We note that representing DE as a function of distance (as is employed in Chapter 7.5 to show sensor performance) is not ideally suited for overall network DE modeling, because the sensor DE function versus distance changes the shape for different peak currents. Therefore it would be necessary to determine the sensor DE function for “all” the peak currents what is almost impossible. In this respect the usage of the sensor DE function versus signal strength as indicated in Fig. is simpler and straighter forward.

One can alter the nature of the network DE estimate by adapting the peak current distribution. If the network DE for first strokes is desired, then the first-stroke peak current distribution should be employed. If an overall network stroke DE is desired, then one would employ a peak current distribution composed of first and subsequent stroke probabilities, in proper proportion. If the Flash DE is the desired metric, meaning that a flash is considered to be detected if *any* stroke in a flash is detected and located, this can be approximated by determining the network DE for first strokes OR any number of subsequent strokes. This calculation requires an estimate of the flash multiplicity (number of strokes in a flash), along with estimates of first and subsequent stroke peak current distributions. Often, the flash DE is approximated by the first stroke DE, since first strokes are generally larger (and easier to detect) than subsequent strokes.

To demonstrate the effect of sensor baseline, location method and sensor availability (simulating temporarily outage of a sensor) we have calculated the DE for a six-sensor network configuration. Assumptions and details of the calculation are given in Appendix A. The sensors are assumed to be located at the corners and the center of a pentagon as shown in Fig. . To demonstrate the effect of baseline length we have set the radius of the pentagon to 150, 200 and 300 km, respectively. To analyze the effect of a sensor outage we have removed the central sensor and a corner sensor. For each network configuration we have calculated the overall DE for the different location methods, requiring 2, 3 or 4 sensors. Contour plots of the DE for the various network configurations are shown in Appendix A and results are summarized in Table . The assumed sensor sensitivity is what would typically be used for sensor baselines of 150-200 km. Table summarizes the overall DE within a region of 600 km x 600 km (150 and 200 km baseline networks) and 800 km x 800 km (300 km baseline network) area for the various conditions.

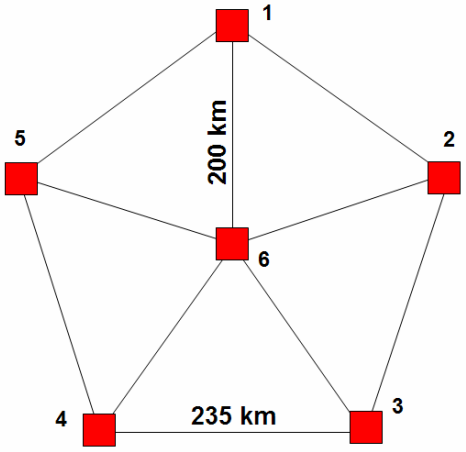

Fig. 4.2 Six sensor network, where sensors are located at the corners and centre of a pentagon

For the assumed network geometry and peak current distribution we can see in Table 4.1 the significant effect of applied location method and sensor baseline. The highest DE (97,0%) is achieved by the 150 km baseline network when only 2 sensors are required (MDF+TOA), whereas the lowest DE (56,3%) is estimated for a network of 300 km baseline, when 4 reporting sensors are necessary to get a location – which is generally required for TOA-only networks to avoid ambiguous locations (see chapter 3.2). DE of a network requiring 4 sensors is obviously much more affected by any changes of baseline length or outage of a sensor.

Given the general model and results discussed above, one can anticipate the following relationship between return stroke peak current, network status, and overall network detection efficiency:

(1) Missed (not located) events: Very low peak current events may not be detected by any sensors and somewhat larger events (a few kA) will be seen by a small number of sensors, but insufficient to obtain an accurate location.

(2) Variable detection of events: Depending on network geometry and status (Up/Down) of sensors intermediate-size (several kA) events can be seen by a sufficient number of sensors to obtain a location for some positions in the network (e.g. center region of network), but not all.

(3) Consistent detection, irrespective of loss of 1-2 local sensors: Large (10's of kA) events which can always be seen by 4 or more sensors. Normally those events radiate electromagnetic signals which are large enough to cross threshold at all sensors within several hundreds of kilometers.

The analysis provided above addresses the primary interaction between LLS DE and peak current, which is a threshold-related phenomenon. It is also important to consider the effect of very high peak current events on LLS DE. These large events may over-range (saturate) one or more nearby sensors in a LLS, or may produce a com-

plex waveform that is not properly detected by nearby sensors. A study of sensors in the U.S. NLDN by Cummins (2000) has shown that “very high” gain IMPACT and LPATS sensors (Gain 6) will improperly detect about half of 100-200 kA strokes at a distance of 300 km. This can lead to poor detection of large events when the network is small (has only a few sensors). Although the numerical effect in DE resulting from missing such large events is small due to the low probability of occurrence, these large events can be the most important to detect because of their potential for severe damage.

We have to note at this point that single events of extremely low or high peak currents are not a reliable indicator for the actual sensitivity range of a given network. There is a good chance that some of those extreme values are the result of miss located strokes and hence data should be carefully analyzed by checking individual sensor reports and the entire location procedure before using such events for further conclusions.

Table 4.1: Model based DE of a 6 sensor network of different network layouts and location methods (2, 3 or 4 sensors required to get a location).

	Network – Sensor locations	Number of sensors required to get a location		
		2	3	4
Sensor Baseline **200 km** (600 km x 600 km area)	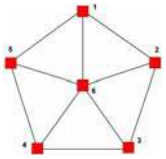	96,5% (Fig. A1)	90,4% (Fig. A2)	76,6% (Fig. A3)
	Centre sensor removed 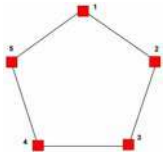	94,0% (Fig. A4)	81,2% (Fig. A5)	58,3% (Fig. A6)
	1 border sensor removed 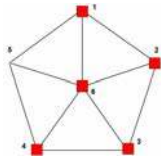	94,5% (Fig. A7)	84,0% (Fig. A8)	60,3% (Fig. A9)
Baseline **150 km** (600 km x 600 km area)	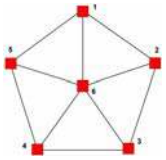	97,0% (Fig. A10)	92,2% (Fig. A11)	80,6% (Fig. A12)
Baseline **300 km** (800 km x 800 km area)	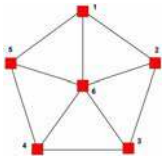	89,5% (Fig. A13)	76,5% (Fig. A14)	56,3% (Fig. A15)

5 Effect of Detection Efficiency on CG Lightning Parameters

In this chapter we turn to the question of how the quality/accuracy of the statistical information provided by LLS networks depends on its flash and stroke detection efficiency. The primary determinant of the accuracy of estimated ground flash density (GFD), peak current distributions, and flash multiplicity distributions is detection efficiency (DE) – the percentage of actual lightning discharges that are detected and located by the network. Location accuracy – a statistical measure of the position difference between the actual ground strike location and the location provided by the network – has a weak secondary effect on these parameters, and will only be touched on briefly in this chapter.

5.1 Estimation of Ground Flash Density

Ground flash density (GFD), typically presented as the number of CG flashes per square km per year, is affected by LLS performance in rather direct ways. If the flash DE is low and nearly constant over longer time periods but can be estimated, than the actual GFD can be estimated by dividing the measured GFD by an estimate of flash DE. Flash DE is usually rather constant over moderate-sized regions (radius of 100-200 km for LLS networks with 200-300 km sensor baselines), making it practical to apply regional DE corrections. Methods for producing DE corrections are presented in Chapter 9.

Two other factors that can affect the accuracy of GFD estimates are location accuracy (LA) and misclassified events. LA defines the lower limit on the size of the grid area over which one should compute statistics. In general, the grid size should not be finer than the median location accuracy of the LLS. For most practical purposes a grid size of 2 km x 2 km is sufficiently small to represent any regional variation in flash density, and is quite consistent with the LA of modern LLS's. Note that some misplacement of flashes into neighboring grid cells simply serves to produce a "smoothing" of the GFD distribution, assuming that the locations errors are predominantly random. Finally, misclassified events – an important example is cloud discharges that may be misclassified as CG strokes – should be compensated for in the calculation of GFD if they contribute a large fraction of the events. As a rule of thumb, effects larger than about 5-10%, which is in the range of expected uncertainty for other uncorrectable effects, should be compensated for if possible.

As a final topic regarding flash density, there are important distinctions between GFD, ground stroke density (GSD) and ground strike-point density (GSPD). GSD is very sensitive to LLS performance, because the stroke DE is usually much lower and more variable than flash DE. Additionally, since about one half of all multi-stroke negative flashes are thought to have two or more ground attachment points separated by a few 10s of meters to over 7 km (Rakov et al., 1994), the traditional GFD underestimates lightning-damage risk associated with a CG flash (Cummins et al., 1998b). Given that current LLS location error is in the range of 500-1000 m (median), the most practical method to estimate GSPD is to multiply the GFD by 1.5 - 1.7, based on multiple strike point statistics accumulated to date (see Section 2.4).

5.2 Estimation of peak current parameters

The shape and parameters (e.g., mean, median) of peak current distributions are extremely sensitive to the detection efficiency of a LLS. In this section we illustrate this fact, and we briefly describe a method used to infer DE changes over time that exploits this relationship.

It is possible to see the influence of DE in the peak current distribution by careful evaluation of the cumulative distribution. This fact is illustrated in Fig. 5.1. A "reference" cumulative peak current distribution was obtained from a small region in the central U.S. using the negative flash (first stroke) information for a several-week period in 1998 (referred to as "All" in Fig. 5.1). Additional cumulative distributions were then obtained by reprocessing the U.S. NLDN data with the exclusion of increasing numbers of sensors, to produce three different relative DE conditions (99%, 89%, and 75%). The exact percentage of events that were detected is known – it is the fraction of the total count of events produced for the reference (All) condition. These cumulative distributions were computed starting with the largest peak current flashes, reaching 100% as the peak current approaches zero. The "99%" distribution superimposes exactly over the curve produced in the "All" condition. Note that as the DE reduces, there is a clear increase in the minimum detectable current (the point on the curve where the cumulative distribution reaches 1.0). This reflects the fact that the primary determinant of DE is the probability of detection as a function of current. Specifically, all events below some minimum peak current are missed, nearly all events above some larger peak current are detected, and values in between are detected with monotonically increasing probability. This behavior has been shown in numerous studies – most recently in a paper by Diendorfer et al. (2002).

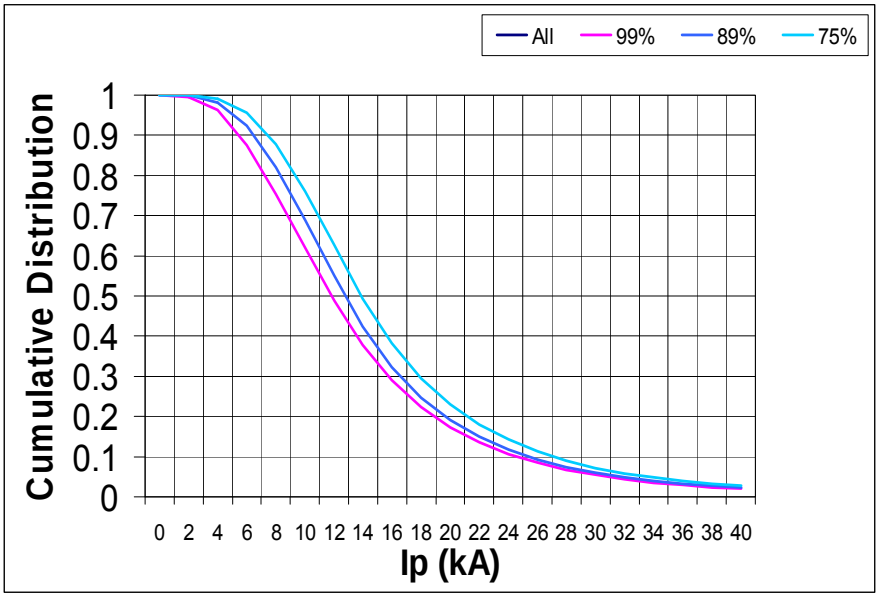

Fig. 5.1 Cumulative negative first stroke peak current distributions for four different detection efficiency conditions in the central U.S. NLDN (plot of "All" and 99% superimpose exactly).

The influence of these DE differences on the mean and median peak current values is shown in Table 5.1. As the relative DE reduces from 99% to 75%, there is a steady increase in both the mean and median peak current parameter values. Note that the "99%" condition has the same values as the reference (100%) condition. When the flash (first stroke) DE is reduced to 75%, the mean value is increased by 13.6% (from -16.9 kA to -19.2 kA) and the median is increased by 15.1% (from -13.9 kA to -16.0 kA). We note that these variations with peak current are sufficient to "mask" any likely regional peak current differences resulting from "real" climatological differences.

Table 5.1: Mean and median peak currents of neg. first strokes for the four different DE conditions shown in Fig. 5.1.

Relative DE	Mean I_p (kA)	Median I_p (kA)
100	-16.9	-13.9
99	-16.9	-13.9
89	-17.9	-14.9
75	-19.2	-16.0

Continuous updates of lightning peak current distributions obtained from LLS's are important to refine the distributions taking into account cyclic variations on lightning intensity. This will be a valuable input to standard bodies working on lightning protection guidelines.

5.3 Estimation of Multiplicity parameters

This section specifically deals with negative CG flashes, since positive flashes seldom involve more than one stroke. Like peak current distributions, the shape and parameters of the multiplicity distribution are also significantly affected by the detection efficiency of an LLS. The multiplicity parameters that will be explored here are average multiplicity and the percentage of single-stroke flashes.

Earlier work by Rubinstein (1995) and Rakov and Huffines (2003) have shown that the overall stroke DE (computed including both first and subsequent strokes) has a strong influence on the measured multiplicity distribution, and that the "true" multiplicity distribution determines the relationship between flash DE and overall stroke DE. Rakov and Huffines applied a simple relationship between "True" average multiplicity (M), measured average multiplicity (m), Flash DE (DE_f) and overall stroke DE (DE_s) that can be expressed in a way to illustrate the sensitivity:

$$m = M * \left(\frac{DE_s}{DE_f} \right) \qquad \textbf{(5.1)}$$

Since M is statistically greater than 1 (usually in the range of 3-5 for negative flashes), the ratio (DE_s/DE_f) is generally viewed as a monotonically increasing function that approaches 1 as DE_s increases (Rubinstein, 1995, figure 2). In the example case by Rubinstein, an overall stroke DE of 30% caused the measured multiplicity (m) to be about ½ of the value of the true multiplicity (M). This formulation implies that any improvement in detection efficiency would produce a larger measured average multiplicity.

The work cited above dealt with a single overall stroke DE, and resulted in a simple (first approximation) relationship between multiplicity and DE. However, it is well-accepted that first stroke DE (DE_1) differs from and is generally higher than subsequent stroke DE (DE_{su}). Also, recent work by Schulz et al. (2005) in Austria, as well as unpublished studies in the U.S., has shown that under some conditions, improved performance actually results in a lower average measured multiplicity. This is apparently because the increase in first stroke DE_1 resulted also in an increased number of very low peak current single-stroke flashes, outweighing the contribution of the increased number of subsequent strokes. This occurrence is not unreasonable, given the growing number of observations showing that on average, peak current for single-stroke flashes is significantly smaller than first stroke peak current for multi-strokes flashes (Rakov and Uman, 1990). Orville et al. (2002) found that the median peak current of single-stroke flashes was approximately 2/3 the median first-stroke value found in flashes with 7 or more strokes. Accordingly, we present a more-general model for the multiplicity distribution that separates out these two DE terms, assuming that all subsequent strokes have equal detection probability. This is known to be a simplification given that subsequent strokes in new channels have generally larger peak current than subsequent strokes in established channels (Rakov and Uman, 1990), but this model is sufficiently flexible to address the major effects on multiplicity parameters. In this formulation, the probability of having detected “k” strokes, given that there were actually “n” strokes in the flash, can be described as follows:

Prob {k detected strokes | n actual strokes} =

Prob {detect 1st stroke}*Prob {detect k-1 Subs}*Prob {missing n-k Subs} *Comb(n-1:k-1) +
Prob { miss 1st stroke}*Prob {detect k Subs} *Prob {missing n-k-1 Subs} *Comb(n-1:k) **(5.2)**

where Comb(a:b) is the number of combinations of “a” things taken “b” at a time.

In this formulation, we consider two general conditions – detecting the first stroke and missing the first stroke. For each condition, we then determine the probability of obtaining exactly “’k-1” subsequent strokes (in the case of detecting the first stroke) and “k” subsequent strokes (when the first stroke is missed). Expressed in terms of DE_1 and DE_{su}:

$$\mathrm{Prob}_{det}\{k \mid n \geq k\} = \sum_{n=k}^{N} \mathrm{Prob}_{true}\{n\} * DE_1 * DE_{su}^{(k-1)} * (1-DE_{su})^{(n-k)} * \mathrm{Comb}(n-1:k-1) + \sum_{n=k+1}^{N} \mathrm{Prob}_{true}\{n\} * (1-DE_1) * DE_{su}^{k} * (1-DE_{su})^{(n-k-1)} * \mathrm{Comb}(n-1:k) \quad \textbf{(5.3)}$$

where N is the highest multiplicity considered in the analysis.

Fig. 5.2 illustrates one element of this calculation, and the effect of lowering the first stroke DE_1 to 0.7 and the subsequent stroke DE_{su} to 0.4. The portion of the "True" 4-stroke flashes that became located three-stroke flashes ($Prob_{det}\{3|n=4\}$) is illustrated as the green portion of the lower multiplicity distribution. The "total" probability of obtaining a 3-stroke flash is this term, plus the terms related to k=3, 5,…N.

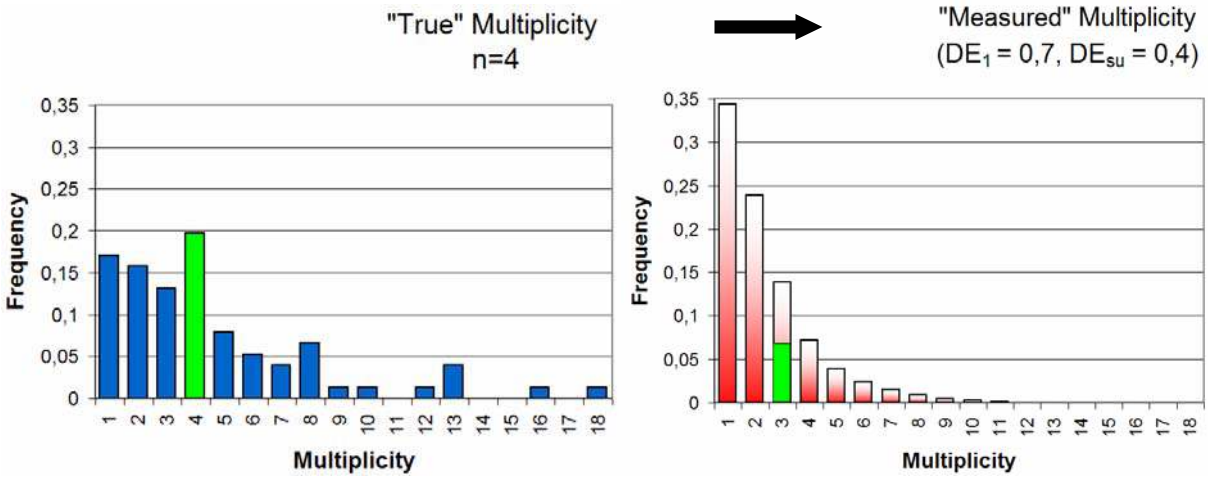

Fig. 5.2 Effect of limited detection efficiency on multiplicity

Fig. 5.2 - Left histogram represent the "True" multiplicity distribution, based on video and electric field records near Tampa Florida. The right histogram is the estimated "measured" multiplicity distribution assuming that 70% of first strokes are detected and 40% of subsequent strokes are detected. The green region of the curve is the portion of the "multiplicity =3" that is contributed by true 4-stroke flashes.

The importance of using this more-general model is illustrated in Fig. 5.3. Two conditions are shown – both of which result in a flash DE_f of 89%. One condition employs the same DE (60%) for first and subsequent strokes. The other condition has a significantly higher first-stroke DE_1 (70%) and a lower subsequent-stroke DE_{su} (40%). Note that the percentage of single-stroke flashes is significantly lower in the condition with equal DE ($DE_1 = DE_{su}$). Table 5.2 summarizes these results, and also provides the average multiplicity values associated with the various conditions. In this example, the average measured multiplicity differed by nearly 30% (3.1 vs. 2.4), with no change in flash DE_f.

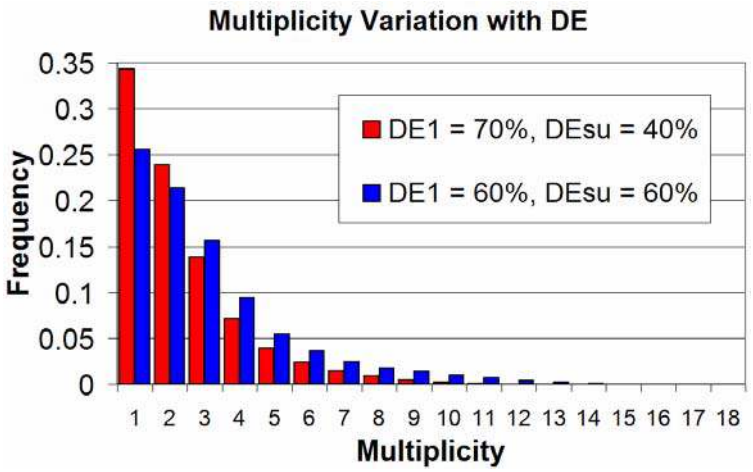

Fig. 5.3 Multiplicity histograms for two different detection efficiency conditions. Both conditions result in flash DE_f of 89%.

Table 5.2: Flash DE_f, percent of single-stroke flashes, and Multiplicity for three detection efficiency conditions.

$DE_1 : DE_{su}$	Flash DE_f	% Single-stroke	Multiplicity
100% : 100%	100%	17%	4.5
60% : 60%	89%	26%	3.1
70% : 40%	89%	34%	2.4

It is clear from Fig. 5.3 and Table 5.2 that it is important to consider different DE values for first and subsequent strokes, and that detection efficiency can have a significant effect on measured multiplicity parameters.

As noted earlier, recent studies in Austria and the U.S. have shown that under some conditions, improved performance (detection efficiency) can actually result in a lower average measured multiplicity. This observation can be explained using the following more-general form of Eq. (5.1) using variable names defined above:

$$m = \frac{(M-1)*DE_{su} + DE_1}{DE_f} \qquad \textbf{(5.4)}$$

From this equation, it is possible to envision that an increase in DE_1 could actually result in a smaller average measured multiplicity, given that the denominator term will also increase. The most-likely case is when there is a high fraction of single-stroke flashes in the "True" multiplicity distribution.

6 Sensor Calibration and Correction for Propagation Effects

In this section we discuss sensor gain calibration and methods for the correction of propagation effects related to the peak field measurement used to infer the peak current of the lightning discharge. We do not cover the MDF sensor alignment errors, the correction of systematical angle error (site error correction) for MDF sensors (e.g. Hiscox et al., 1984; Schulz, 1997) or the correction for systematic time errors, all of which affect the accuracy of the location and the peak current estimate (Schulz and Diendorfer, 2000). These topics are outside of the scope of this document.

6.1 Calibration of E-field sensors

Typically E-field sensors (e.g. LPATS III, LPATS IV) measure the electric field employing a vertical rod antenna. It is well known that depending on local site conditions, the measured electric field will differ from the undisturbed incident field due to local field enhancement. Therefore E-field sensors placed on objects of different height and shape (e.g. sensor placed on the roof of a building) will measure and report different field peak values. Therefore a gain calibration procedure is required.

In older LLS employing only E-field sensors a calibration was typically done using a two steps procedure. In step (1) the relative gain for each sensor was determined by equalizing their average range normalized field strength values. In step (2) the median field strength was then set to a value resulting in a median negative flash peak current of a given value (typically 30 kA, as this is the published median peak current of negative first strokes – see Table 2.1). Nevertheless this type of network is not calibrated in terms of absolute field peaks.

For mixed networks (MDF and TOA sensors) it is possible to calibrate the E-field sensors with the aid of the magnetic field signals reported by the calibrated MDF sensors, since the magnetic field does not suffer from local field enhancement effects. It is important to note that the calibration of the E-field sensors has to be done for a certain attenuation constant of the fields (see chapter 6.2). Thus changing the setting of the attenuation constants in the central processor (e.g. LP2000) of a network requires a recalibration of all the E-field sensors.

Basically there are three options for calibrating an E-field sensor:

- Adjust the length of the rod antenna
- Change the gain setting of the antenna receiver
- Set and apply appropriate software gain correction factor in the central processor (e.g. LP2000).

Table 6.1 summarizes the advantages and disadvantages of each of the three approaches.

Table 6.1: Advantages and disadvantages of each calibration method

Calibration method	Advantage	Disadvantage
Adjust length of the rod antenna	Gain identical to other sensors	Site visit necessary - to find appropriate length by try and error is required;
Change Gain of the antenna receiver	Gain identical to other sensors Easy to do	During sensor hardware replacement gain has to be configured
Set Gain correction factor in central processor	Easy to do	Sensors have different sensitivities

A combination of the above listed measures is also possible to calibrate the sensors by roughly adjusting the length of the antenna in a first step and then do the fine adjustment by setting gain correction factors in the central processor.

6.2 Correction of propagation effects

LLS infer the peak current from the range normalized peak fields (range normalized signal strength RNSS) and by using Eq.(6.1). The field-to-current conversion constant SNF is typically set to 0.23 or 0.185 (see Diendorfer et al., 1998). The factor 0.23 which was originally supplied as default setting by the manufacturer of the LLS was theoretically derived assuming a transmission line model (Uman and McLain, 1969) with a return stroke velocity of 1/3 of the speed of light (1.10^8 m/s – see also chapter 3.6). The factor SNF=0.185 was derived from triggered lightning and correlated U.S. NLDN data analysis (see also Cummins et al., 1998a).

$$I[kA] = SNF * \overline{RNSS} \qquad \textbf{(6.1)}$$

In Eq.(6.1) $\overline{RNSS}$ is the mean of the RNSS values of all sensors participating in the location.

The range normalized signal strength (RNSS) of the individual sensors is calculated using Eq. 6.2 [see Cummins et al. (1998a)]. In this equation SS is the raw signal strength and r is the distance in km from the sensor to the estimated ground strike point. Parameters b and L are taking into account effects of field propagation over ground of finite conductivity.

$$RNSS = SS * \left(\frac{r}{100}\right)^{b} * \exp\left(\frac{r-100}{L}\right) \qquad \textbf{(6.2)}$$

When we assume a purely inverse-distance dependency of the lightning radiated field, which is valid only in the case of infinite ground conductivity, we have to set b = 1.0 and the space constant L to a very large value (e.g. L = 10^5 km). Different values for the attenuation "power law" constants b have been proposed in literature, e.g. b= 1.13 by Orville (1991) or b= 1.09 by Idone et al. (1993). Herodotou et al. (1993) and Cramer et al. (2004) have shown the importance of applying an appropriate attenuation model, and they suggest that an exponential model employing a space constant L results in a better fit than a power-law model.

To demonstrate the procedure to find the "best" value for the space constant L, we used data from the European lightning location system EUCLID (see paragraph 7.1) which is a combined network of about 100 LPATS and IMPACT sensors. For the peak current calibration and validation of the setting of the attenuation parameters we have reprocessed raw sensor data from August 2004. The following paragraphs describe the individual steps used to determine the optimum parameters L and SNF for the attenuation model of the given LLS.

(1) In a first step we have disabled the use of the signal information for all of the LPATS sensors to prevent these uncalibrated signal strengths from being included in the peak current calculation of the strokes. Then we have reprocessed the data with different attenuation constants. For all the recalculations the attenuation exponent was kept constant (b = 1.0) and only the space constant L was changed to find the best value. To be able to compare the results with data obtained without applying any attenuation model, a reprocessing sequence was performed with the values b=1.0 and L=10^7 km. From the range normalized signal strength of the sensor ($RNSS_{Sensor}$) and the average range normalized signal strength ($\overline{RNSS}$) a parameter called sensor gain (SG) was calculated according to Eq.(6.3) for each stroke and for each individual sensor. $\overline{RNSS}$ is the mean of $RNSS_{Sensor}$ from all the sensors contributing to each stroke location.

$$\mathbf{SG_{Sensor}} = \frac{\mathbf{RNSS_{Sensor}}}{\overline{\mathbf{RNSS}}} \qquad \textbf{(6.3)}$$

In a next step mean and standard deviation of SG_{Sensor} were calculated for each sensor for all strokes located by that particular sensor within 500 km. The central processor (LP2000) location algorithm was configured to calculate the stroke peak current by using only signal strength information from sensors located within 625 km of the stroke location.

In a last step we calculated the overall mean of all the $\overline{SG_{Sensor}}$ and the mean of the standard deviations of all these $\overline{SG_{Sensor}}$ values. This procedure was done for differ-

ent settings of L in the range of 800 km to 1,300 km and results are shown in Fig. 6.1.

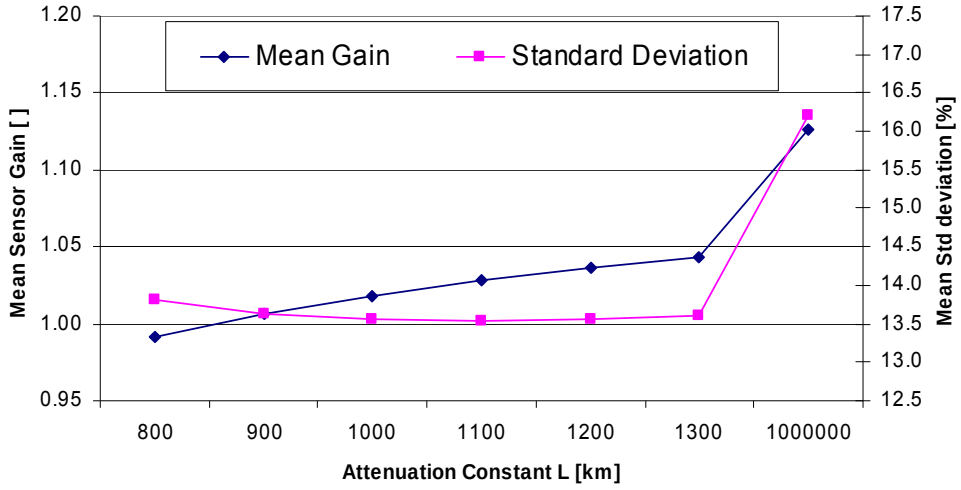

Fig. 6.1 Mean of sensor gain and mean of standard deviation as a function of L

The “best” value for L is defined as the value that provides an average gain very close to unity, and minimizes the standard deviation of that statistic. Fig. 6.1 shows that the mean sensor gain for L=900 km is approximately 1.0 and the standard deviation has a minimum in the range of L=1000 km to L=1300 km. In this case the difference between L=900 km or L=1000 km is small and both values resulted in significant improvements compared to the configuration with $L=10^7$ km. Applying L=1000 km in the attenuation model reduces the mean random error of the range normalized signal strength from about 16% to 13.5% - a relative improvement of about 18%.

(2) After selecting the space constant L = 1000 as the appropriate value for the attenuation model all the gain correction (GC) values of the LPATS sensors were derived from the reprocessed data and applied to the sensor configuration of the central processor.

(3) A final sequence of reprocessing with the adjusted sensor configuration was performed, this time allowing LPATS signal strength information to be used by the central processor to infer the stroke peak current. Validity of the adjusted LPATS gain corrections was confirmed by the results of this reprocessing sequence (near-unity gains and small standard deviations).

7 Relative Network and Sensor Detection Efficiency of an Operational Network

To demonstrate the effect of different network settings on the overall network performance we have reprocessed data from summer 2001 (July and August 2001) with different configurations.

We have used data from the European LLS EUCLID (**EU**ropean **C**ooperation for **LI**ghtning **D**etection) as a reference to calculate the relative DE of the **A**ustrian **L**ightning **D**etection & **I**nformation **S**ystem (ALDIS) and to demonstrate the effect of different network settings on the resulting peak current and multiplicity distribution.

7.1 EUCLID network

In 2001 several countries (Austria, France, Germany, Italy, Norway and Slovenia) started a cooperation called EUCLID. It is the goal of this cooperation to provide European wide lightning data with nearly homogeneous quality. In summer 2001 the EUCLID network employed 87 sensors, 12 LPATS III, 17 LPATS IV, 33 IMPACT and 25 IMPACT ES/ESP sensors. In Fig. 7.1 only a section of the EUCLID network around Austria is shown.

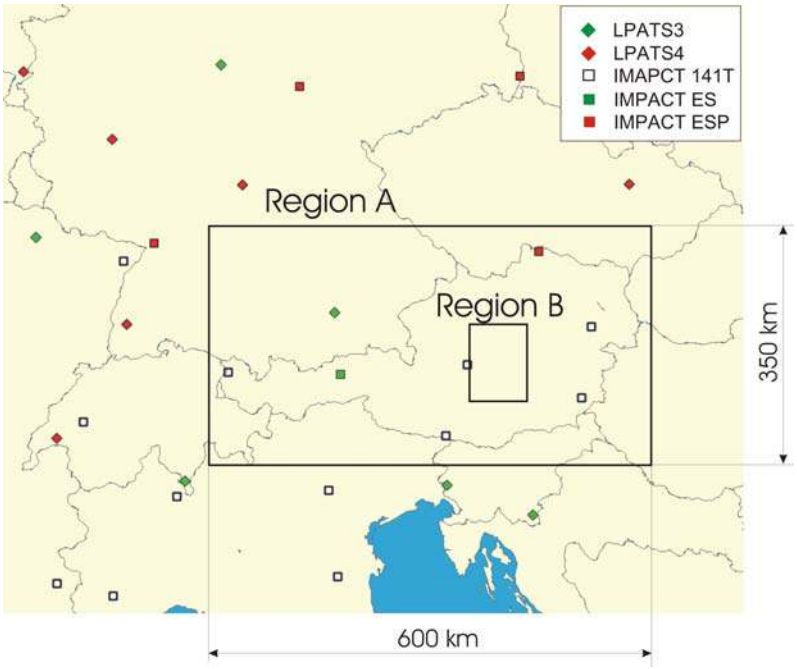

Fig. 7.1 EUCLID network configuration around Austria for summer 2001 with regions of investigations (Region A: 600 km x 350 km, Region B: 75 km x 110 km)

7.2 ALDIS network

The Austrian lightning location system ALDIS started operation in January 1992. Mean baseline between the 8 sensors in Austria is in the range of about 120 km and hence is one of the high gain networks in the world with the smallest sensor baselines, and for this reason it has been selected as a particularly significant example of LLS.

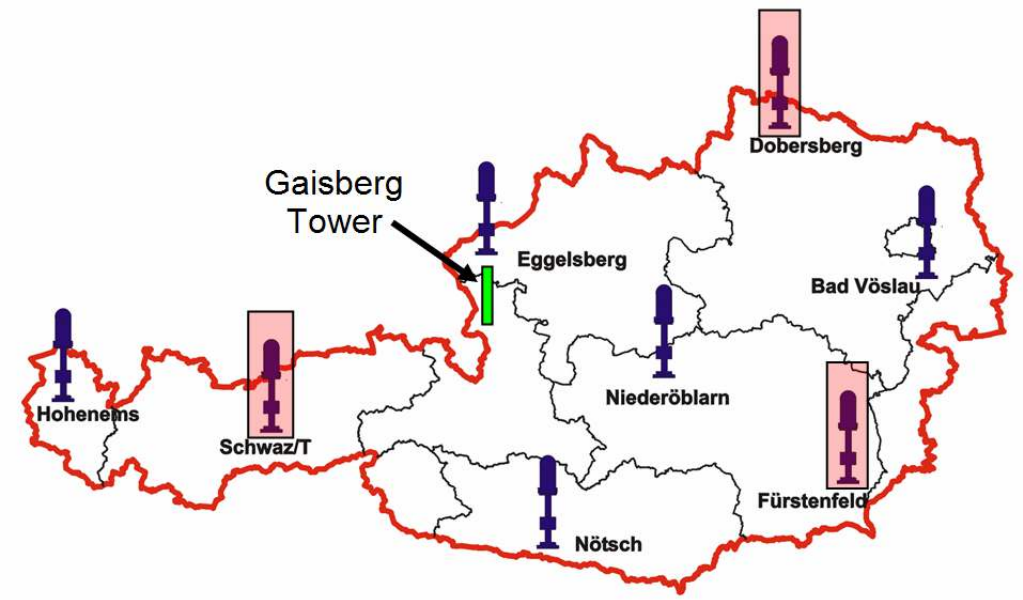

Fig. 7.2 Austrian lightning location network with 8 IMPACT type sensors

In summer 2001 the system employed eight IMPACT 141T sensors and a LP2000 as central processor. The LP2000 is able to process all the available sensor information and computes a separate position for each individual stroke. The located strokes are grouped to flashes and a multiplicity is assigned to the flash as described in section 3.5.

We have reprocessed the raw data for three different network configurations referred in the following section as LLS_8AT, LLS_3AT and LLS_8T, respectively.

LLS_8AT: Time and angle information is used from all the 8 ALDIS sensors shown in Fig. 7.2 – supposed to examine the performance changes due to not using sensors from neighboring networks participating in EUCLID.

LLS_3AT: Only time and angle information of a 3 sensor sub-network (sensors marked by surrounding rectangles in Fig. 7.2) is used. This configuration represents a small network of longer baselines.

LLS_8T: Only time information from the 8 sensors is used, simulating a pure TOA system. In this configuration a minimum of either 3 (LLS_8T/3) or 4 (LLS_8T/4) measurements were required to compute a location.

7.3 Overall network comparison

From the results of the different reprocessing sequences we extracted and analyzed data within the two rectangular regions (A) and (B) shown in Fig. 7.1. Region (A) covers the area 9.5° to 17.5° East and 46.00° to 49.25° North. Region (B) is a sub-region of (A) and covers the area 14° to 15° East and 47° to 48° North.

All reprocessing sequences were done without applying any attenuation model and with the same field-to-current conversion factor of 0.23.

In Table 7.1 we have summarized some performance parameters for the different network configurations, the flash DE_f for negative CG flashes relative to the EUCLID network, the median and 1% peak current of the negative flash current distribution and the mean multiplicity of negative flashes. Stroke-to-flash grouping criteria remained unchanged in the different network settings.

Table 7.1: Performance parameters for the different network setups in region A

	Flash DE_f relative to EUCLID	Median negative peak current	1% negative peak current	Mean multiplicity
EUCLID	100%	-10.0 kA	-2.6 kA	2.3
LLS_8AT	89% (-11%)	-9.8 kA (-2%)	-2.3 kA	2.1
LLS_3AT	61% (-39%)	-11.2 kA (+12%)	-3.4 kA	1.8
LLS_8T/3	59% (-41%)	-12.3 kA (+23%)	-3.7 kA	2.0
LLS_8T/4	43% (-57%)	-14.4 kA (+44%)	-5.3 kA	1.9

From Table 7.1 it is interesting to note that a pure TOA system of equal baseline and requiring 4 measurements (LLS_8T/4) detects only 43% of the flashes of the reference network, whereas the reduction in DE_f for the LLS_8AT is only -11%. Somewhat unexpectedly, we see that the LLS_8AT network with a significantly smaller DE_f (89%) shows a smaller median negative peak current (-9.8 kA) and a smaller 1% peak current (-2.3 kA) when compared to the EUCLID network. The slightly smaller median peak current of the ALDIS network is a result of poor detection of very high peak current strokes in a small network with high gain sensors (Cummins 2000). Typically, we expect a higher median peak current for networks of lower DE because it is mainly the strokes with small peak currents that are missed in LLS with lower DE.

To separate out effects of including border areas in our analysis we have determined the same performance parameters within area (B) which is a subarea well centered within all the tested networks. This region is even within the LLS_3AT sub-network, a network of only 3 sensors. When compared to region (A) where the LLS_8AT network detected 89% of the flashes seen by the EUCLID network (see Table 7.1), region (B) has only a 1% difference in the DE of the LLS_8AT and the EUCLID network

(Table 7.2). This confirms that the integration of neighboring sensors results mainly in an increase in DE in the border areas.

Table 7.2: Performance parameters for the different network setups in region B

	Flash DE_f relative to EUCLID	Median negative peak current	1% negative peak current	Mean multiplicity
EUCLID	100%	-9.7 kA	-2.8 kA	2.6
LLS_8AT	99% (-1%)	-9.2 kA (-5%)	-2.6 kA	2.5
LLS_3AT	82% (-18%)	-10.1 kA (+4%)	-3.5 kA	2.2
LLS_8T/3	85% (-15%)	-10.5 kA (+8%)	-3.6 kA	2.4
LLS_8T/4	69% (-31%)	-12.0 kA (+24%)	-4.6 kA	2.3

In subarea (B) the reduction in DE_f is less significant than in region (A). In this subarea the LLS_8AT network has a relative DE of 99%, whereas the LLS_8T/4 network missed 31% of the flashes. It is interesting to note that LLS_3AT, a 3 sensor combined MDF/TOA network and an 8 sensor TOA network (LLS_8T/3) have similar DE_f values in both regions with 61% and 59%, respectively in region (A) and 82% and 85%, respectively in sub-region (B).

Model simulation results listed in Table show the same trends listed in Table 7.2. There is a significant difference in DE between a combined MDF/TOA network and a TOA network when a 4^{th} sensor is required to get a location. In the 6 sensor model network the absolute DE reduces from 96,5% to 76,6% and in Table 7.2 the relative DE_f reduces from 99% (LLS_8AT) to 69% (LLS_8T/4) for the 8 sensor network in Austria.

A comparison of the normalized peak current distributions for the LLS_8AT and the LLS_8T/4 configuration is shown in Fig. 7.3. It is clear that the LLS_8AT configuration detects more flashes with small peak currents, when compared to the LLS_8T/4 configuration. This is in agreement with section 4 when we consider that in the LLS_8AT configuration only 2 reporting sensors are required and for the LLS_8T/4 configuration a minimum of 4 sensors is required to get a stroke location. A higher peak current is required in order to exceed the detection threshold at 4 or more sensors (ALDIS_8T/4), therefore the resulting peak current distribution for this configuration is biased towards higher peak currents.

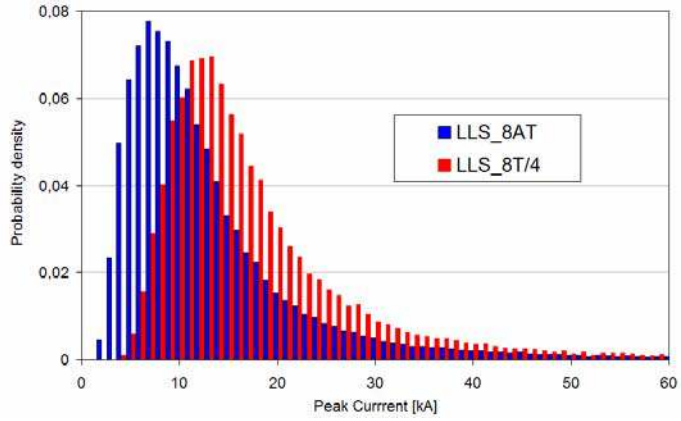

Fig. 7.3 Comparison of the resulting peak current distributions in region (A) for the LLS_8AT and LLS_8T/4 network settings

7.4 Spatial network comparison

In the following figures we show the spatial distribution of relative flash DE_f when EUCLID data are used as a reference for a somewhat larger area compared to region (A) analyzed in chapter 7.3. This spatial comparison clearly shows the relative DE decreases outside the network.

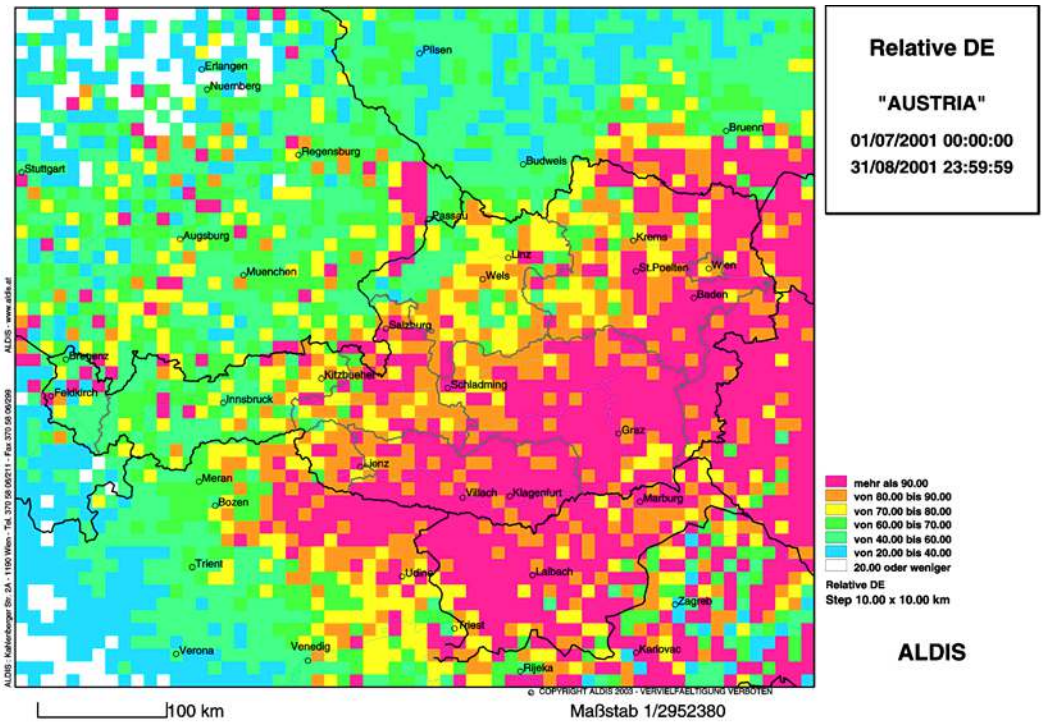

Fig. 7.4 DE of the LLS_8AT network relative to the EUCLID network

In the southeast region of the area shown in Fig. 7.4 the DE of the EUCLID network is mainly determined by the ALDIS network (equal to LLS_8AT) itself because few other EUCLID sensors are near this region. Therefore the relative DE in this region is

high (>90%) and there is a steadily and significant decrease in DE towards the west, north-west and south-west. The performance of the LLS_8AT system in the western part of Austria is lower compared to the eastern part of Austria due to the network configuration, which is constrained by the shape of Austria. This clearly illustrates that integration of neighboring sensors was most effective and beneficial to the ALDIS network in the western part of the country.

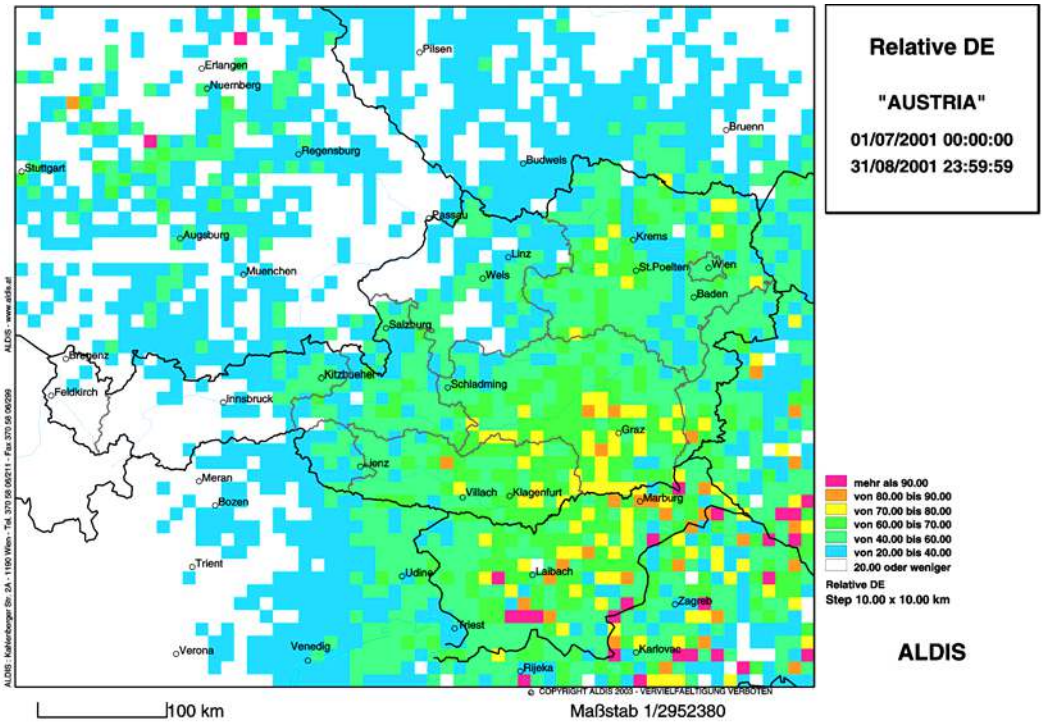

Fig. 7.5 Relative DE of the LLS_8T/3 network

When only time information of the eight Austrian sensors is used (LLS_8T/3), the DE relative to the EUCLID network decreases further. Fig. 7.5 shows that the DE of this TOA network in the western part of Austria is less than 20%.

7.5 Single Sensor DE

For a given peak current (given by I) the function of sensor DE(I) versus distance D is determined by three parameters

1) the maximum sensor detection efficiency, DE_{max}
2) the saturation limit (D_1) and
3) the threshold limit (D_2).

Fig. 7.6 shows an idealized sensor DE(I) function (dashed line), where the distances D_1 and D_2 are related to the saturation and the threshold limits, respectively. Both values depend on the given lightning peak current I, the angle of incidence and the signal attenuation. This is an idealized sensor DE(I) function because in reality a sensor will not detect 100% of all of the flashes with peak fields within the limits of

saturation and threshold. Local noise, sensor dead time, waveform discrimination, etc. cause a certain limitation of the $DE(I)_{max}$ to less than 100%, even in the range of normal system operation. Whenever a sensor processes a stroke it has a certain dead time (typically 1 – 3 ms, depending on sensor type) and the sensor is unable to process a further stroke during that short time period. We note that the most modern sensors do not have any significant dead time.

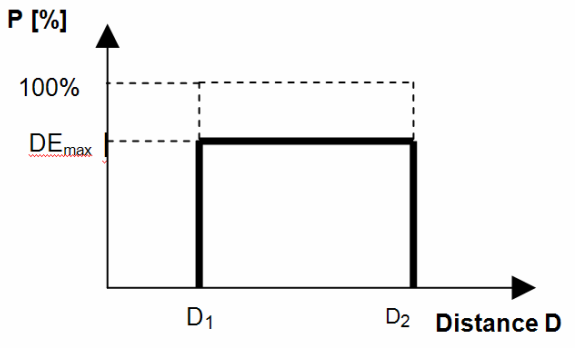

Fig. 7.6 Idealized sensor DE for a given peak current I (D_1 .. Saturation limit, D_2 … Threshold limit)

When a stroke of the given peak current occurs within a distance $D<D_1$, the sensor will be saturated. If the striking point is located at a distance $D>D_2$, the signal at the sensor site is below the threshold limit and therefore it will not “trigger” the sensor.

A field waveform that is just slightly above the trigger level will most likely not satisfy any applied waveform criteria and therefore it is unlikely to be reported by the sensor. It is typically assumed that a lightning field has to be at least twice as high as the sensor threshold setting to be further processed.

To achieve a more realistic model of the sensor DE we have to modify the instantaneous change of the DE at the saturation and the threshold distance, as it is unlikely that a sensor will not detect flashes if they are slightly closer than the calculated saturation distance D_1 or slightly farther than the threshold distance D_2. A more continuous increase and decrease of DE starting at the saturation limit and the threshold limit, respectively, is assumed (Fig.7.7).

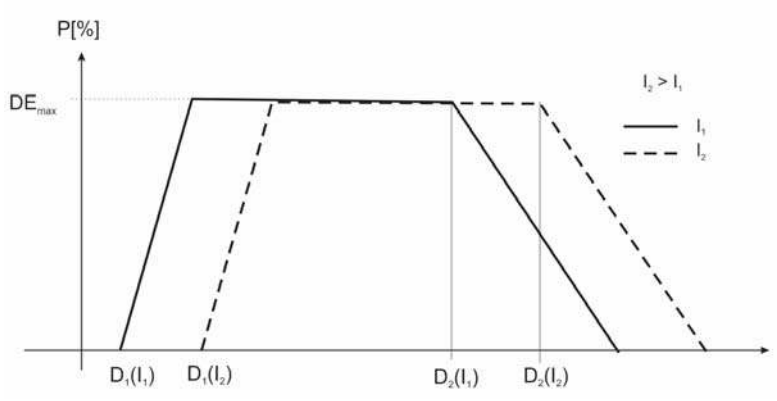

Fig. 7.7 Schematic sensor detection efficiency for two different peak currents I_1 and I_2

Typically the distance range for the transition from non-detection to DE_{max} at the saturation limit is smaller than the range for the threshold limit. Analysis of real sensor data reveals that a more continuous decrease of DE is observed at the threshold limit. Fig.7.7 shows the schematic DE function of a sensor for two different peak currents I_1 and I_2. Obviously I_1 is smaller than I_2 because I_2 saturates the DF up to a larger distance $D_1(I_2)$. On the other hand peak current I_2 triggers the sensor up to a larger distance $D_2(I_2)$.

When we analyze sensor DE functions based on real data some differences in the performance of different sensor types become obvious. In Fig. 7.8a-c, we show relative sensor DE versus distance for a normal performing IMPACT 141T, IMPACT ESP and an LPATS III sensor for peak currents of about 20 kA (exactly in the range from 19 kA to 21 kA).

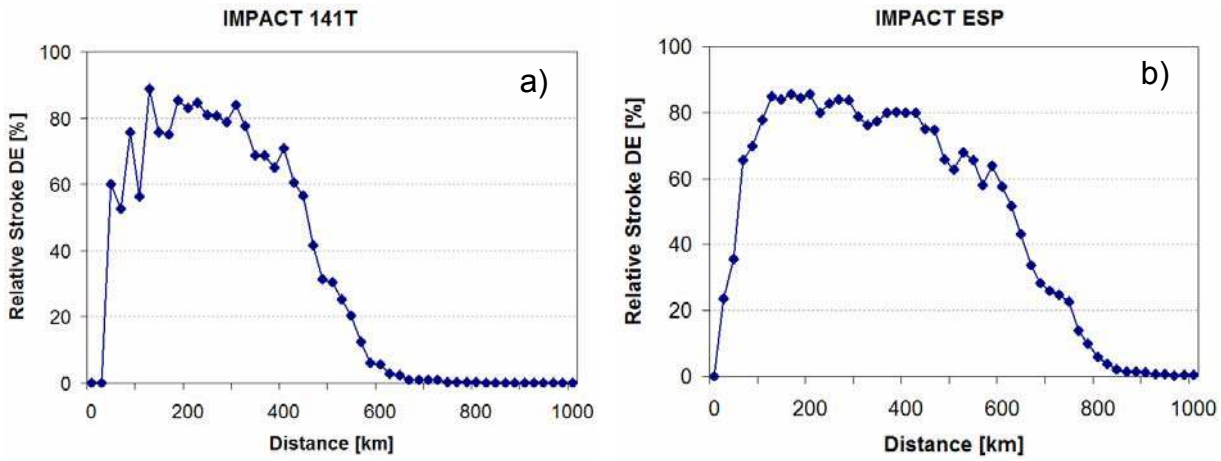

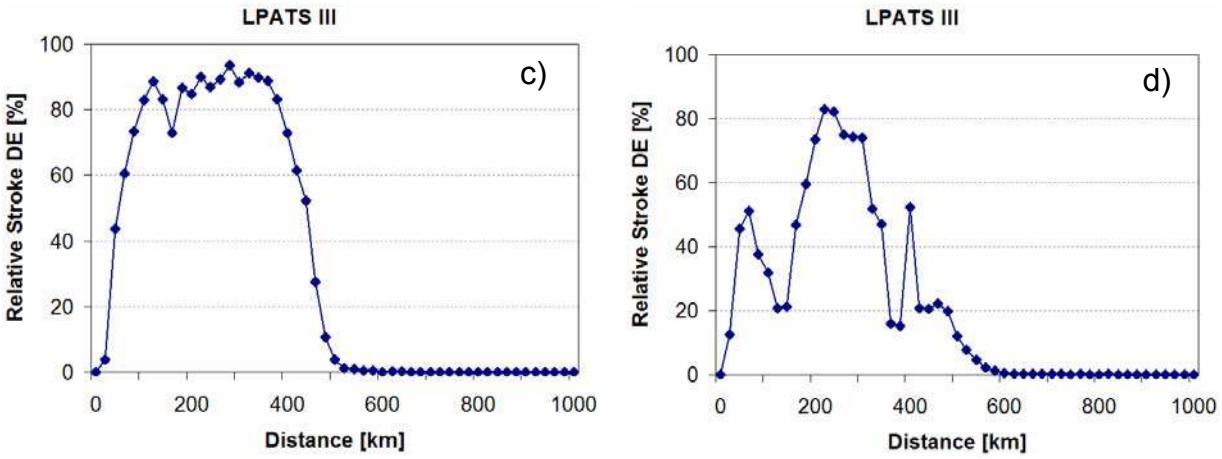

Fig. 7.8 Relative sensor DE versus distance for peak currents of 20kA ±1kA for different sensor types and gain derived from real data. a), b) and c) are examples of regular performing sensors - d) shows a poor performing sensor

The relative DE function also depends on the GAIN of the sensor. IMPACT ESP is a so called Gain-6 sensor. For the LPATS III sensor the decrease of DE at the threshold limit is more rapid than for an IMPACT sensor. Fig. 7.8d shows an example of relative sensor DE of a poor performing LPATS III sensor. Such a result in the performance analysis indicates sensor problems either caused by temporary communication outages, sensor hardware failures, or local noise at the sensor site.

8 Ground Truth References

A variety of ground truth approaches have been employed to prove and quantify the performance of a LLS. In this section only CG lightning is considered. First studies were done by Mach et al. (1986) and Mac Gorman and Rust (1988). For a 4 DF magnetic direction finder system a flash detection efficiency of about 70% was determined obtaining independent data on lightning strikes with a TV camera on a mobile laboratory. However, over the last 15 years the technologies of the sensors and the capabilities of the applied location algorithm have evolved considerably, so results of these early studies are no longer representative of today's LLS.

The most fundamental performance parameters of a LLS are:

- Detection Efficiency (DE): As mentioned in section 4 we have to distinguish between flash detection efficiency (DE_f) and stroke detection efficiency (DE_s), where DE_f is typically higher than the DE_s, because a flash is successfully located whenever at least one of the strokes within a multi-stroke flash is located.
- Location Accuracy (LA): LLS-reported locations are defined by the centroid of the LLS error ellipse. For a given stroke, the distance between the LLS location and the ground truth striking point is defined to be the stroke location error.
- Peak Current Estimate (PCE): LLS infer peak currents from measured peak fields. Simple models to account for field attenuation are partially integrated into the lightning location software. It is important to distinguish between the ability of a LLS to infer the correct peak current for a given stroke and the ability to provide correct values for peak current distributions. The former are typically use for case studies (e.g. investigation of power line flashover caused by a given lightning stroke) whereas peak current distributions are used in lightning protection standards and many lightning related statistical analyses.

An appropriate set of ground truth reference data is fundamental for any performance evaluation of LLS. Ideally such a data set includes precise knowledge of time, type of discharge (CG versus CC), location (latitude/longitude) and peak current of all the strokes in all CG flashes within a given area and time period. Unfortunately today no such complete data set is practically available, because any method of lightning observation independent from LLS has its own limitations:

(1) Measurements of natural lightning to elevated objects (e.g. Berger et al., 1975, Diendorfer et al., 2002a, Lafcovici et al., 2006) are strictly valid only for the given location. The majority of the discharges to elevated objects is initiated by upward propagating leaders similar to triggered lightning and thus different from typical discharges to ground, which are initiated by a downward propagating stepped leaders.

(2) Triggered lightning is limited to a single location and the artificially initiated discharges do not show a first stroke preceded by a downward propagating stepped leader (e.g. Rakov and Uman 2003). Only subsequent strokes occurring after cessation of the initial continuing current (ICC) phase are assumed to be similar to the dart-leader-return-stroke sequences in natural lightning.

(3) Video surveys have been carried out over limited areas (e.g. Idone et al., 1998; Parker and Krider 2003; Berger and Pedeboy 2003; Kehoe and Krider 2004; Biagi et al., 2007). The main restriction in these studies is the limited time resolution in the range of 5-30 ms defined by the frame rate of the camera, making it difficult to resolve same-channel strokes with an inter-stroke interval shorter than the frame rate. Rakov and Uman (1990) used simultaneous E-field and video records to get around this issue. The time interval between subsequent strokes in a flash is usually several tens of milliseconds although it can be as small as one millisecond or less.

In this section we will focus on some of the most recent available data based on ground truth studies because only those results are applicable to the currently used technology of sensors and associated location algorithms. Reference data are either obtained from direct current measurements on instrumented towers as the Gaisberg Tower in Salzburg (Austria) and CN Tower in Toronto (Canada), or from triggered lightning or video observations. In this document we do not consider cross-comparisons of networks covering a common area because typically these relative comparisons face a number of difficulties and deficiencies in the final interpretation of the results. We first present results for the main LLS system performance parameters (DE, LA and PCE) derived from each one of the ground truth case studies. The results are unique to each case study because they are affected by both the LLS network covering the area where the ground truth data have been collected, and by the ground truth method. In the chapter summery we will then discuss each performance criterion versus the different ground truth data sets.

8.1 Lightning to the Gaisberg Tower

8.1.1 Lightning Data

Since 1998 direct lightning strikes to a radio tower have been measured at Gaisberg, a mountain next to the City of Salzburg in Austria (Diendorfer et al., 2000b). This project was initially started with the aim to evaluate the performance of the Austrian lightning location system ALDIS. This 100 m tower is located on the top of Gaisberg (see Fig. 7.2). The tower coordinates are 47.805 N and 13.112 E, and the mountain top is 1287 m above sea level. Lightning flashes to the tower occur in summer as well as during winter. The overall current waveforms are measured at the base of the air terminal installed on the top of the tower with a current-viewing shunt resistor of 0.25 mΩ having a bandwidth of 0 Hz to 3.2 MHz. A fiber optic link is used for transmission of the shunt output signal to a digital recorder installed in the building next to the tower. Two separate fiber optic channels of different sensitivity are used: 0-2 kA to measure low amplitude currents like the initial continuing current (ICC) and 2-40 kA to measure return stroke peak currents. The signals are recorded by an 8 bit digitizing board (upper frequency response 15 MHz; memory 16 MB) installed in a

personal computer. The trigger threshold of the recording system is set to 200 A with a pre trigger recording time of 15 ms. The lower measurement limit given by the 8 bit digitizer resolution is about 20 A. A digital filter with an upper frequency of 250 kHz and offset correction is applied to the current records before the lightning parameters (peak current, charge transfer, action integral) are determined.

As typical for elevated objects, more than 90% of the flashes to the tower are upward initiated. The upward leader bridges the gap between the grounded object and cloud and establishes an initial continuous current (ICC) with a duration of some hundreds of milliseconds and an amplitude of some tens to some thousands of amperes. In more than half of the cases current pulses are superimposed on the slowly varying continuous current and these pulses are often referred to as Initial Continuous Current pulses or α-pulses. After the cessations of the ICC, one or more downward leader/upward return stroke sequences may occur – the associated current pulses are called β-pulses. Typically α-pulses are relatively small, less than 10 kA, while β-pulses have peaks mostly in the range above 5 kA (Miki et al., 2005).

For the following analysis we used recorded data from 2000 to 2005 with a total of 219 negative upward flashes containing 985 pulses (509 α–pulses and 476 β-pulses) with amplitudes greater than 2 kA. Fig. 8.1 shows a typical overall current waveform recorded on the Gaisberg tower with the ICC superimposed by α–pulses and followed by β-pulses. About 100 upward flashes recorded during the same period with no pulses or pulses < 2 kA are not considered in the following analysis. This type of lightning is not applicable to CG lightning.

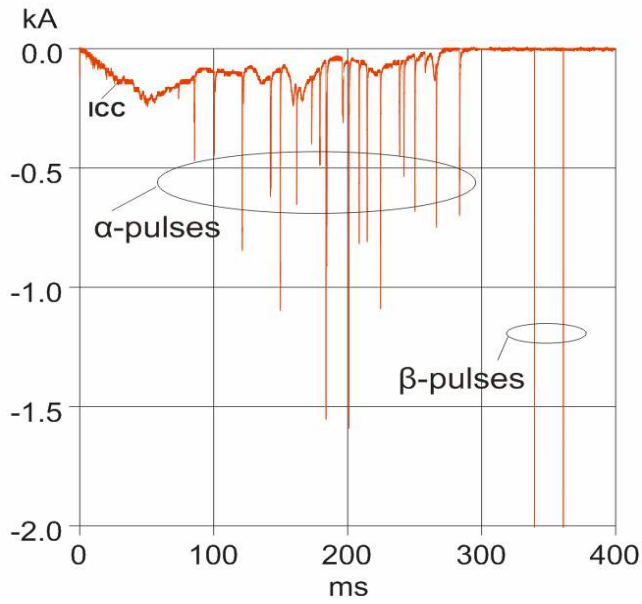

Fig. 8.1 ICC and α and β-pulses of a typical upward initiated flash to the Gaisberg tower

In general β-pulses are assumed to be the best representation of subsequent strokes in natural downward lightning. Hence, the results of our analysis are thought to be applicable to subsequent strokes occurring in a pre-existing channel in natural light-

ning, but not necessarily to negative first strokes, new-channel subsequent strokes, or positive strokes. A typical current waveform of a β-pulse measured at Gaisberg tower is shown in Fig. 8.2

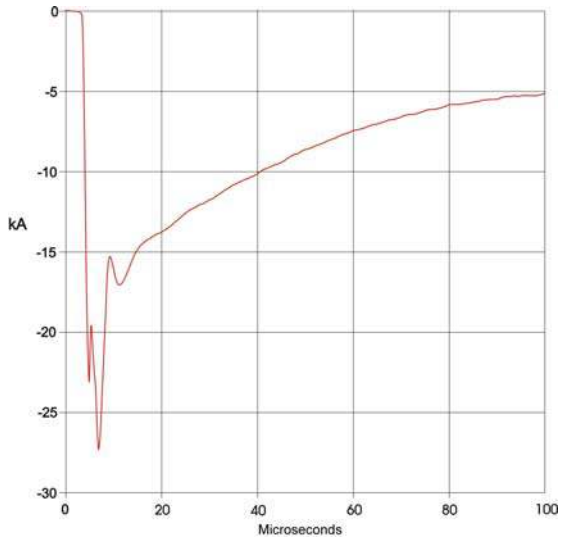

Fig. 8.2 Typical current wave shape of a β-pulse

Peak current distributions of the two distinct pulse categories are shown in Fig. 8.3. For the distribution of β-pulses a median of 9.6 kA (N = 476, σ_{log10} = 0.23) was determined. The smallest β-pulse peak current measured was 2.1 kA and the maximum was 68 kA (NOTE: the 68 kA pulse was above the 40 kA measuring limit of Gaisberg instrumentation and 68 kA is the peak current provided by the LLS for that event).

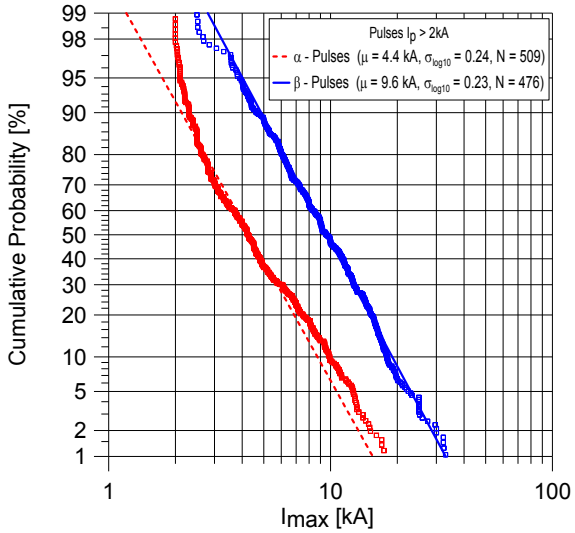

Fig. 8.3 Peak current distribution of α and β-pulses measured at the Gaisberg tower from 2000 – 2005 (straight lines represent best fit of log-normal distributions)

8.1.2 LLS covering the Gaisberg area

Gaisberg tower is located at the border area between Austria and Germany and is well covered by sensors contributing to the EUCLID network (see section 7.1). Sensor locations, sensor type and distance to the tower of the 5 nearest sensors are listed in Table 8.1.

Table 8.1: Type and distance of the five EUCLID sensors next to the Gaisberg tower (see Fig. 7.2)

Sensor Location	Sensor Type	Sensor distance to Gaisberg Tower [km]
Eggelsberg (A)	IMPACT 141T	31
Niederoeblarn (A)	IMPACT 141T	77
Schwaz/T (A)	IMPACT ES	116
Muenchen (D)	LPATS III	118
Noetsch (A)	IMPACT 141T	142

Model calculations estimate for the Salzburg area a DE_f of greater 90% and a location accuracy with a semi-major axis value of the 50%-error ellipse of less than 500 m.

8.1.3 Detection Efficiency

8.1.3.1 Flash Detection Efficiency (DE_f)

In Table 8.2 we have summarized the Gaisberg flash data for the period 2000–2005. In this document we consider only negative flashes to the tower having at least one current pulse with a peak greater then - 2 kA. Positive flashes, bipolar flashes and tower discharges exhibiting solely initial current phase (ICC with possible pulses below ±2 kA) are outside the scope of this document. We define flash peak current I_{FL} as the largest amplitude of all pulses within the flash. Detection of at least one stroke of a multiple-stroke flash was required to consider the flash to be detected. Detection efficiency values were computed from this information as ratios of the LLS-detected events to all directly measured lightning events.

N_{tot} in Table 8.2 refers to the total number of flashes independent of the type of pulses (α- or β-pulse). N_β refers to flashes only where the ICC phase of the upward discharge was followed by at least one β-pulse. The overall flash detection efficiency $(DE_f)_{tot}$ is 89% (154 out of 174) for all flashes with I_{FL} > 2 kA and increases to 97% for I_{FL} > 5 kA (139 out of 144). EUCLID detected 108 out of 110 [$(DE_f)_\beta$=98%] of the flashes with at least one β-pulse. We determined a median value of 15.6 kA (σ_{log10} = 0.22 kA, N=110) for the peak current distribution of this subset of flashes to the tower. We have assigned the flash peak current with peak current of the largest stroke in the flash because no conventional first stroke exists in upward lightning.

We note that two flashes occurred during a period of malfunction of the GPS synchronization for the tower instrumentation, but they are excluded from the dataset. They were probably located by the LLS, but could not be time correlated.

Table 8.2: Gaisberg flash data (2000-2005)

I_{FL} [kA]	N_{tot} Gaisberg	N_{tot} LLS	$(DE_f)_{tot}$	N_β Gaisberg	N_β LLS	$(DE_f)_\beta$
> 2	174	154	89%	110	108	98%
> 3	165	153	93%	110	108	98%
> 4	158	149	94%	110	108	98%
> 5	144	139	97%	109	107	98%
> 6	139	135	97%	105	103	98%
> 7	130	129	99%	102	101	99%
> 8	124	123	99%	99	98	99%
> 9	115	114	99%	95	94	99%
> 10	104	104	100%	86	86	100%

8.1.3.2 Stroke Detection Efficiency (DE_s)

We have also analyzed DE_s as a function of stroke type (α- or β-pulses) and peak current range (see Table 8.3).

In upward lightning initiated on high towers some of the α-pulses have waveforms similar to the waveform characteristic of return stroke pulses. Their risetimes are in the range of a few μs and the peaks are larger than 2 kA. In triggered lightning the α-pulses (ICC pulses) have longer risetimes and their waveshapes are more similar to M-components (Miki et al., 2005).

Table 8.3: DE_s of strokes of different amplitude ranges (2000 – 2005)

	GAISBERG			Lightning Location System (LLS)				
I [kA]	N	N_α	N_β	N_α	N_β	Stroke $(DE_s)_\alpha$ [%]	Stroke $(DE_s)_\beta$[%]	Stroke DE_s[%]
2 – 3	150	139	11	21	4	15,1	36,4	16,7
3 – 4	98	83	15	29	3	34,9	20,0	32,7
4 – 5	119	90	29	50	17	55,6	58,6	56,3
5 – 6	72	33	39	23	27	69,7	69,2	69,4
6 – 7	79	36	43	31	31	86,1	72,1	78,5
7 – 8	66	23	43	19	37	82,6	86,0	84,8
8 – 9	61	26	35	23	31	88,5	88,6	88,5
9 – 10	60	20	40	20	37	100,0	92,5	95,0
> 10	269	48	221	47	219	97,9	99,1	98,9
Total	**974**	**498**	**476**	**263**	**406**	**52,8**	**85,3**	**68,7**

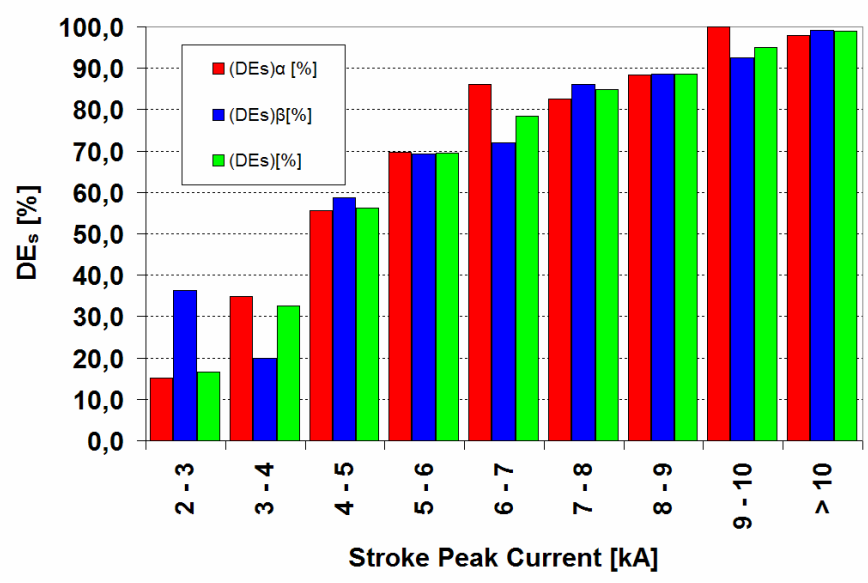

Fig. 8.4 Stroke Detection Efficiency DE_s as a function of peak current for strokes to the Gaisberg tower

The DE_s increased with increasing peak currents. About 70% of the strokes with peak currents in the range from 5-6 kA were detected, whereas the DE_s increases to 99% for all strokes with I_p > 10 kA. Model estimates of LLS DE are typically provided in terms of an overall DE_s for all strokes exceeding a given value (e.g. 5 kA). For comparison with results from such model calculations, Fig. 8.5 shows a plot of the observed DE_s as a function of minimum peak current.

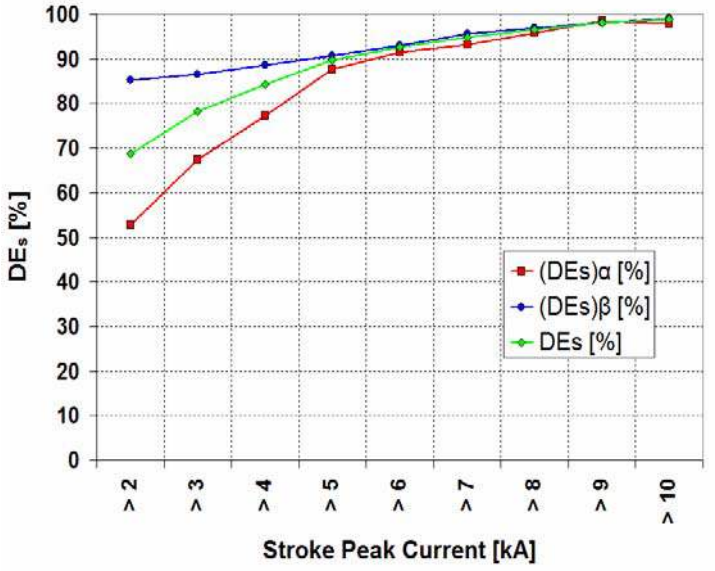

Fig. 8.5 Stroke DE_s as a function of minimum peak current

It is interesting to note in Fig. 8.5, that the DE_s for all α-pulses (I_S > 2 kA) is 53%, which significantly lower then for β-pulses (DE_s = 85%). Reasons for the lower DE_s

for α-pulses are (1) the overall higher fraction of small amplitude α-pulses (see Fig. 8.3) and (2) a considerable number of α-pulses are unlikely to be detected because of their slow rising current front. Considering all directly measured β-pulses with a peak current I_S > 2 kA (N = 476) the LLS detected 406 and therefore missed 70 ($(DE_s)_\beta$ = 85,3%); for I_S > 5 kA (N = 421) the LLS located 382 and missed 39 strokes ($(DE_s)_\beta$ = 91%).

As model based calculations of the DE_s of the EUCLID network for the Gaisberg region result in a very low probability to miss strokes with amplitudes > 10 kA, we have analyzed in detail the 2 missed strokes with I_S > 10 kA. In both cases the strokes were actually located by a number of sensors but sensor messages indicate that a separate stroke occurred within 1 – 2 milliseconds at a different location and hence the central processor location algorithm did not successfully group the correlated sensor messages to the two different strokes and failed to provide a correct location.

These results allow us to infer a lower bound on flash and stroke DE for the EUCLID LLS in this region. When we postulate that (1) subsequent strokes in typical downward CG lightning are well represented by the β-pulses in this analysis and (2) the peak current distribution of downward subsequent CG strokes is comparable to the analyzed sample, we can conclude that for strokes with minimum peak currents of 5 kA we can achieve a DE_s in the range of 90% and a DE_f of 95%. This result should be representative of performance for other LLS when the network is comparable to the EUCLID network (in this region), in terms of mean sensor baseline, sensor- and central processor configuration. Given that natural first strokes typically have higher peak currents than subsequent strokes in existing channels, overall flash DE for natural lightning could be even higher.

8.1.4 Location Accuracy

Tower strikes are a perfect reference to evaluate the location accuracy of the EUCLID network, because the tower location (47.805°N / 13.112°E) is known with high accuracy. Fig. 8.6 is a plot of the EUCLID stroke location error. The plot origin corresponds to the actual tower location.

There is no significant difference in the location accuracy of α- and β- pulses. A median location error of 368 m and a standard deviation of 768 m was determined for all the 674 strokes (see Fig. 8.7), with a minimum error of 23 m and a maximum of 9.4 km. Typically location errors exceeding 2 km were observed for strokes located by only two or three sensors or when the location was calculated based on erroneously grouped sensor messages resulting from discharges that occurred almost simultaneously at two separate locations.

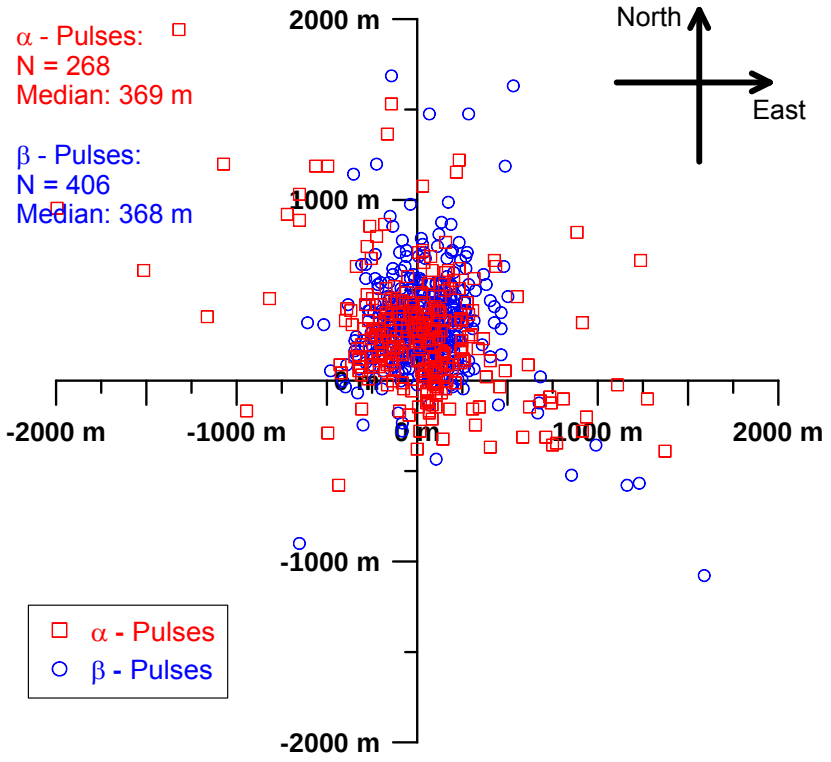

Fig. 8.6 Plot of EUCLID stroke locations for 674 strokes during 2000–2005 (Origin corresponds to the tower location).

The plot in Fig. 8.6 exhibits a bias of the LLS stroke locations by about 300 meters to the north. Reasons for that bias are assumed to be a combination of (1) timing errors as a result of pulse propagation over ground of finite conductivity and different sensor bandwidth and (2) a result of propagation elongation caused field propagation over high mountains (Schulz and Diendorfer, 2000).

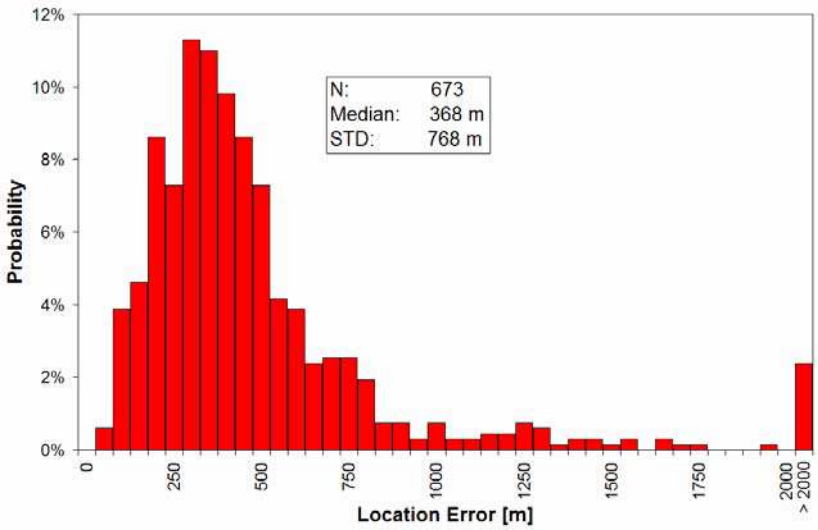

Fig. 8.7 Histogram of EUCLID absolute location error for 486 strokes to the tower during 2000-2005. All bins are 50 m except for the last bin, which includes all errors greater than 2000 m, with a maximum of 9.407 m

8.1.5 Peak Current Estimate

LLS infer the peak current from the range normalized signal strength (RNSS) which is calculated from the raw sensor signal strength SS, corrected for the propagation distance and attenuation due to the finite conductivity propagation path (see section 6.2).

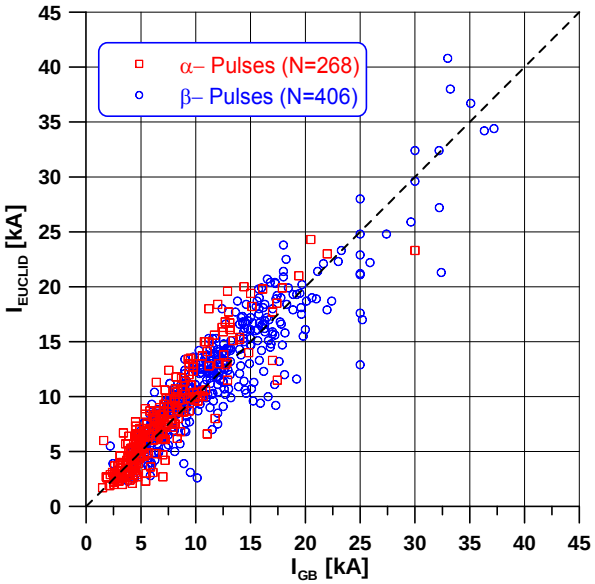

Fig. 8.8 EUCLID peak currents plotted versus peak currents measured at the Gaisberg tower during the season 2000–2005.

Note: During the period 2000 – 02/2005 (N = 612) in the EUCLID network no attenuation model was applied and a peak field to peak current conversion coefficient SNF=0.23 (see Eq.(6.1)) was used. Since 03/2005 (N=62) attenuation parameters are set to SNF=0.185, b=1.0 and L=1000 (see Eq.(6.2)) and test showed that there are negligible effects when these two data sets are analyzed together..

Fig. 8.8 shows the EUCLID estimated peak current versus peak current measured directly at the tower, plotted separately for α- and β-pulses recorded during 2000–2005. There is a strong positive linear correlation between the measured and EUCLID-estimated peak currents and no obvious differences in the quality of peak current estimates of α- and β-pulses are observed.

8.1.6 Peak Current Estimate for First Strokes

To our knowledge there are very few directly measured first stroke peak currents with corresponding amplitudes inferred by a lightning location system. Five flashes measured at the Gaisberg tower exhibited current records from the shunt measurement that started with a fast rising pulse without any ICC current prior to the first pulse. Thus we conclude that these pulses represent first-stroke attachments to the tower top. In 4 of the 5 events the ALDIS network located one or more strokes in the near vicinity of the tower (within several hundred meters) and within some hundred milliseconds before the return-stroke-type current was observed on the tower top. Those nearby located strokes resulted in time correlated very short current pulses in the shunt current record and triggered the current measurement. It is unclear whether these short pulses are (1) unsuccessful short upward leaders from the tower top triggered by the nearby downward leaders attaching to ground or the tower structure

below the top (side flashes) or (2) these short pulses are high frequency induced currents in the measuring system due to the electromagnetic field from the nearby discharge channel. From the current records we conclude that these 4 events (Flash # 252, #310, #323 and #324) are not first strokes of a typical CG discharge, but they are likely to be subsequent strokes with new attachments produced by a "natural" upward leader. Details of all 5 events are summarized in Table 8.4 and the current waveforms of the first measured stroke currents at the tower top are shown in Fig. 8.9.

Fig. 8.10 shows the peak currents of these first (new attachment to tower top) strokes in the 5 discharges recorded at the Gaisberg tower and the corresponding peak current inferred by the EUCLID lightning location network.

Comparison of Fig. 8.8 and Fig. 8.10 indicates similar relationship between peak field and peak current for these “new attachment” pulses as was found for α- and β-pulses (Fig. 8.8), although the number of events is too small for any final conclusion.

We note that LLS infer the peak current of positive and negative strokes by applying exactly the same field-to-current conversion. This conversion has not been validated for positive discharges yet by comparison with correlated ground truth data.

Table 8.4: Flashes to the Gaisberg tower, where the first stroke measured at the tower top was not preceded by any initial continuing current

Flash #	Date	Time	Number of preceding strokes located by ALDIS	Number of strokes measured on tower top	Tower Ip [kA]	ALDIS Ip [kA]
252	08.11.2001	19:27:28.8693762	15	1	-14.0	-12.1
310	06.07.2002	13:52:28.3657010	9	2	-12.0	-14.3
323	16.07.2002	23:53:12.4556237	1	1	-23.3	-23.3
324	16.07.2002	23:56:08.8381122	3	1	-27.4	-24.8
368	15.12.2003	06:32:22.4898087	0	9	-9.0	-12.4

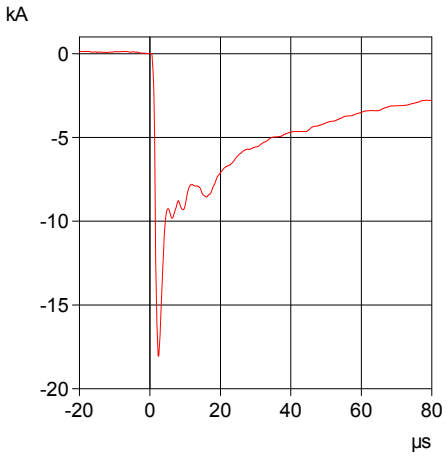

a) First measured stroke in Flash #252

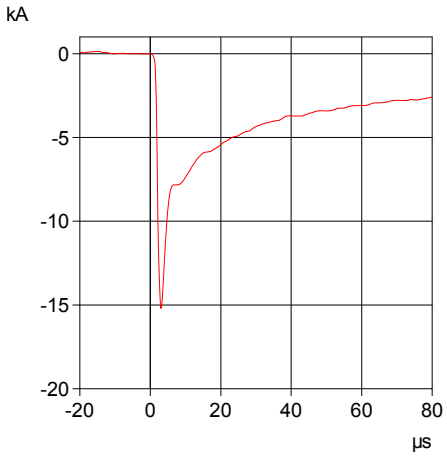

b) First measured stroke in Flash #310

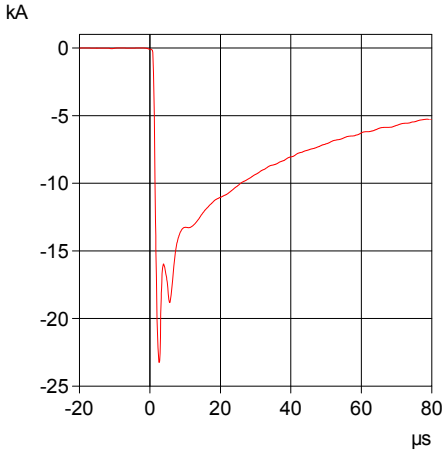

c) First measured stroke in Flash #323

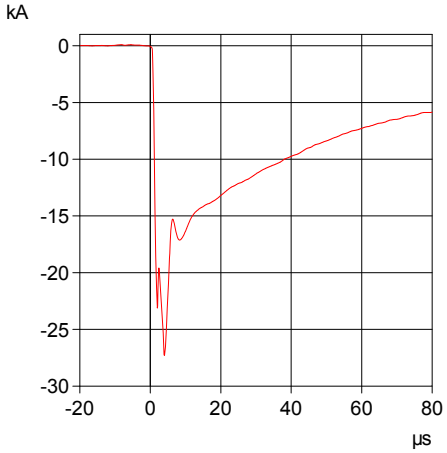

d) First measured stroke in Flash #324

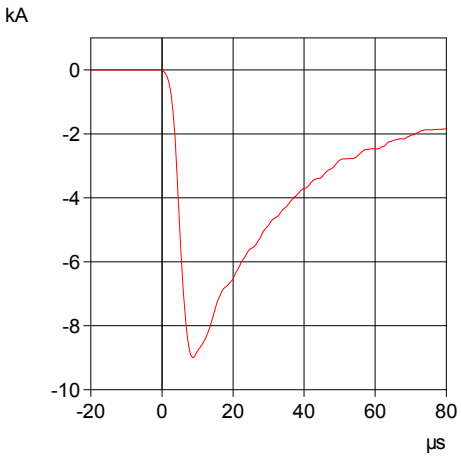

e) First measured stroke in Flash #368

Fig. 8.9 Current waveforms of first measured current pulses on tower top without any preceding ICC

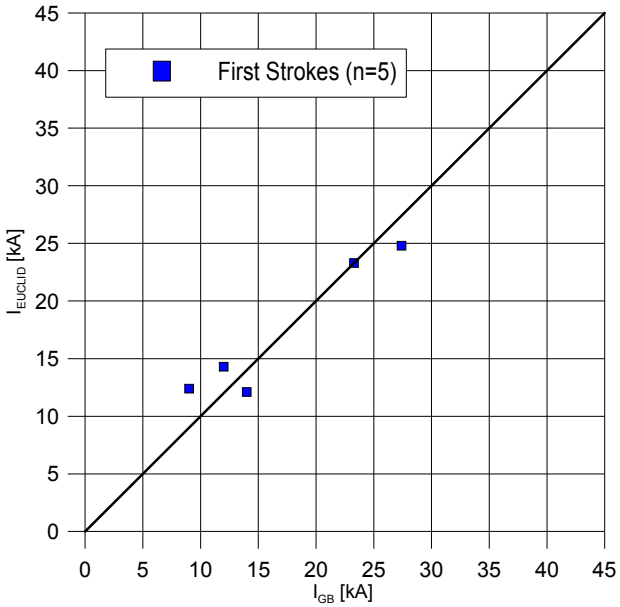

Fig. 8.10 Correlation of measured and detected peak currents of first strokes in downward flashes to the Gaisberg Tower

8.2 Lightning to the CN Tower

Lafcovici et al. (2006) describe a comprehensive evaluation of the North American Lightning Detection Network (NALDN) performance characteristics in the Toronto area based on the lightning data acquired at the 553 m CN Tower over the summer of 2005. NALDN is composed of the U.S. NLDN and the Canadian Lightning Detection Network (CLDN).

8.2.1 Lightning Data

The CN Tower with a height of 553 m receives several tens of strikes each year (Hussein et al. 1995, Hussein et al. 2005). As described by Hussein et al. (2004), the CN Tower is equipped with two current sensing Rogowski coils. The first is a 3 m, 40 MHz coil, which was installed at the CN Tower in 1990. It is placed at the 474 m above ground level and encircles one fifth of the tower's pentagon steel structure. A newer 6 m, 20 MHz coil encircling the whole steel structure at the 509 m level was installed in summer 2004. The current measurement system is equipped with a GPS clock allowing time stamping, accurate to 1 µs, for each recorded return stroke. In addition, electric and magnetic fields are measured at a 2 km distance and strikes to the tower are recorded by a high-speed digital camera and a VHS and digital video system with 33 ms time resolution. The current derivative waveforms provided by the Rogowski coil were numerically integrated to obtain the peak current of the strokes. GPS time stamping on all acquired data allows a direct match with the NALDN data.

8.2.2 NALDN Network

The sensor configuration of the NALDN in the region surrounding the CN Tower is shown in Fig. 8.11. Since the CN Tower is located on the border of the U.S. NLDN

and CLDN, two out of the three closest sensors to the tower are in fact U.S. NLDN sensors (see Table 8.5)

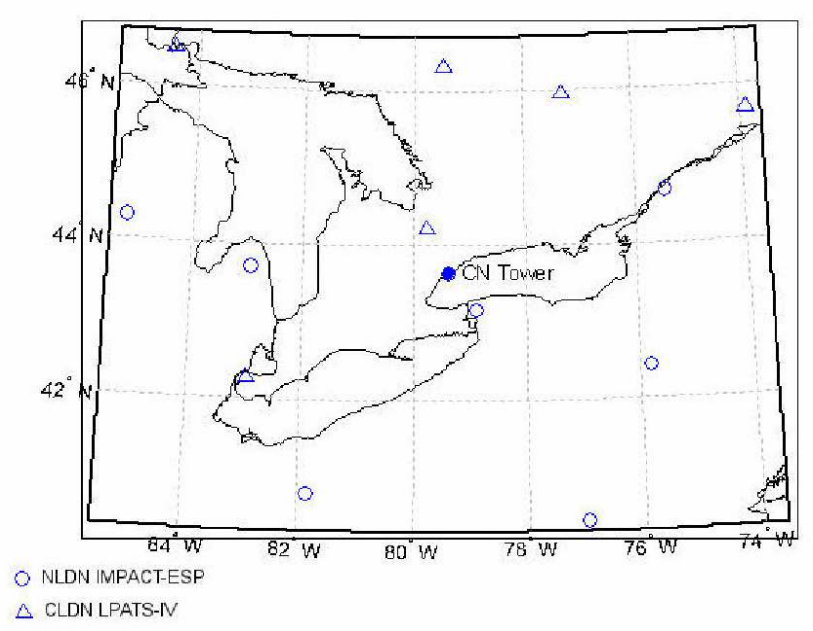

Fig. 8.11 Map showing the locations of U.S. NLDN IMPACT-ESP and CLDN LPATS-IV sensors in the region around the CN Tower

Table 8.5: Type and distance of the five NALDN sensors next to the CN Tower

Sensor Location	Sensor Type	Sensor distance to CN Tower [km]
Sanborn (U.S.)	IMPACT ESP	66.8
Egbert	LPATS IV	73.1
Ubly (U.S.)	IMPACT ESP	286.1
North Bay	LPATS IV	298.8
Petawawa	LPATS IV	304.9

8.2.3 Detection Efficiency

In 2005 the NALDN detected 7 out of 7 flashes recorded at the CN Tower, resulting in 100% flash DE. Furthermore, the NALDN detected 21 out of 38 return strokes resulting in a stroke DE of 55%. Fig. 8.12 shows a histogram of the NALDN stroke DE plotted as a function of the return stroke peak current obtained by the CN Tower measurement system. It is interesting to note that strokes to the CN tower with directly measured peak currents of 8 kA and above were always detected by the NALDN.

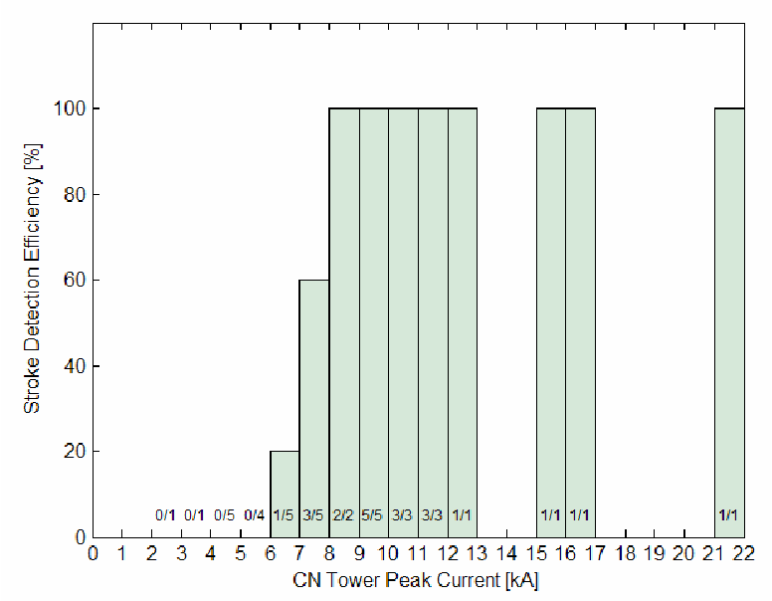

Fig. 8.12 NALDN stroke detection efficiency plotted as a function of the return stroke peak current measured at the CN Tower

8.2.4 Location Accuracy

Fig. 8.13 displays a histogram of the NALDN absolute location errors for 21 detected strokes from 7 flashes. The median location error is 358 m, while the mean error is 395 m. This is better than the projected 500 m median accuracy for the Toronto area.

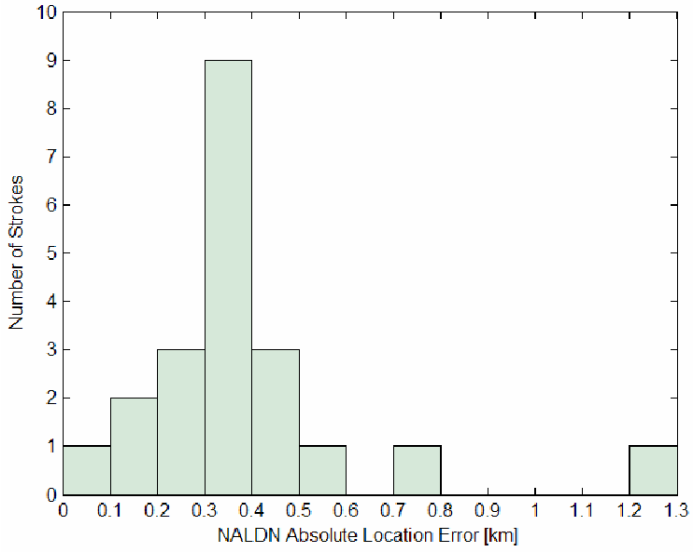

Fig. 8.13 Histogram of the NALDN absolute location errors of the detected return strokes

8.2.5 Peak Current Estimate

Fig. 8.14 shows the NALDN estimated peak current plotted versus the CN Tower peak current for the 21 detected strokes from 7 flashes. Lafkovici et al. (2006) determined the linear regression equation $I_{NALDN} = 2.61*I_{CNT} - 1.83$, indicating that the NALDN estimated peak currents were notably larger than the peak currents measured at the CN Tower. These large discrepancies between directly measured peak currents and LLS inferred peaks appear to be the result of an enhancement of the radiated electromagnetic fields that occurs when lightning strikes a very tall object, as theoretically shown by Bermudez et al. (2005). As noted earlier, peak currents were actually calculated by integrating the measured current derivative of approximately one-fifth of the total current. Performance of a careful revaluation of the current measuring system at the CN Tower, including coil calibration, is suggested by Lafkovici et al. (2006) before reaching a final conclusion concerning this issue.

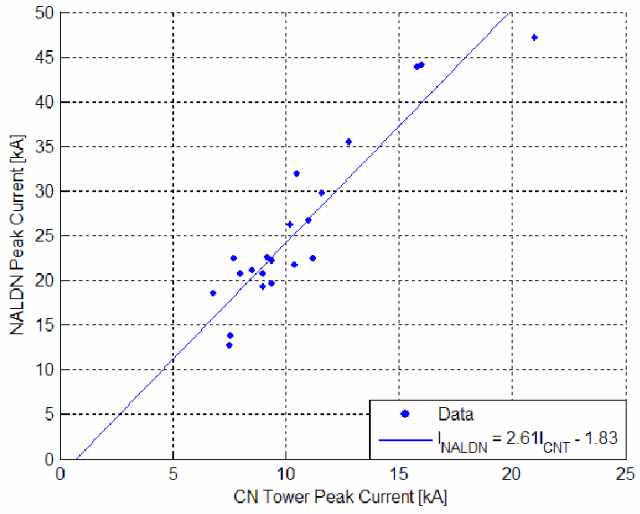

Fig. 8.14 NALDN estimated peak current versus the CN Tower peak current of each detected return stroke

8.3 Triggered Lightning

Similar to tower strikes, rocket-triggered lightning is also initiated by an upward leader. In this case, the leader propagates from the upper end of a vertical grounded wire extended below the charged cloud by a small rocket. Following the electrical "explosion" of the triggering wire and its replacement by an upward-leader plasma channel, the phenomenology of rocket-triggered lightning (e.g., Rakov, 1999) is apparently similar to that of the upward lightning initiated from tall structures discussed in chapter 8.1 and 8.2 except the triggered lightning channel terminates at the rocket launcher at a height typically not exceeding 10 m, while tower-initiated-lightning channel terminates on a tall metallic tower (e.g. 100 m above ground for the Gaisberg tower and 553 m for the CN Tower).

8.3.1 Measured lightning data

During the summers of 2001, 2002, and 2003, a total of 37 flashes containing a total of 159 strokes were triggered at the International Centre for Lightning Research and Testing (ICLRT) at Camp Blanding, Florida (Jerauld et al., 2005). A summary of the triggered flashes is presented in Table 8.7.

The measuring system and data recording equipment are described in detail in Jerauld et al. (2005). The total number of strokes for which peak currents were obtained (122) is less than the total number of strokes recorded (159) due to some limitations and malfunctions of the measuring system.

The distribution of peak currents for all triggered strokes in which current was recorded, obtained during 2001-2003 (122 strokes total), is given in Fig. 8.15 Fig. 8.14and has a median of 13,3 kA (σ_{log10} = 0,2). Unlike natural upward lightning discussed in section 8.1, no ICC pulses (α-pulses) were included in the triggered lighting study of Jerauld et al. (2005).

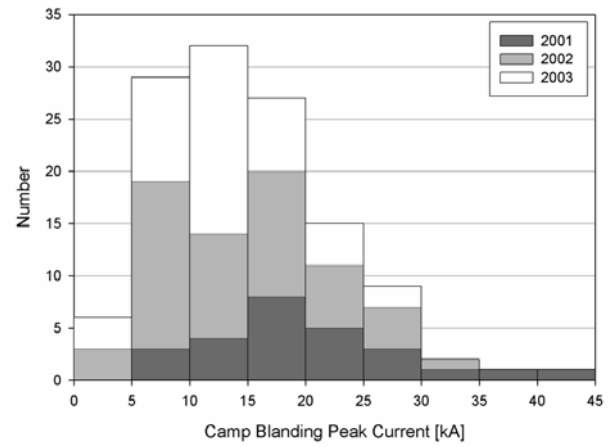

	2001	2002	2003	**2001-2003**
AM, kA	19.9	14.5	13.0	**15.1**
SD, kA	8.7	7.1	5.8	**7.4**
GM, kA	18.2	12.7	11.7	**13.3**
SD (log_{10}I)	0.2	0.2	0.2	**0.2**
Min, kA	6.0	3.6	2.9	**2.9**
max, kA	42.9	32.7	28.5	**42.9**
Sample Size	26	52	44	**122**

Fig. 8.15 Histogram of Camp Blanding triggered lightning return-stroke peak currents for 2001-2003. Shown next to the histogram are statistics for the peak current data for individual years, as well as for the complete 2001-2003 data. Statistics given are sample size, arithmetic mean (AM), standard deviation (SD), geometric mean (GM), standard deviation of the log10 of the parameter (SD[log_{10}(I)]), minimum value (min), and maximum value (max). Adapted from Jerauld et al. (2005).

8.3.2 Location network (U.S. NLDN)

Since 1989, the U.S. NLDN has provided lightning data covering the contiguous United States. During the evaluation period (2001-2003) a network-wide upgrade was underway, and was near completion at the end of 2003. In 2001, the U.S. NLDN employed a combination of MDF and TOA sensors to determine the lightning location (Cummins et al., 1998a). A total of 106 sensors were in the network in 2001. Six sensors have been added since then, and all sensors have been upgraded to the latest MDF/TOA technology. A map showing the locations of U.S. NLDN sensors in the

Florida region, as of early 2004, is given in Fig. 8.16 and Table 8.6 shows type of sensor and distance to the triggering site for the 5 nearest sensors.

Table 8.6: Type and distance of the five U.S. NLDN sensors next to Camp Blanding (adapted from Jerauld et al., 2005)

Sensor Location	Sensor Type (2003)	Sensor distance to Camp Blanding [km]
Ocala, FL	IMPACT ESP	89
Tampa, FL	LPATS IV	227
Wakulla, FL[1)]	IMPACT ESP	228
Savanna, GA	IMPACT ESP	255
Quincy, FL [1)]	LPATS IV	256

[1)] Note: Sensor Quincy was replaced by sensor Wakulla in 2003

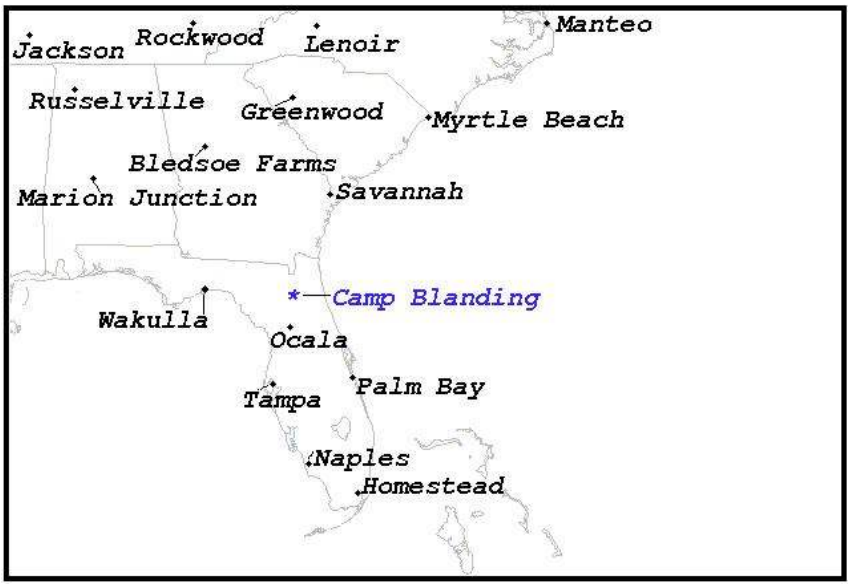

Fig. 8.16 Map showing the locations of U.S. NLDN sensors in and around the Florida region, as of late 2003. The approximate location of Camp Blanding is also shown

Cummins et al. (1998b) estimated the flash detection efficiency for the U.S. NLDN using the detection efficiency model described in their Appendix. For flashes having peak currents of 5 kA and larger, the estimated DE was on the order of 80 to 90%, depending on the region. The median stroke location accuracy for this network has been theoretically estimated to be about 500 m over much of the United States, based on the calculated 50% error ellipses, assuming that the angle and time errors are Gaussian (Cummins et al., 1998b).

Unlike the EUCLID network, the U.S. NLDN employs an attenuation model to account for propagation effects. For the period 2001-2003, this model employed a power-law attenuation with distance (see Eq.(6.2), with the exponent b = 1.13 derived empirically by Orville (1991). The space constant (L) was set to 10^5 km, essentially removing the exponential function from the model. The raw signals strengths measured by individual sensors are normalized to 100 km using the aforementioned pow-

power-law relationship. These range-normalized signal strength (RNSS) values, from all reporting stations within 625 km (to avoid polarity reversals due to ionospheric reflection), are averaged and converted to a peak current estimate (I_p) using the empirical linear relationship (obtained using the triggered-lightning data of Idone et al., 1993)

$$I_p = 0.185 * RNSS \quad \textbf{(8.1)}$$

As stated previously, the years 2001-2003 comprised an upgrade period for the U.S. NLDN – see Jerauld et al. (2005) for further details.

8.3.3 Detection Efficiency

A flash detection efficiency of 82% (9 out of 11) in 2001, 86% (12 out of 14) in 2002 and 83% (10 out of 12) in 2003 with an overall flash detection efficiency of 84% (31 out of 37) for the 3-year period is reported for triggered lightning by Jerauld et al. (2005) (see Table 8.7). These values are consistent with the expected flash detection efficiency of 80% to 90% estimated by Cummins et al. (1998a). Since these triggered flashes do not include natural first strokes that typically have higher peak currents, the measured flash DE is likely an underestimate of the flash DE for natural CG lightning (Cummins et al., 2006).

Table 8.7: Summary of flashes and strokes recorded at Camp Blanding during the summers of 2001-2003, along with the corresponding U.S. NLDN detection efficiencies. Adapted from Jerauld et al. (2005).

Year	Number of Flashes Triggered	Number of U.S. NLDN Detected Flashes	U.S. NLDN Flash Detection Efficiency	Number of Strokes	Number of U.S. NLDN Detected Strokes	U.S. NLDN Stroke Detection Efficiency
2001	11	9	82%	33	17	52%
2002	14	12	86%	77	44	57%
2003	12	10	83%	49	34	69%
2001- 2003	**37**	**31**	**84%**	**159**	**95**	**60%**

The observed stroke detection efficiency was 52% (17 out of 33) in 2001, 57% (44 out of 77) in 2002 and 69% (34 out of 49) in 2003, with an overall stroke detection efficiency of 60% (95 out of 159) for the 3-year period. Fig. 8.17 shows the U.S. NLDN stroke detection efficiency as a function of peak current for a total of 122 strokes measured at Camp Blanding.

For 2001, no strokes with peak currents below 5 kA were triggered, but 7 strokes were triggered having peak currents from 5 to 15 kA, none of which was detected by the U.S. NLDN. Above 15 kA, stroke detection efficiency increased with increasing peak current and reached 100% between 25 and 30 kA (notably near the median value for natural negative first strokes reported by Berger et al. (1975) although trig-

gered-lightning strokes are similar to subsequent strokes in natural lightning and their median peak current is between 10 and 15 kA).

The combined data for 2001-2003 suggest that the detection efficiency is probably near 100% for strokes having peak currents in excess of 30 kA. The stroke detection efficiency decreases to 60-70% as current decreases from 30 to 10 kA, and drops to less than 30% for currents in the 5 to 10 kA range. Jerauld et al. noted that there was evidence of improved stroke DE in 2003 (near the completion of the NLDN upgrade) for peak currents in the 5-15 kA range. No strokes with measured peak currents below 5 kA were detected by the U.S. NLDN.

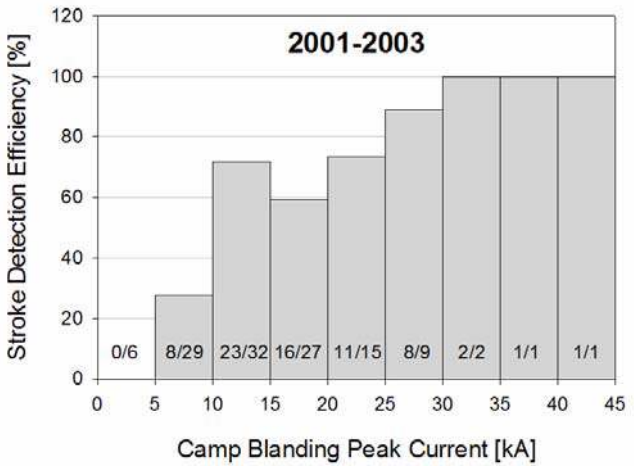

Fig. 8.17 U.S. NLDN stroke detection efficiency as a function of peak current measured at Camp Blanding. For each peak current range (bin size of 5 kA), the ratio given inside the column indicates the number of strokes detected by the U.S. NLDN (numerator) and the number of strokes recorded at Camp Blanding (denominator), for that peak current range. The total number of strokes whose currents were measured at Camp Blanding is 122, of which 70 were detected by the U.S. NLDN. Adapted from Jerauld et al. (2005).

8.3.4 Location Accuracy

U.S. NLDN stroke location errors for 95 strokes in 31 flashes triggered during the seasons of 2001-2003 at Camp Blanding have also been analyzed by Jerauld et al. (2005). For the 2001 and 2003 data, the location errors are distributed more or less uniformly about the strike location with a median stroke location error of 600 meters. Part of the 2002 data contains a large bias towards the north as a result of temporary sensor outages in the vicinity of the triggering site. The north component of these large location errors ranges from about 2 km to about 11 km.

Fig. 8.18 is a histogram of the U.S. NLDN absolute stroke location errors for the 95 strokes. The overall distribution has a long “tail” due to the relatively large location errors observed in 2002. When Jerauld et al. (2005) plotted the U.S. NLDN absolute location errors versus the peak current, measured at Camp Blanding, for 70 strokes in 22 flashes triggered during 2001-2003, the majority of large (>2 km) location errors occur in the 5-10 kA range during 2002 (no strokes were detected with measured peak currents below 5 kA).

For 2003, the location accuracy for smaller peak currents appears to have improved as a result of upgrading the U.S. NLDN, although there is not as much data in that range as in 2002.

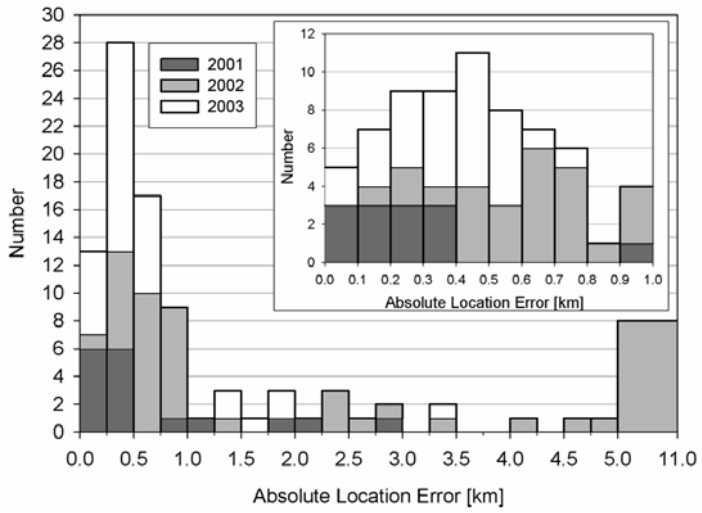

	2001	2002	2003	**2001-2003**
AM, km	0.66	2.42	0.64	**1.47**
SD, km	0.85	2.75	0.67	**2.13**
GM, km	0.31	1.31	0.44	**0.68**
MD, km	0.27	0.83	0.45	**0.60**
min, km	0.05	0.17	0.04	**0.04**
max, km	2.88	11.00	3.33	**11.00**
Sample Size	17	44	34	**95**

Fig. 8.18 Histogram of the U.S. NLDN absolute location errors for 95 strokes in 31 flashes triggered during 2001-2003 at Camp Blanding. All bins are 0.25 km except for the last bin, which includes all errors greater than 5 km, with a maximum of 11 km. The inset shows the histogram with bins of 0.1 km for errors less 1 km. Statistics given are sample size, arithmetic mean (AM), standard deviation (SD), geometric mean (GM), median (MD), minimum value (min), and maximum value (max). Adapted from Jerauld et al. (2005).

8.3.5 Peak Current Estimate

Fig. 8.19 shows the U.S. NLDN-estimated peak current ($I_{U.S.\ NLDN}$) plotted versus peak current measured directly at Camp Blanding (I_{CB}), for 70 strokes in 22 flashes triggered during the period 2001-2003. Jerauld et al. (2005) found that the U.S. NLDN underestimated the measured peak currents by about 18 percent.

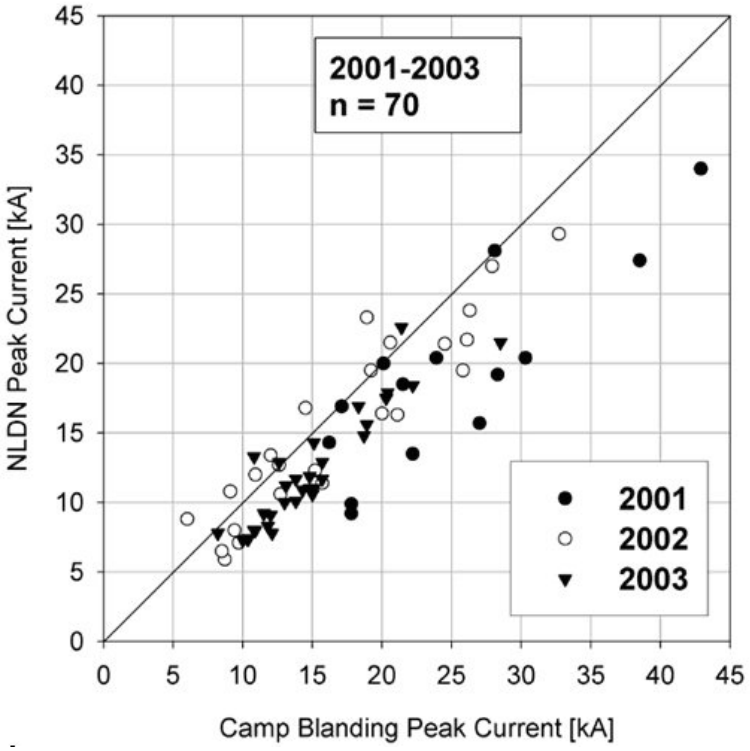

Fig. 8.19 U.S. NLDN-reported peak current plotted versus peak current measured at Camp Blanding, for 70 strokes in 22 flashes triggered during 2001-2003. The slanted line (slope = 1) is the locus of points for which the U.S. NLDN peak current is equal to the Camp Blanding peak current. Adapted from Jerauld et al. (2005).

Cummins at al. (2006) presented a re-calculation of the estimated peak currents of 55 time-matched rocket-triggered strokes from 2002-2003 data when applying a revised propagation model (b=1; L=1000 km in Eq.(6.2)). Using the new propagation model resulted in a regression line with a slope close to 1 for the measured peak current versus U.S. NLDN inferred peak current.

8.4 Optical measurements

To evaluate the U.S. NLDN network performance prior to and after an initial IMPACT sensor upgrade (U.S. NLDN was upgraded to IMPACT sensors during 1994 and 1995) Idone et al. (1998a, 1998b) preformed one of the first systematic studies using a large data set of video observations of CG lightning in the area of Albany, New York. They observed a substantial range of variation between storms, both for DE_f and DE_s and attributed this to significant variations in the properties of lightning between individual storms under the assumption that the U.S. NLDN was not compromised to any significant changes in performance within short periods. A time coincidence window of 24 ms was applied in the correlation process of U.S. NLDN stroke reports and the video events. Based upon 517 video documented CG flashes in the year 1993 Idone et al. (1998a) found a DE_f of 67%. In 1994, 86% of 893 flashes and 67% of 2162 strokes were detected; in 1995, 72% of 433 flashes and 47% of 1242 strokes were detected. During 1994 additional sensors were deployed locally and resulted in a higher DE than in the following year 1995. For a subset of 92 strokes

Idone et al. (1998a) estimated the stroke peak current from measured electric field changes and a clear dependence of the DE from the peak current was found. Strokes with amplitudes greater than 14 kA were almost always detected, whereas none of 14 strokes with estimated peak currents below 6 kA were detected.

The same video observation data were used by Idone et al. (1998b) to evaluate the location accuracy of the U.S. NLDN. In 1995, after the network upgrade a subset of 79 common strokes (strokes that were detected by the U.S. NLDN and for which correlated video recording was available allowing stroke location determination) resulted in a median and mean stroke location of 435 m and 625 m, respectively. They also found that the U.S. NLDN location error is a function of the estimated peak current, with the weakest peak currents having the poorest locations. Typically strokes with peak currents of intermediate magnitude (20 – 30 kA) were the most accurately located. Strokes of very large peak currents are often located with larger errors because sensors at close range are all saturated and therefore only signals from more distant sensors are available for calculation of the stroke location. This results in a larger error, because waveform distortion due to field propagation over longer distances introduces larger timing errors for the sensor measurements.

Parker and Krider (2003) used a portable data acquisition system (digital camcorder, electric field antenna, GPS clock) for precise time synchronized optical and electromagnetic measurements of lightning. For a preliminary assessment of the DE of the U.S. NLDN near Tucson, Arizona, they used only the video imagery from isolated storms that had at least 25 visible strokes. A subset (109 flashes in five storms) of video data collected in summer 2001 was correlated to the U.S. NLDN stroke reports. The flash and stroke detection efficiency of the U.S. NLDN near Tucson Arizona (southwestern U.S.) were about 71% and 41%, respectively, with a 33-ms requirement for time coincidence between video time stamp and U.S. NLDN report. They determined a 55% DE_1 for first strokes which is higher than the DE_{su} for subsequent strokes due to they typically higher peak currents for first strokes. When they reduced the time coincidence window to 24 ms, like Idone et al. (1998a) the DE_f and DE_s reduce to 61% and 36%, respectively. For this region along the southern border of the NLDN, a model-based DE_f of 74% was predicted for the 2001 network configuration (Cummins et al., 1998b).

The same portable system was used by Kehoe and Krider (2004) to record 671 CG flashes containing at least 2290 strokes in 18 thunderstorms near Tucson, Arizona during summer 2003. By comparing the GPS times of the video flashes and strokes with reports from the U.S. NLDN they observed an average DE_f and DE_s of about 95% and 78%, respectively. The higher values in 2003 are a result of improved performance provided by the U.S. NLDN upgrades that were implemented in 2002 (see Cramer et al., 2004) when all U.S. NLDN sensors were replaced by IMPACT-ESP sensors. Prior to this upgrade, typically 3-4 sensors were required in order to compute a location, since 60% of the sensors in the network only provided TOA information. This change allows the network to detect much smaller events. On the other hand, due to the enhanced sensitivity of the IMPACT-ESP sensors, an increased percentage of miscategorized IC events was reported by Cramer et al., 2004, where most of positive small CG events (<10 kA) were actually cloud discharges.

Biagi et al. (2006) conducted four video field campaigns in southern Arizona (AZ) and in northern Texas and southern Oklahoma (TX-OK) in 2003 and 2004 to evaluate the performance of the U.S. NLDN after completion of the 2003 upgrade in noted above (see also paragraph 8.3.2). Average flash DE_f in AZ was 93% and the stroke DE_s was 76%; corresponding values in TX-OK were 92% and 86%, respectively. The observed average DE_1 for first strokes (92%) was larger than the DE_{su} for subsequent strokes that produced a new ground contact (81%), and larger than the DE_{su} for subsequent strokes that remained in the pre-existing channel (67%).

The primary cause of the U.S. NLDN missing strokes was that the peak of the radiated electromagnetic field (or the inferred peak current I_p) was below the detection threshold.

Biagi et al. (2006) determined a median random position error of 424m in AZ and 282 m in TX-OK by analyzing the locations of subsequent strokes that remained in the same channel as the first stroke (confirmed by the video observation). These values do not include any residual systematic (or non-random) errors in the stroke locations.

By evaluating the classification of lightning type by the U.S. NLDN Biagi et al. (2006) found that only a small fraction (1,4% to 7%, depending on whether events that exhibited no luminous activity were included in the statistics or not) of positive U.S. NLDN reports with $I_p \leq +10$ kA actually resulted from CG strokes. In the range $+10 \text{ kA} < I_p \leq +20$ kA 4,7% to 26% of positive U.S. NLDN reports corresponded to CG observations. When positive peak currents were large ($I_p \geq +20$ kA), 67% to 95% of the reports were CG strokes. 50% to 87% of the negative, single-stroke U.S. NLDN reports with $|I_p| \leq 10$ kA were produced by CG discharges.

The performance of RINDAT (Brazilian Integrated Lightning Detection Network) was evaluated in the Sao Paulo area by Ballarotti et al. (2006) based on GPS time correlated high speed video records (1000 frames/s). RINDAT detected 226 from 413 strokes with clearly visible channels to ground on the video images (stroke DE_s= 55%). A flash detection efficiency DE_f of 87% was determined for the same region, where at least one stroke in 180 flashes (out of 206) was located by RINDAT.

8.5 Discussion

From the different studies presented in the previous paragraphs we can draw the following conclusions for the major performance criteria of LLS:

By deploying most recent technology of sensors a DE_f of 95% or higher is achievable. In a network with small sensor baselines and low sensor threshold settings (requires sensor sites with low electromagnetic background noise) a DE_f close to 100% is possible. DE_s is generally lower than DE_f and can reach values in the range of 80-90%, where most likely strokes of very small peak currents are missed by the LLS.

The effect of the number and type of sensors located within a few hundred kilometers around any strike point becomes obvious when we compare the DE results of lightning to the Gaisberg tower and triggered lightning in Florida. The stroke DE_s in the

Gaisberg tower area is significantly higher as 5 sensors are within a distance of 150 km. In the U.S. NLDN only one sensor is within 100 km from the Camp Blanding site and the 4 next nearest sensors are at distances from 200 km to 250 km, resulting in predominantly poor detection of triggered strokes with small peak currents. In addition, when a subset of the nearby sensors only provide TOA information (as in the Florida area in 2001-2002), the LLS was not able to produce a position when only two sensors detected an event.

The different ground truth studies confirmed a location accuracy with a median location error in the range of 500 m range, as predicted by model calculations. The most-accurate locations are observed for peak currents in the intermediate peak-current range of 20-30 kA range, since a sufficient number of sensors report the event and the peak field values are below the saturation limit of the nearby sensors.

Triggered lightning and upward initiated lightning to elevated towers represents mostly same-channel subsequent strokes in natural downward lightning. First strokes in downward lightning typically have larger peak currents than subsequent ones and therefore the DE values based for triggered and tower lightning data represent lower bounds on DE for the given LLS.

Peak current estimates from LLS are dependent on the sensor calibration, the applied attenuation model and the field to current conversion factor. Some of the differences observed in the peak current estimate of triggered lightning located by the U.S. NLDN and strikes to the Gaisberg tower located by EUCLID are most likely caused by the following reasons. To account for propagation effects, power-law or exponential (space constant) attenuation with distance is applied in the U.S. NLDN, whereas no attenuation model is used in the EUCLID network. On the other hand in the U.S. NLDN range normalized signals are converted to peak current by I_p = 0.185*RNSS whereas EUCLID uses I_p = 0.23*RNSS. Another source of differences might be the so called tower effect, where it is assumed that lightning fields from strikes to elevated towers are enhanced as a result of current waves traveling along the tower structure and being reflected at ground level and the tower top (see e.g. Bermudez et al., 2005 and Baba and Rakov, 2005). The observed pronounced overestimation of peak currents by the NALDN from lightning to the CN Tower could also be caused at least partly by this tower effect. Pavanello et al. (2007a) tested the theoretical field peak enhancement predicted by Bermudez et al. versus experimental data of fields and currents associated with lightning strikes to the Toronto CN Tower and found a reasonably good agreement. Pavanello (2007c) used the tower correction factor proposed by Bermudez et al. (2005) to correct the NALDN current peak estimates the correction resulted in an excellent estimation of the lightning current peaks. Further investigations, including the calibration of the current measurement system are needed to confirm these results.

Concerning the mean and median value of the LLS inferred statistics, it is worth mentioning that as the elevated tower is more attractive for flashes of large peak currents, the measured distribution from instrumented towers is biased to higher values. The effect of tall object on the lightning peak current frequency distribution was first investigated by Sargent (1972). Pettersson (1991) has proposed an analytical formula to obtain the statistical distribution of lightning peak current at ground starting from that

obtained from elevated instrumented towers. Such a formula has been derived under the two assumptions that the peak current distribution at ground level is lognormal and the relationship between the lightning current peak and the corresponding attractive radius of the tower is exponential. The Pettersson's formula has been applied by Sabot (1995) to adjust the lightning current amplitude distribution adopted by Cigré [Sabot (1995)].The relationship between the probability density function of stroke current peaks I_p to an elevated structure, f_s, and the probability density function of stroke current peaks to open ground, f_g may be expressed as (Brown (1978) and Rizk (1994))

$$f_s\left(h, I_p\right) = \frac{r^k\left(h, I_p\right) f_g\left(I_p\right)}{\int_0^\infty r^k\left(h, I_p\right) f_g\left(I_p\right) dI_p} \qquad \textbf{(8.2)}$$

where h is the structure height and k is equal to 2 if the structure is a tower and equal to 1 if it is an horizontal conductor (line). From Eq.(8.2), Rizk (1994) has inferred the conclusion that if $r(h,I_p)$ can be expressed as a product of two explicit functions in h and I_p, then the stroke current distribution f_s is independent of structure height. Borghetti et al. (2004) have presented a method that allows the calculation of f_g, being f_s and r known, based on a Monte Carlo approach. Depending on the expression used to calculate the attractive radius of the tower, Borghetti et al. (2004) calculated distributions of the peaks to ground level with median values lower than those of the original distribution, relevant to instrumented tower data, ranging from more than 20% to about 40%, depending on the attractive radius expression adopted for the calculation. The results confirm that, for all but one of the considered attractive radius models examined in that paper, it is the presence of the tower, more than its height, to have the major impact on the median value of the peak current distribution. The results by Borghetti et al. are in agreement with the conclusions of Rizk (1994) and with the analysis presented by Mousa and Srivastava (1984). Indeed, CIGRE concluded that experimental data from Europe and South Africa show that first-stroke peak currents are not greatly influenced by the height (ranging from 25 to 300 m) of the structure on which they were measured (CIGRE Document 118, 1997, page 16). Clearly, additional experimental data would be very useful to validate these theoretical findings.

9 Methods for compensation of relative network detection efficiency

The material presented in Chapter 5 clearly shows that the DE (flash or stroke) for a given LLS has a significant effect on lightning parameters derived using data produced by that LLS. Therefore, if we hope to separate out true differences in lightning characteristics when comparing LLS-derived lightning parameters between regions, it is essential that differences in LLS performance are taken into account. In this chapter we present methods to correct ground flash density values for differences in stroke DE, and we discuss additional methods to help to assess the quality of derived lightning parameters. Ideally, any study that compares LLS-derived lightning parameters between regions would include some form of quality analysis for each LLS, making it possible to assess the significance of the regional differences.

9.1 Stroke DE correction using peak current distributions

The discussion of the effect of DE on peak current distributions in Section 5.2 provides the rationale for a method to estimate the relative stroke DE between two regions or conditions (Reference and Test Conditions). If there is a specific peak current value (I_0) above which all events are seen in a Test condition (that peak current being higher than the I_0 value for a Reference condition that had higher stroke DE), then it must be possible to represent this by "scaling" the Test distribution by a constant that is equal to the fraction of events detected by the Test network. The Test and Reference distributions should then be identical for peak currents greater then I_0. This fact is illustrated in Fig. 9.1, where the Test distributions (same datasets shown in Fig. 5.1) have been "normalized" by scaling them down to the known stroke DE values. Note that the curves are essentially identical for peak currents above 11 kA. Note also that the curves grow farther apart as peak current decreases, which reflects the variable (but decreasing) detection efficiency with decreasing peak current in the Test configuration. Fig. 9.1 clearly shows that no flashes with peak currents below 4 kA were seen in the "75%" Test condition.

The experiment described above suggests that it is possible to estimate the relative detection efficiency associated with two data sets through an analysis of the cumulative peak current distributions. This stroke DE estimation method simply becomes the task of identifying the peak current value (I_0) above which the cumulative peak current distributions from the Test and Reference distributions "match." There are a number of assumptions that must be met in order for this correction method to produce reliable results. The critical assumptions are as follows:

- The underlying distributions of peak currents (actual, not measured) in the Test and Reference regions are the same. Under normal conditions, this assumption is likely to be met for negative flashes accumulated over a full year.
- The lightning detection network performance was consistent over the regions(s) of interest during the Test time period, and also during the Reference time period. Obviously, it is assumed that the performance during the Reference time period is different then during the Test time period.

- The signal strength calibration of the sensors, and the method used to convert signal strength to estimated peak current, did not change during both the Test and Reference time periods.

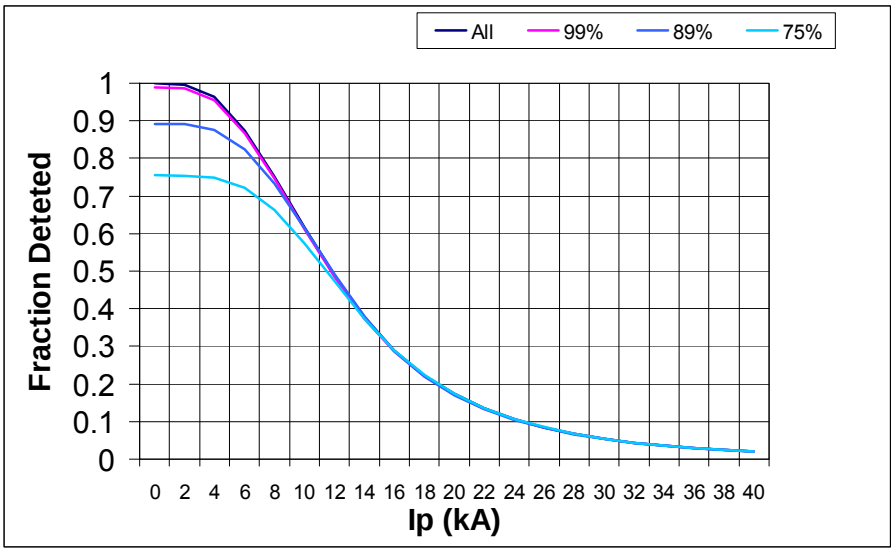

Fig. 9.1 First stroke peak current distributions scaled by their associated relative first stroke DE values, for four different detection efficiency conditions in the central U.S. NLDN. Unscaled distributions are shown in Fig. 5.1

The procedure for determining I_0 and relative stroke DE are as follows. As noted above, the task of estimating the relative stroke DE between a Test and Reference region begins with the task of identifying the minimum peak current value (I_0) above which the cumulative peak current distributions from the Test and Reference distributions can be made to "match." This "match" is obtained by computing the "best" fractional constant that can be used to scale the Test cumulative distribution to look like the Reference distribution, for peak currents greater than I_0. The following procedure has been developed to obtain these parameters:

1. Produce the normalized cumulative peak current distributions for the Test and Reference periods/regions, such that the cumulative fractions are zero at very large current values and total to 1.0 at zero peak current. The "bin" size for these cumulative distributions should be 1-2 kA. These distributions are illustrated in Fig. 9.2a below.

2. Starting at a very high peak current value (known to be larger then I_0), for each current "bin" in the cumulative distribution, determine the least-squared error scaling factor (SF) which makes the Test cumulative distribution ($I > I_0$) match the shape of the Reference cumulative distribution. One particular set of values is illustrated in Fig. 9.2d. The least-squared-error method to obtain the scaling constants is the following:

$$SF(I_o) \equiv \frac{\sum_{i=I_{max}}^{i=I_o} C_t(i) * C_r(i)}{\sum_{i=I_{max}}^{i=I_o} C_r(i) * C_r(i)} \quad \textbf{(9.1)}$$

where C_t is the cumulative distribution for the Test region/period, C_r is the cumulative distribution for the Reference region/period, and I_{max} is the maximum peak current in the cumulative distributions.

3. Determine the quality of the match in (1) above, based on the Pearson Product-moment Correlation Coefficient (R) for each of the ($I > I_0$) intervals. The result of this step is illustrated in Fig. 9.2c. R is a dimensionless index that ranges from -1.0 to 1.0 inclusive and reflects the extent of a linear relationship between two data sets. The “Fit Error” is the percentage deviation of the fit from linearity, as defined by R:

$$Fit = 100 * (1 - |R(I_o)|) \quad \textbf{(9.2)}$$

$$R(I_o) \equiv \frac{N\left(\sum_{i=I_{max}}^{i=I_o} C_t(i)C_r(i)\right) - \left(\sum_{i=I_{max}}^{i=I_o} C_t(i)\right)\left(\sum_{i=I_{max}}^{i=I_o} C_r(i)\right)}{\sqrt{\left[N\sum_{i=I_{max}}^{i=I_o} C_t^2(i) - \left(\sum_{i=I_{max}}^{i=I_o} C_t(i)\right)^2\right]\left[N\sum_{i=I_{max}}^{i=I_o} C_r^2(i) - \left(\sum_{i=I_{max}}^{i=I_o} C_r(i)\right)^2\right]}} \quad \textbf{(9.3)}$$

4. Identify the I_0 associated with the best Fit, where “best” is defined as smallest value of I_0 where the Fit reaches a minimum, and determine the associated scaling factor (SF). The scaling factor determined in Eq.(9.1) is the estimated relative DE. Fig. 9.2b is a graphical representation of the match between the Test and the Reference distributions, after scaling the Test distribution by the estimated relative DE. In this example, the best fit (error ~ 0.1) occurs at 10 kA (see Fig. 9.2c), which corresponds to a best-fit estimator (SF) of ~0.74, taken from Fig. 9.2d.

The corrected (blue) Test distribution is shown in Fig. 9.2b. The figure shows a good match between the Test and Reference distributions for peak currents above 10 kA, followed by a steadily increasing difference between 10 and about 5 kA. Note that the Test distribution shows no detected events below 5 kA (horizontal curve), whereas the Test distribution continues to increase (up to 1.0) for currents as low as about 2 kA. The characteristics correspond nicely with the theoretical basis for the method.

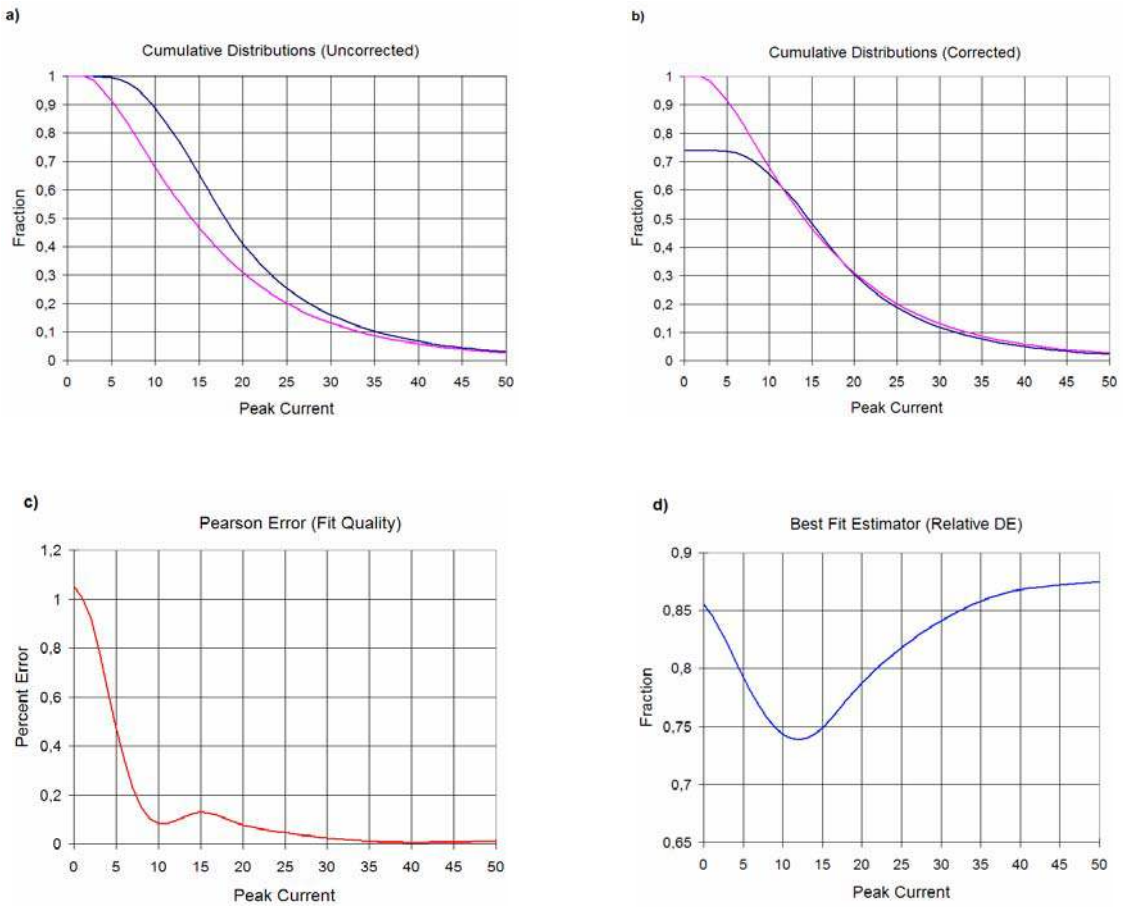

Fig. 9.2 Illustration showing the complete DE correction method. See text for details.

This DE correction method can be used to correct stroke DE for first, subsequent, or "all" strokes. The choice is determined by the specific peak current distributions that are employed in the analysis. The method is not directly applicable for flash DE_f, which is dependent on the number of strokes in a flash and the stroke DE as shown in Eq. (5.1). However, Eq.(5.1) can be rewritten to express flash DE_f in terms of stroke DE_s and multiplicity:

$$DE_f = \frac{M}{m} * DE_s \qquad \textbf{(9.4)}$$

This form can be used to determine the ratio of the "test" flash DE (DE_{ft}) to the "reference" flash DE (DE_{fr}):

$$\frac{DE_{ft}}{DE_{fr}} = \frac{m_r}{m_t} * \frac{DE_{st}}{DE_{sr}} \qquad \textbf{(9.5)}$$

Where DE_{st}/DE_{sr} is the ratio of the "test" stroke DE to the "reference" stroke DE, and m_r/m_t is the ratio of the "reference" multiplicity to the "test" multiplicity.

Since the stroke DE_s estimation method discussed earlier in this section provides the relative stroke DE_s (the ratio DE_{st}/DE_{sr}), Eq.(9.5) provides a simple method to produce relative flash DE_f.

This technique has been successfully used to obtain flash DE_f corrections for the U.S. National Lightning Detection Network (U.S. NLDN) for the years 1999 through 2004, with the coverage area broken down into 2º x 2º regions, in order to allow corrections for network performance resulting from an upgrade that took place in 2001-2002.

As noted early in this section, there are three critical conditions that must be met in order for this method to accurately reflect changes in DE. If the assumptions are violated, there can be significant errors, as is discussed by Murphy and Holle (2005) who used a similar technique to estimate U.S. NLDN DE in northern Mexico. The following subsection provides a simpler graphical method for estimating the relative DE which is somewhat less sensitive to the basic assumptions.

9.2 Graphical Approach to DE Estimation

The stroke DE_s calculation described in Section 9.1 is mathematically complicated. In this section we describe a graphical method that relies in the same principles but does not require the calculations of Eq.(9.1) through Eq.(9.3).

This approach is illustrated using a "simulated" peak current distribution derived from a log-normal distribution, shown in Fig. 9.3. The blue (cumulative) curve represents the "true" peak current distribution and the green curve results from removing all events with peak current below 20 kA. The red curve is the adjusted cumulative distribution after having applied the correction method discussed in Section 9.1.

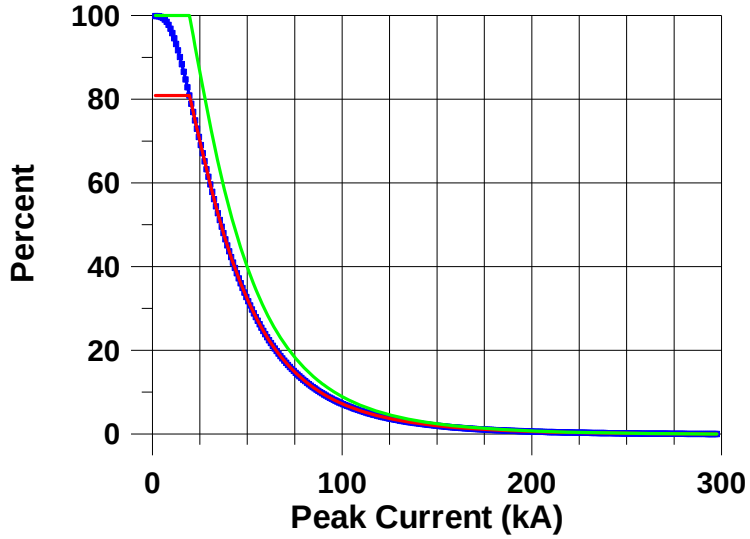

Fig. 9.3 Cumulative distributions for simulated long-normal peak current distribution (blue), same distribution after removing all events below 20 kA (green), and the DE-corrected distribution (red).

When these data are plotted in semi-log format, one can easily tell how to “adjust” the green curve for it to match the “reference” (blue) curve for the higher peak-current values. A correction is determined sliding the green curve down in order for the Test and Reference curves to be aligned at higher-current levels (DE-corrected curve is shown in red). The relative DE of the test condition (compared to the Reference condition) can be read off of the y-axis (in this case, 80%).

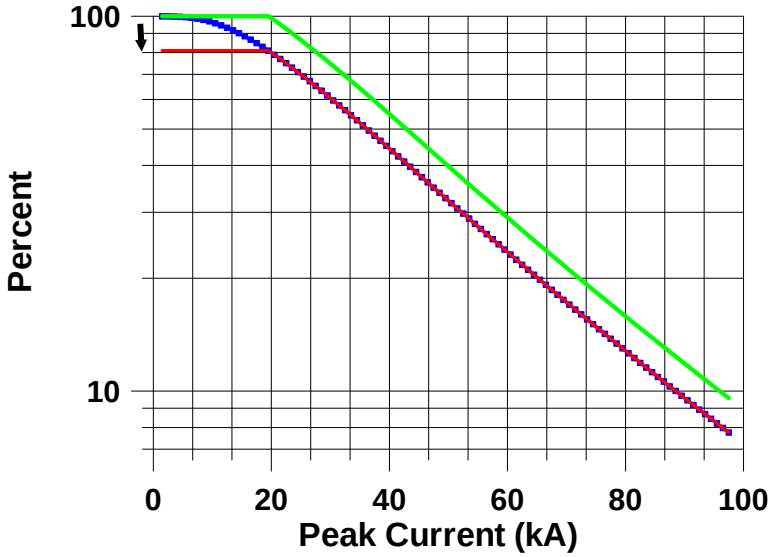

Fig. 9.4 Data from Fig. 9.3, replotted in semi-log format

These data can be plotted in log-probability format in order to better appreciate the impact of the error in the original Test distribution (green curve). The red curve is the DE-corrected Test curve.

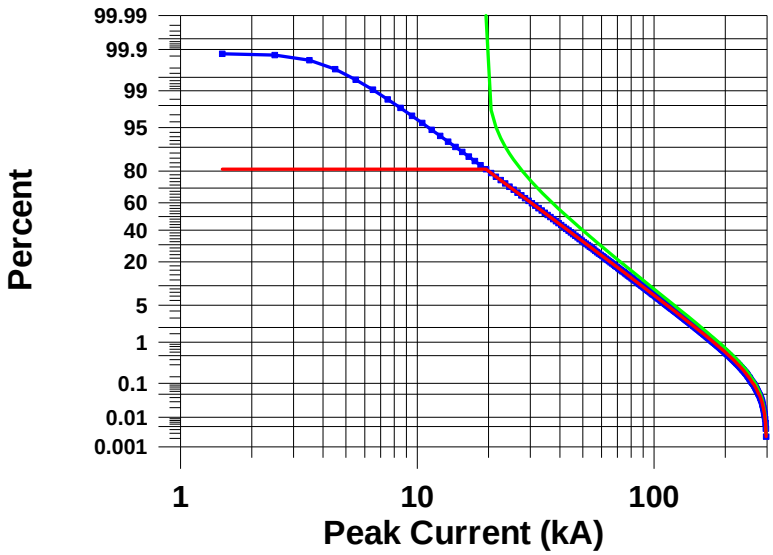

Fig. 9.5 Data from Fig. 9.3, replotted in log-probability format

It is important to note that „real world“ distributions will not match as nicely as the curves shown in Fig. 9.4 and Fig. 9.5. The perfect straight-line relationship between 20 and 100 kA in Fig. 9.4 will be compromised due to factors such as small datasets, contamination by cloud discharges, and differences in propagation corrections between Test and Reference datasets. It is most important to match the log-plotted curves in the lower-current ranges (where there are more events, and to allow the curves to deviate for higher-current (lower probability) values. This is illustrated in the example shown in Fig. 9.6, taken from a region in the central U.S.

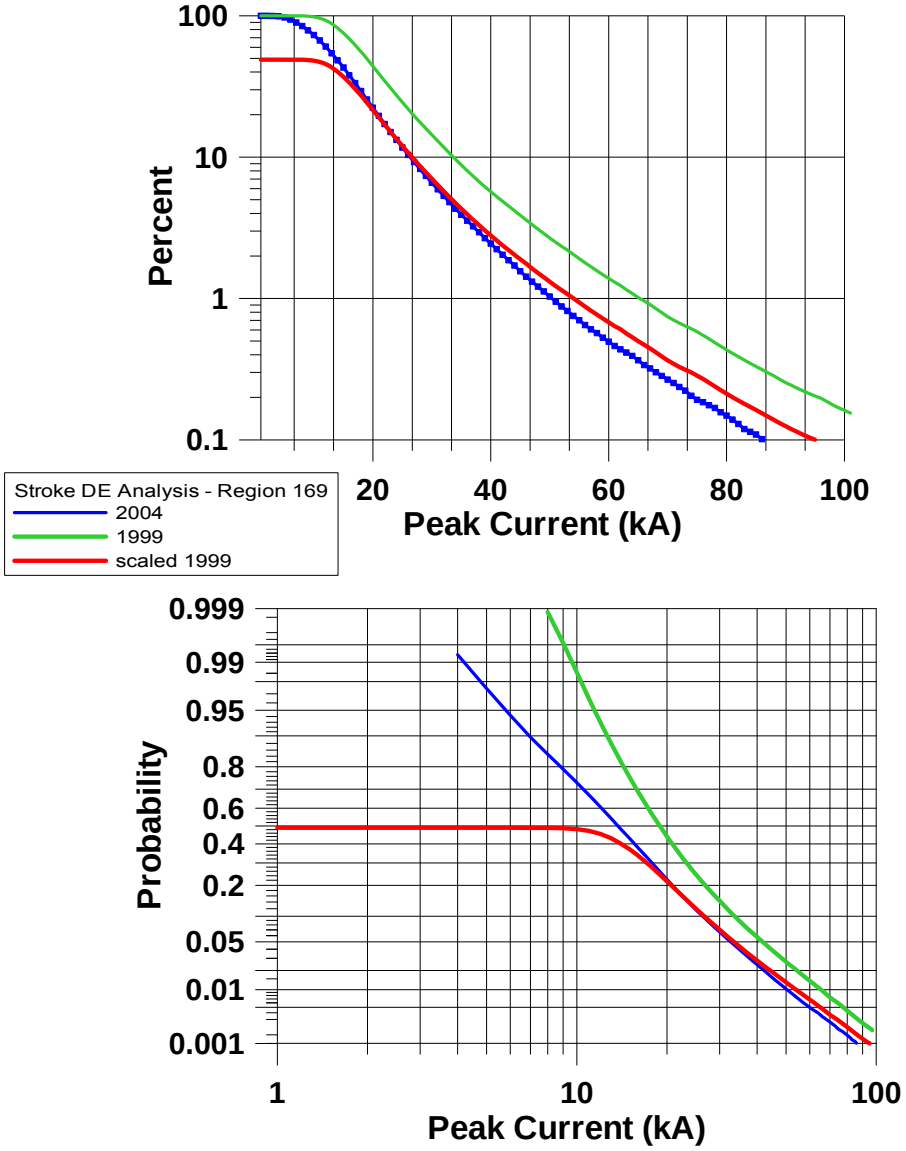

Fig. 9.6 Practical example of the graphical approach to DE estimation

10 Bibliography

/1/ Anderson, R. B. and A. J. Eriksson (1980), Lightning parameters for engineering application, Electra 69: 65-102.

/2/ Anderson, R. B., A. J. Eriksson, H. Kröninger, D. V. Meal, and M. A. Smith (1984), Lightning and Thunderstorm Parameters, Proc. IEE Int. Conf. on Lightning and Power Systems, London, UK

/3/ Asakawa, A., K. Miyake, S. Yokoyama, T. Shindo, T. Yokota, and T. Sakai (1997), Two types of lightning discharges to a high stack on the coast of the Sea of Japan in winter, IEEE Trans. Pow. Del. 12: 1222-31.

/4/ Baatz, H. (1951), Blitzeinschlag-Messungen in Freileitungen, Elektrotech. Z. Ausg. A 72: 191-8.

/5/ Baba, Y. and V. A. Rakov (2005), Lightning electromagnetic environment in the presence of a tall grounded strike object, J. Geophys. Res., 110, D09108, doi:10.1029/2004JD005505.

/6/ Ballarotti, M.G., M. M. F. Saba, O. Pinto Jr. (2006), A new performance evaluation of the Bazilian Lightning Location System (RINDAT) based on high-speed camera observations of natural negative ground flashes, 19th International Lightning Detection Conference (ILDC), Tucson, Arizona.

/7/ Beierl, O. (1992), Front shape parameters of negative subsequent strokes measured at the Peissenberg tower, In Proc. 21st Int. Conf. on Lightning Protection, Berlin, Germany, pp. 19-24.

/8/ Bent, R. S. and W. A. Lyons (1984), Theoretical evaluations and initial operational experiences of LPATS (Lightning Position and Tracking System) to monitor lightning ground strikes using a time-of-arrival (TOA) technique, in Preprints, 7th Int. Conf. on Atmospheric Electricity, Albany, New York, (pp. 317–324). Sponsored by American. Meteorological Society.

/9/ Berger, G. and S. Pedeboy (2003), Comparison between real CG flashes and CG flashes detected by a lightning detection network, ICOLSE, Blackpool.

/10/ Berger, K. (1955a), Die Messeinrichtungen fuer die Blitzforschung auf dem Monte San Salvatore, Bull. Schweiz. Elektrotech. Ver. 46: 193-204.

/11/ Berger, K. (1955b), Resultate der Blitzmessungen der Jahre 1947-1954 auf dem Monte San Salvatore, Bull. Schweiz. Elektrotech. Ver. 46: 405-24.

/12/ Berger, K. (1962), Front duration and current steepness of lightning strokes to Earth, In Gas Discharges and the Electricity Supply Industry, eds. J.S. Forrest, P.R. Howard, and D.J. Littler, pp. 63-73, London: Butterworths.

/13/ Berger, K. and E. Vogelsanger (1965), Messungen und Resultate der Blitzforschung der Jahre 1955-1963 auf dem Monte San Salvatore, Bull. Schweiz. Elektrotech. Ver. 56: 2-22.

/14/ Berger, K. (1967a), Novel observations on lightning discharges: Results of research on Mount San Salvatore, J. Franklin Inst. 283: 478-525.

/15/ Berger, K. (1967b), Gewitterforschung auf dem Monte San Salvatore, Elektrotechnik (Z-A) 82: 249-60.

/16/ Berger, K. and E. Vogelsanger (1969), New results of lightning observations, In Planetary Electrodynamics, 1, eds. S.C. Coroniti, and J. Hughes, pp. 489-510, New York: Gordon and Breach.

/17/ Berger, K. (1972), Methoden und Resultate der Blitzforschung auf dem Monte San Salvatore bei Lugano in den Jahren 1963-1971, Bull. Schweiz. Elektrotech. Ver. 63: 1403-22.

/18/ Berger, K., R. B. Anderson, and H. Kroninger (1975), Parameters of lightning flashes. Electra 80: 223-37.

/19/ Berger, K. (1980), Extreme Blitzstroeme und Blitzschutz. Bull. Schweiz. Elektrotech. Ver. 71: 460-4.

/20/ Berger, K. and E. Garabagnati (1984), Lightning current parameters. Results obtained in Switzerland and in Italy, URSI Conf., Florence, Italy.

/21/ Bermudez, J. L., F. Rachidi, M. Rubinstein, W. Janischewskyj, V. O. Shostak, D. Pavanello, J. S. Chang, A. M. Hussein, C. A. Nucci, and M. Paolone (2005), Far-Field–Current Relationship Based on the TL Model for Lightning Return Strokes to Elevated Strike Objects, IEEE Transactions on Electromagnetic Compatibility, Vol. 47, No. 1.

/22/ Biagi, C. J., K. L. Cummins, K. E. Kehoe, and E. P. Krider (2007), National Lightning Detection Network (NLDN) performance in southern Arizona, Texas, and Oklahoma in 2003–2004, J. Geophys. Res., 112, D05208, doi:10.1029/2006JD007341.

/23/ Biswas, K. R. and P. V. Hobbs (1990), Lightning over the Gulf Stream, Geophys. Res. Lett. 17: 941-3.

/24/ Boccippio, D. J., W. Koshak, R. Blakeslee, K. Driscoll, D. Mach, D. Buechler, W. Boeck, H. J. Christian, and S. J. Goodman (2000), The Optical Transient Detector (OTD): instrument characteristics and cross-sensor validation, J. Atmos. Oceanic Technol. 17: 441-58.

/25/ Borghetti, A., C.A.Nucci, M.Paolone (2004), Estimation of the Statistical Distributions of Lightning Current Parameters at Ground Level From the Data Recorded by Instrumented Towers, IEEE Transactions on Power Delivery, Vol.19, No.3.

/26/ Brown G.W. (1978), Joint Frequency Distribution of Stroke Current Rates of Rise and Crest Magnitude to Transmission Lines, IEEE Trans. Power Apparatus and Systems, Vol. PAS-97, No. 1, pp. 53-58.

/27/ Brook, M., M. Nakano, P. Krehbiel, and T. Takeuti (1982), The electrical structure of the Hokuriku winter thunderstorms, J. Geophys. Res. 87: 1207-15.

/28/ Brook, M. (1992), Breakdown electric fields in winter storms, Res. Lett. Atmos. Electr. 12: 47-52.

/29/ Casper, P. W. and R. B. Bent (1992), Results from the LPATS USA national lightning detection and tracking system for the 1991 lightning season, in Proc. 21st Int. Conf. on Lightning Protection, Berlin, (pp. 339–342). Sponsored by the Association of German Electrical Engineers (VDE) and VEAG (Berlin) and SIEMENS AG (Erlangen).

/30/ Changnon, S. A. (1988), Climatography of thunder events in the conterminous United States. Part II: Spatial aspects. J. Clim. 1: 399-405.

/31/ CIGRE Report 63 (1991), Guide to Procedures for Estimating the Lightning Performance of Transmission Lines, WG 33.01

/32/ CIGRE Report 94 (1995), Lightning Characteristics Relevant for Electrical Engineering: Assessment of Sensing, Recording and Mapping Requirements in the Light of Present Technological Advancements, TF 33.01.02

/33/ CIGRE Document 118 (1997), Lightning Exposure of Structures and Lightning Interception of Air Terminals, TF 33.01.03

/34/ CIGRE Report 172 (2000), Characterization of Lightning for Applications in Electric Power Systems, TF 33.01.02

/35/ Cooray, V. and K. P. S. C. Jayaratne (1994), Characteristics of lightning flashes observed in Sri Lanka in the tropics, J. Geophys. Res. 99: 21,051-6.

/36/ Cooray, V. and H. Perez (1994), Some features of lightning flashes observed in Sweden, J. Geophys. Res. 99: 10,683-8.

/37/ Cramer, J. A., K. L. Cummins, A. Morris, R. Smith, and T. R. Turner (2004), Recent upgrades to the U.S. national lightning detection network, 18th International Lightning Detection Conference (ILDC), Helsinki, Finland

/38/ Cummins, K. L., R. O. Burnett, W. L. Hiscox, and A. E. Pifer (1993), Line reliability and fault analysis using the National Lightning Detection Network, paper presented at Precise Measurements in Power Conference, Arlington, Va., USA, National Science Foundation and Ctr. for Power Engineering at Virginia Tech. Univ.

/39/ Cummins, K. L., E. P. Krider, and M. D. Malone (1998a), The U.S. National Lightning Detection Network and Applications of Cloud-to-Ground Lightning by Electric Power Utilities," in IEEE Transactions on Electromagnetic Compatibility, Vol. 40, No. 4, pp. 465-480.

/40/ Cummins, K. L., M. J. Murphy, E. A. Bardo, W. L. Hiscox, R. B. Pyle, and A. E. Pifer (1998b), A combined TOA/MDF technology upgrade of the U.S. National Lightning Detection Network, J. Geophys. Res. 103: 9035-44.

/41/ Cummins, K. L. and M. J. Murphy (2000), Overview of Lightning Detection in the VLF, LF, and VHF Frequency Ranges, 16th International Lightning Detection Conference (ILDC), Tucson, Arizona

/42/ Cummins, K. L. (2000), Continental-scale detection of cloud-to-ground lightning, T.IEE Japan, Vol. 120-B, No. 1.

/43/ Cummins, K. L., J. A. Cramer, C. J. Biagi, E. P. Krider, J. Jerauld, M. A. Uman, and V. A. Rakov (2006), The U.S. National Lightning Detection Network: Post-upgrade status. 2nd Conf. on Meteorological Application of Lightning Data, Amer. Meteorol. Soc., Atlanta, paper 6.1

/44/ Diendorfer, G., W. Schulz, and V. Rakov (1998), Lightning characteristics based on data from the Austrian lightning location system, IEEE Transactions on EMC, Vol. 40, No. 4.

/45/ Diendorfer, G., M. Mair, W. Schulz, and W. Hadrian (2000a), Lightning current measurements in Austria – Experimental setup and first results, In Proc. 25th Int. Conf. on Lightning Protection, Rhodes, Greece, pp. 44-47.

/46/ Diendorfer, G., W. Schulz, and M. Mair (2000b), Evaluation of a LLS based on lightning strikes to an instrumented tower, 16th International Lightning Detection Conference (ILDC), Tucson, Arizona.

/47/ Diendorfer, G., W. Hadrian, F. Hofbauer, M. Mair, and W. Schulz (2002), Evaluation of Lightning Location Data Employing Measurements of Direct Strikes to a Radio Tower, CIGRE Session, Paris.

/48/ Dodge, P. P. and R. W. Burpee (1993), Characteristics of rainbands, radar echoes, and lightning near the North Carolina coast during GALE. Mon. Wea. Rev. 121: 1936-55.

/49/ Dulzon, A. A. and V. A. Rakov (1980), Estimation of errors in lightning peak current measurements by frame aerials (in Russian). Izv. VUZov SSSR, ser. Energetika 11: 101-4.

/50/ Eriksson, A. J. (1978), Lightning and tall structures, Trans. South African IEE 69: 2-16.

/51/ Eriksson, A. J. (1980), The lightning ground flash - an engineering study. Ph.D. Dissertation, Univ. Natal, South Africa (available as CSIR Special Report ELEK 189, National Electrical Engineering Research Institute, Pretoria, South Africa).

/52/ Fisher, R. J., G. H. Schnetzer, R. Thottappillil, V. A. Rakov, M. A. Uman, and J. D. Goldberg (1993), Parameters of triggered-lightning flashes in Florida and Alabama. J. Geophys. Res. 98: 22,887-902.

/53/ Fuchs, F., E. U. Landers, R. Schmid, and J. Wiesinger (1998), Lightning current and magnetic field parameters caused by lightning strikes to tall structures relating to interference of electronic systems, IEEE Trans. Electromagn. Compat. 40: 444-51.

/54/ Fuquay, D. M. (1982), Positive cloud-to-ground lightning in summer thunderstorms. J. Geophys. Res. 87: 7131-40.

/55/ Garbagnati, E., E. Giudice, and G. B. Lo Piparo (1978), Measurement of lightning currents in Italy - results of a statistical evaluation, Elektrotechnische Zeitschrift ETZ-A 99: 664-8.

/56/ Garbagnati, E. and G. B. Lo Piparo (1982), Parameter von Blitzstroemen. Elektro-Technische Zeitschrift ETZ-A 103: 61-5.

/57/ Gorin, B. N., V. I. Levitov, and A. V. Shkilev (1977), Lightning strikes to the Ostankino tower (in Russian), Elektrichestvo 8: 19-23.

/58/ Gorin, B. N. and A. V. Shkilev (1984), Measurements of lightning currents at the Ostankino tower (in Russian). Elektrichestvo 8: 64-5.

/59/ Goto, Y. and K. Narita (1992), Observations of winter lightning to an isolate tower. Res. Lett. Atmos. Electr. 12: 57-60.

/60/ Goto, Y. and K. Narita (1995), Electrical characteristics of winter lightning, J. Atmos. Terr. Phys. 57: 449-59.

/61/ Harris, D. J. and Y. E. Salman (1972), The measurement of lightning characteristics in northern Nigeria. J. Atmos. Terr. Phys. 34: 775-86.

/62/ Herodotou, N., W. A. Chisholm, and W. Janischewskyj (1993), Distribution of lightning peak stroke currents in Ontario using an LLP system, IEEE transactions on Power delivery, Vol. 8, Nb. 3.

/63/ Hidayat, S. and M. Ishii (1998), Spatial and temporal distribution of lightning activity around Java. J. Geophys. Res. 103: 14,001-9.

/64/ Hidayat, S. and M. Ishii (1999), Diurnal Variation of Lightning Characteristics Around Java Island. J. Geophys. Res., 104 (D20): 24,449-24,454.

/65/ Hiscox, W. L., E. P. Krider, A. E. Pifer, and M. A. Uman (1984), A systematic method for identifying and correcting "site errors" in a network of magnetic direction finders; paper presented at the International Aerospace and Ground Conference on Lightning and Static Electricity. Natl. Interagency Coord. Group, Natl. Atmos. Electr. Hazard Program, Orlando, Florida, June 26-28.

/66/ Hojo, J., M. Ishii, T. Kawamura, F. Suzuki, H. Komuro, and M. Shiogama (1989), Seasonal variation of cloud-to-ground lightning flash characteristics in the coastal area of the Sea of Japan, J. Geophys. Res. 94: 13,207-12.

/67/ Holle, R. L. and R. E. Lopez (1993), Overview of real-time lightning detection systems and their meteorological uses. NOAA Technical Memorandum ERL NSSL-102, National Severe Storms Laboratory, Norman, Oklahoma, 68 p.

/68/ Holzer, R. E. (1953), Simultaneous measurement of sferics signals and thunderstorm activity, In Thunderstorm Electricity, ed. H.R. Byers, pp. 267-75. Chicago, Illinois: Univ. of Chicago Press.

/69/ Hussein, A. M., W. Janischewskyj, J.-S. Chang, V. Shostak, W. A. Chisholm, P. Dzurevych, and Z.-I. Kawasaki (1995), Simultaneous measurement of lightning parameters for strokes to the Toronto Canadian National Tower, J. Geophys. Res. 100, 8853-61.

/70/ Hussein, A. M. (2003), CN Tower Lightning Parameters, A Review. 2003 International Workshop on EM Radiation from Lightning to Tall Structures, Bologna, Italy.

/71/ Hussein, A. M., W. Janischewskyj, M. Milewski, V. Shostak, W. Chrisholm, and J.S. Chang (2004), Current Waveform Parameters of CN Tower Lightning Return Strokes, J. of Electrostatics, 60, 149-162.

/72/ Hussein, A.M., M. Milewski, A. Abdelraziq, W. Janischewskyj and F. Jabbar (2006) Visual Characteristics of CN Tower Lightning Flashes, Proceedings of the 28th International Conference on Lightning Protection (ICLP), pp. 89-94, Kanazawa, Japan

/73/ Idone, V. P., S. B. Arsalan, R. W. Henderson, P. K. Moore, and R. B. Pyle (1993), A Reexamination of the Peak Current Calibration of the National Lightning Detection Network, J. Geophys. Res. Vol. 98, No. D10, p. 18,323-18,332.

/74/ Idone, V. P., D. A. Davis, P. K. Moore, Y. Wang, R. W. Henderson, M. Ries, and P. F. Jamason (1998a), Performance evaluation of the U.S. National Lightning Detection Network in eastern New York 1. Detection efficiency, J. Geophys.Res. Vol.103, No. D8, p. 9045-9055.

/75/ Idone, V. P., D. A. Davis, P. K. Moore, Y. Wang, R. W. Henderson, M. Ries, and P. F. Jamason (1998b), Performance evaluation of the U.S. National Lightning Detection Network in eastern New York 2. Location accuracy, J. Geophys.Res. Vol.103, No. D8, p. 9057-9069.

/76/ Ishii, M. and J. Hojo (1989), Statistics on fine structure of cloud-to-ground lightning field waveforms, J. Geophys. Res. 94: 13,267-74.

/77/ Ishii, M., K. Shimizu, J. Hojo, and K. Shinjo (1998), Termination of multiple-stroke flashes observed by electromagnetic field, In Proc. 24th Int. Conf. on Lightning Protection, Birmingham, United Kingdom, pp. 11-6.

/78/ Ishii, M., M. Saito, F. Fujii, J. Hojo, M. Matsui, N. Itamoto and K. Shinjo (2005), LEMP from Lightning Discharges Observed by JLDN, IEEJ Trans. PE, Vol. 125, No. 8, pp.765-770.

/79/ Jacobson, E. A. and E. P. Krider (1976), Electrostatic field changes produced by Florida lightning, J. Atmos. Sci. 103-17.

/80/ Janischewskyj, W., A. M. Hussein, V. Shostak, I. Rusan, J.-X. Li, and J.-S. Chang (1997), Statistics of lightning strikes to the Toronto Canadian National Tower (1978-1995), IEEE Trans. Pow. Del. 12: 1210-21.

/81/ Jerauld, J., V. A. Rakov, M. A. Uman, K. J. Rambo, D. M. Jordan, K. L. Cummins, and J. A. Cramer (2005), An evaluation of the performance characteristics of the U.S. National Lightning Detection Network in Florida using rocket-triggered lightning, J. Geophys. Res., 110, D19106, doi:10.1029/2005JD005924.

/82/ Kehoe, K. E. and E. P. Krider (2004), NLDN performance in Arizona, 18th International Lightning Detection Conf., Vaisala Oyj, Helsinki, Finland, Paper 50 (CD-ROM)

/83/ King, T. S. and R. C. Balling (1994), Diurnal variations in Arizona monsoon lightning data, Mon. Wea. Rev. 122: 1659-64.

/84/ Kitagawa, N., M. Brook, and E. J. Workman (1962), Continuing currents in cloud-to-ground lightning discharges, J. Geophys. Res. 67: 637-47.

/85/ Kitagawa, N. (1989), Long-term variations in thunderday frequencies in Japan, J. Geophys. Res. 94: 13, 183-9.

/86/ Kitterman, C.G. (1980), Characteristics of lightning from frontal system thunderstorms, J. Geophys. Res. 85: 5503-5.

/87/ Kononov, I. I., I. A. Petrenko, and V. S. Snegurov (1986), Radiotechnical Methods for Locating Thunderstorms, 222 p. Leningrad, Russia: Gidrometeoizdat.

/88/ Kononov, I. I. and I. A. Petrenko (1996), Experience of lightning location systems elaboration in Russia, In Proc. 23rd Int. Conf. on Lightning Protection, Florence, Italy, pp. 236-40.

/89/ Krider, E. P., C. Leteinturier, and J. C. Willett (1996), Submicrosecond fields radiated during the onset of first return strokes in cloud-to-ground lightning. J. Geophys. Res. 101: 1589-97.

/90/ Krider, E. P., R. C. Noggle, and M. A. Uman (1976), A gated wideband magnetic direction-finder for lightning return strokes, J. Appl. Meteor., (15), pp. 301–306.

/91/ Krider, E. P., R. C. Noggle, A. E. Pifer, and D. L. Vance (1980), Lightning direction finding systems for forest fire detection, Bull. Amer. Meteor. Soc., (61), pp. 980–986.

/92/ Lacerda, M., O. Pinto, I. R. C. A. Pinto, J. H. Diniz, and A. M. Carvalho (1999), Analysis of negative downward lightning current curves from 1985 to 1994 at Morro do Cachimbo research station (Brazil), In Proc. 11th Int. Conf. on Atmospheric Electricity, Guntersville, Alabama, pp. 42-45.

/93/ Lafkovici, A., A. M. Hussein, W. Janischewskyj, and K. Cummins (2006), Performance analysis of the North American Lightning Detection Network using CN Tower Lightning data," International Lightning Detection Conference, pp. 1-32, Tucson, Arizona.

/94/ Le Boulch, M. and T. Plantier (1990), The Meteorage thunderstorm monitoring system: A tool for new EMC protection strategies, In Proc. 20th Int. Conf. on Lightning Protection. Interlaken, Switzerland, Paper 6.13P, 8 p.

/95/ Lee, A. C. L. (1989), Ground truth confirmation and theoretical limits of an experimental VLF arrival time difference lightning flash locating system, Quart J. Roy. Meteor. Soc., (115), pp. 1147–1166.

/96/ Leteinturier, C., C. Weidman, and J. Hamelin (1990), Current and electric field derivatives in triggered lightning return strokes, J. Geophys. Res. 95: 811-28.

/97/ Leteinturier, C., J. H. Hamelin, and A. Eybert-Berard (1991), Submicrosecond characteristics of lightning return-stroke currents, IEEE Trans. Electromagn. Compat. 33: 351-7.

/98/ Lewis, E. A., R. B. Harvey, and J. E. Rasmussen (1960), Hyperbolic direction finding with sferics of transatlantic origin, J. Geophys. Res., (65), pp. 1879–1905.

/99/ Lewis, W. W. and C. M. Foust (1945), Lightning investigation on transmission lines, Pt. 7. Trans. AIEE 64: 107-15.

/100/ Livingston, J. M. and E. P. Krider (1978), Electric fields produced by Florida thunderstorms, J. Geophys. Res. 83: 385-401.

/101/ Lopez, R. E. and R. L. Holle (1986), Diurnal and spatial variability of lightning activity in Northeastern Colorado and Central Florida during the Summer, Mon. Wea. Rev. 114: 1288-312.

/102/ Lucas, C. and R. E. Orville (1996), TOGA COARE: Oceanic lightning Mon. Wea. Rev. 124: 2077-82.

/103/ Lyons, W. A., M. Uliasz, and T. E. Nelson (1998), Large peak current cloud-to-ground lightning flashes during the summer months in the contiguous United States, Mon. Wea. Rev. 126: 2217-23.

/104/ Mach, D. M., D. R. MacGorman, W. D. Rust, and R. T. Arnold (1986), Site errors and detection efficiency in a magnetic direction finder network for locating lightning strikes to ground, Journal of Atmospheric and Oceanic Technology, 3.67-74.

/105/ Mach, D. M. and W. D. Rust (1989), Photoelectric return-stroke velocity and peak current estimates in natural and triggered lightning, J. Geophys. Res. 94: 13,237-47.

/106/ Mackerras, D. and M. Darveniza (1994), Latitudinal variation of lightning occurrence characteristics, J. Geophys. Res. 99: 10,813-21.

/107/ Mackerras, D., M. Darveniza, R. E. Orville, E. R. Williams, and S. J. Goodman (1998), Global lightning: Total, cloud and ground flash estimates. J. Geophys. Res. 103: 19,791-809.

/108/ McCann, D. G. (1944), The measurement of lightning currents in direct strokes, Trans. AIEE 63: 1157-64.

/109/ MacGorman, D. R. and W. D. Rust (1988), An evaluation of the LLP and LPATS lightning ground strike mapping systems, Proceedings 8th International Conference on Atmospheric Electricity, 668-673, Uppsala, Sweden, June 13-16.

/110/ Miki, M., V. A. Rakov, T. Shindo, G. Diendorfer, M. Mair, F. Heidler, W. Zischank, M. A. Uman, R. Thottappillil, and D. Wang (2005), Initial Stage in Lightning Initiated from Tall Objects and in Rocket-Triggered Lightning, Journal of Geophysical Research, VOL. 110, D02109, doi:10.1029/2003JD004474.

/111/ Miyake, K., T. Suzuki, and K. Shinjou (1992), Characteristics of winter lightning current on Japan Sea coast, IEEE Trans. Pow. Del. 7: 1450-6.

/112/ Montandon, E. (1992), Lightning positioning and lightning parameter determination experiences and results of the Swiss PTT research project, In Proc. 21st Int. Conf. on Lightning Protection, Berlin, Germany, pp. 307-312.

/113/ Moore, P. K. and R. E. Orville (1990), Lightning characteristics in lake-effect thunderstorms, Mon. Wea. Rev. 118: 1767-82.

/114/ Mousa A.M. and K.D. Srivastava (1989), The implications of the electrogeometric model regarding effect of height of structure on the median amplitude of collected lightning strokes, IEEE Trans. Power Delivery, vol. 4, no. 2, pp. 1450 –1460.

/115/ Murray, N. D., R. E. Orville, and G. R. Huffines (2000), Effect of pollution from Central American fires on cloud-to-ground lightning in May 1998, Geophys. Res. Lett., Vol. 27, No15, p. 2249-2252.

/116/ Norinder, H. and O. Dahle (1945), Measurements by frame aerials of current variations in lightning discharges, Arkiv. Mat. Astron. Fysik 32A: 1-70.

/117/ Orville, R. E. and H. Songster (1987), The East Coast lightning detection network, IEEE Trans. PWRD-2: 899-907.

/118/ Orville, R. E., R. A. Weisman, R. B. Pyle, R. W. Henderson, and R. E. Orville Jr. (1987), Cloud-to-ground lightning flash characteristics from June 1984 through May 1985, J. Geophys. Res. 92: 5640-4.

/119/ Orville, R. E. (1990a), Peak-current variations of lightning return strokes as a function of latitude, Nature 343: 149-51.

/120/ Orville, R. E. (1990b), Winter lightning along the East Coast, Geophys. Res. Lett. 17: 713-5.

/121/ Orville, R. E. (1991), Calibration of a Magnetic Direction Finding Network Using Measured Triggered Lightning Return Stroke Peak Currents, J. Geophys. Res. Vol. 96, No. D9, p. 17,135-17,142.

/122/ Orville, R. E. (1994), Cloud-to-ground lightning flash characteristics in the contiguous United States: 1989-1991, J. Geophys. Res. 99: 10,833-41.

/123/ Orville, R. E. and G. R. Huffines (1999), Lightning ground flash measurements over the contiguous United States: 1995-1997, Mon. Wea. Rev. 127: 2693-703.

/124/ Orville, R. E., G. R. Huffines, J. Nielsen-Gammon, R. Zhang, B. Ely, S. Steiger, S. Phillips, S. Allen, and W. Read (2001), Enhancement of Cloud-To-Ground Lightning Over Houston, Texas. Geophys. Res. Lett., 28, 13, 2597-2600.

/125/ Orville, R. E., G. R. Huffines, W. R. Burrows, R. L. Holle, and K. L. Cummins (2002), The North American Lightning Detection Network (NALDN) – First Results: 1998-2000, Monthly Weather Review, Vol. 130.

/126/ Parker, N. G. and E. P. Krider (2003), A Portable, PC-Based System for Making Optical and Electromagnetic Measurements of Lightning, J. Appl. Met., 42. 739-751.

/127/ Pavanello, D., F. Rachidi, W. Janischewskyj, M. Rubinstein, A. M. Hussein, E. Petrache, V. Shostak, I. Boev, C. A. Nucci, W. A. Chisholm, M. Nyffeler, J. S. Chang, and A. Jaquier (2007a), On Return-Stroke Currents and Remote Electromagnetic Fields Associated with Lightning Strikes to Tall Structures: 2. Experiment and Model Validation, Journal of Geophysical Research, 112, 1-12.

/128/ Pavanello, D. (2007b), Electromagnetic radiation from lightning return strokes to tall structures, 134 pp, PhD Thesis, EPFL, Lausanne, Switzerland.

/129/ Pettersson P. (1991), A unified probabilistic theory of the incidence of direct and indirect lightning strikes, IEEE Trans. Power Delivery, vol. 6, no. 3, pp. 1301 -1310.

/130/ Pierce, E. T. (1970), Latitudinal variation of lightning parameters. J. Appl. Meteor. 9: 194-195.

/131/ Pinto, O. Jr., I.R.C.A. Pinto, M. Lacerda, A. M. Carvalho, J. H. Diniz, and L. C. L. Ccherchiglia (1997), Are equatorial negative lightning flashes more intense than those at higher latitudes? J. Atmos. and Solar-Terr. Phys. 59: 1881-3.

/132/ Prentice, S. A. and D. Mackerras (1977), The ratio of cloud to ground-ground lightning flashes in thunderstorms. J. Appl. Meteor. 16: 545-50.

/133/ Rachidi, F., J. L. Bermudez, M. Rubinstein, and V. A. Rakov (2004), On the estimation of lightning peak currents from measured fields using lightning location systems, Journal of Electrostatics, Vol. 60, pp. 121-129.

/134/ Rakov, V. A. and A. A. Dulzon (1984), On latitudinal features of thunderstorm activity, Meteor. Gidrol. No. 1: 52-7.

/135/ Rakov, V. A. (1985), On Estimating the Lightning Peak Current Distribution Parameters Taking Account of the Measurement Threshold Level (in Russian), Elektrichestvo, No. 2, 57-59.

/136/ Rakov, V. A. and A. A. Dulzon (1986), Study of some features of frontal and convective thunderstorms, Meteor. Gidrol. 9: 59-63.

/137/ Rakov, V. A. and A. A. Dulzon (1988), Lightning research in Western Siberia, In Proc. 8th Int. Conf. on Atmos. Electr., Uppsala, Sweden, pp. 766-9.

/138/ Rakov, V. A., A. K. Adjiev, M. M. Akchurin, and Y. R. Shoivanov (1989), Study of spatial distribution of ground flash density using the "Ochag" lightning locating system, Meteor. Gidrol. No. 2: 48-53.

/139/ Rakov, V. A. and M. A. Uman (1990a), Long continuing current in negative lightning ground flashes, J. Geophys. Res. 95: 5455-70.

/140/ Rakov, V. A. and M. A. Uman (1990b), Some properties of negative cloud-to-ground lightning flashes versus stroke order, J. Geophys. Res. 95: 5447-53.

/141/ Rakov, V. A. (1992), Data acquired with the LLP lightning locating systems, Meteor. Gidrol. No. 7: 105-14.

/142/ Rakov, V. A., R. Thottappillil, and M. A. Uman (1992b), On the empirical formula of Willett et al. relating lightning return-stroke peak current and peak electric field, J. Geophys. Res. 97: 11,527-33.

/143/ Rakov, V. A. and M. A. Uman (1994), Origin of lightning electric field signatures showing two return-stroke waveforms separated in time by a millisecond or less, J. Geophys. Res. 99: 8157-65.

/144/ Rakov, V. A., M. A. Uman, and R. Thottappillil (1994), Review of lightning properties determined from electric field and TV observations, J. Geophys. Res. 99: 10,745-50.

/145/ Rakov, V. A. (2001), Transient response of a tall object to lightning, IEEE Trans. on EMC, 43, 654-661.

/146/ Rakov, V. A. (2003a), A Review of the Interaction of Lightning with Tall Objects, Recent Res. Devel. Geophysics, 5, pp. 57-71, Research Signpost, India.

/147/ Rakov, V. A. (2003b), A Review of Positive and Bipolar Lightning Discharges, Bull. Amer. Meteorol. Soc., June 2003, 767-775.

/148/ Rakov, V. A. and M. A. Uman (2003), Lightning: Physics and Effects. Cambridge University Press.

/149/ Rakov, V. A. and G. R. Huffines (2003), Return-stroke multiplicity of negative cloud-to-ground lightning flashes, J. Appl. Meteor., Vol. 42, No. 10, pp. 1455-1462.

/150/ Rakov, V. A. (2004), Lightning Return-Stroke Speed: A Review of Experimental Data, in Proc. of the 27th Int. Conf. on Lightning Protection, Avignon, France, September 13-16, 2004, pp. 139-144.

/151/ Rakov, V. A. (2005), Lightning Flashes Transporting Both Negative and Positive Charges to Ground", Recent Progresses in Lightning Physics, ed. C. Pontikis, Research Signpost, submitted.

/152/ Reap, R. M. (1986), Evaluation of cloud-to-cloud lightning data from the western United States for the 1983-1984 summer seasons, J. Clim. Appl. Meteor. 25: 785-99.

/153/ Reap, R. M. (1994), Analysis and prediction of lightning strike distributions associated with synoptic map types over Florida. Mon. Wea. Rev. 122: 1698-715.

/154/ Rizk F. A. M. (1994), Modelling of lightning incidence to tall structures. Part I: theory. Part II: application, IEEE Trans. Power Delivery, vol. 9, no. 1, pp. 162-193.

/155/ Rubinstein, M. (1995), On the determination of the flash detection efficiency of lightning location systems given their stroke detection efficiency, EMC Conference Proceedings, Zurich.

/156/ Rust, W. D. (1986), Positive cloud-to-ground lightning, In The Earth's Electrical Environment, pp. 41-5. Washington, D.C.: National Academy Press.

/157/ Sabot A. (1995), An engineering review on lightning, transient overvoltages and the associated elements of electrogeometric compatibility, in Proc. 9th Int. Symposium on High Voltage Engineering, Graz, Austria.

/158/ Sargent, M.A. (1972), The Frequency Distribution of Current Magnitudes of Lightning Stroke to Tall Structures, IEEE Trans, Vol. PAS-91, n°5, pp 2224-2229.

/159/ Schonland, B. F. J. (1956), The lightning discharge, Handb. Phys. 22: 576-638.

/160/ Schulz, W. (1997), Performance evaluation of lightning location systems. Ph.D. Thesis, Technical University of Vienna.

/161/ Schulz, W. and G. Diendorfer (1999), Lightning Characteristics as a Function of Altitude Evaluated from Lightning Location Network Data, International Conference on Lightning and Static Electricity (ICOLSE), Toulouse.

/162/ Schulz, W. and G. Diendorfer (2000), Evaluation of a lightning location algorithm using an elevation model, 25th International Conference on Lightning Protection (ICLP), Rhodos.

/163/ Schulz, W., K. Cummins, G. Diendorfer, and M. Dorninger (2005), Cloud-to-ground lightning in Austria: A 10-year study using data from a lightning location system, J. Geophys. Res., 110, D09101, doi:10.1029/2004JD005332.

/164/ Smith, D. A., X. M. Shao, D. N. Holden, C. T. Rhodes, M. Brook, P. R. Krehbiel, M. Stanley, W. Rison, and R. J. Thomas (1999), A distinct class of isolated intracloud lightning discharges and their associated radio emissions, J. Geophys. Res., 104, 4189-4212

/165/ Stekolnikov, I. S. and A. A. Lamdon (1942), Lightning currents in USSR supply systems during the period 1937-1940 (in Russian). J. Tech. Phys. 12: 204-10.

/166/ Takeuti, T., M. Nagatani, and H. Nakada (1975), Thunderstorm activities and related meteorological conditions in the northwest subtropical Pacific. Proc. Res. Inst. Atmospherics Nagoya Univ. 22: 27-31.

/167/ Takeuti, T. (1976), On cloud-to-sea discharges, In Proc. Res. Inst. Atmospherics Nagoya Univ. 23: 17-20.

/168/ Thomson, E. M. (1980), The dependence of lightning return stroke characteristics on latitude, J. Geophys. Res. 85: 1050-6.

/169/ Thottappillil, R., V. A. Rakov, M. A. Uman, W. H. Beasley, M. J. Master, and D. V. Shelukhin (1992), Lightning subsequent-stroke electric field peak greater than the first stroke peak and multiple ground terminations, J. Geophys. Res. 97: 7503-9.

/170/ Uman, M. A. (1969), Lightning, 264 p., New York: McGraw-Hill.

/171/ Uman, M. A. and D. K. McLain (1969), Magnetic field of the Lightning Return Stroke, J. Geophys. Res. Vol. 74.

/172/ Uman, M. A. and D. K. McLain (1970), Lightning return stroke current from magnetic and radiation field measurement, J. Geophys. Res. 75: 5143-7.

/173/ Uman, M. A., D. K. McLain, R. J. Fisher, and E. P. Krider (1973a), Electric field intensity of lightning return stroke, J. Geophys. Res. 78: 3523-9.

/174/ Uman, M. A., D. K. McLain, R. J. Fisher, and E. P. Krider (1973b), Currents in Florida lightning return strokes, J. Geophys. Res. 78: 3530-7.

/175/ Uman, M. A., D. K. McLain, and E. P. Krider (1975), The electromagnetic radiation from a finite antenna, Am. J.Phys. 43.

/176/ Uman, M. A. (1984), Lightning, 298 p., New York: Dover.

/177/ Valine, W. C. and E. P. Krider (2002), Statistics and characteristics of cloud-to-ground lightning with multiple ground contacts. J. Geophys. Res., 107 (D20), 4441, doi: 10.1029/2001JD001360.

/178/ Visacro, S., A. Soares, M. A. O. Schroeder, L. C. L. Cherchiglia, and V. J. D. Sousa (2004), Statistical analysis of lightning current parameters: measurements at Morro do Cachimbo Station, J. Geophys. Res., 109, D01105, doi: 10.1029/2003JD003662.

/179/ Wacker, R. S. and R. E. Orville (1999), Changes in measured lightning flash count and return stroke peak current after the 1994 U.S. National Lightning Detection Network upgrade: 1. Observations, J. Geophys. Res., 104(D2), 2151–2158.

/180/ Watson-Watt, R. A. and J. F. Herd (1926), An instantaneous direct-reading radio goniometer, J. Inst. Elec. Engrs., (64), pp. 611–622.

/181/ Westcott, N. E. (1995), Summertime cloud-to-ground lightning activity around major Midwestern urban areas, J. Appl. Meteor. 34: 1633-42.

/182/ Willett, J. C., J. C. Bailey, V. P. Idone, A. Eybert-Berard, and L. Barret (1989), Submicrosecond intercomparison of radiation fields and currents in triggered lightning return strokes based on the transmission-line model, J. Geophys. Res. 94: 13,275-86.

Acknowledgement:

For the development of this document many people have contributed their talent and valuable time. I would like to express my special thanks to Vladimir Rakov, Kenneth Cummins, Wolfgang Schulz and Ali Hussein and all the other members of the Task Force who delivered significant input to this brochure. Significant written comments to the draft version were received from Alain Sabot and C.A. Nucci helping to improve the document.

Gerhard Diendorfer (TF convenor)

11 Appendix A - Detection Efficiency Simulations

The following DE model simulations are based on a set of assumptions as listed below:

1) Sensor DE function: Each sensor detects 80% of all field signals, as long as the calculated signal of a given stroke is above threshold level at the sensor site (see Chapter 7.5). Saturation of a sensor in case of nearby lightning is not considered in the model calculations.
2) Sensor threshold is set to 0.52 V/m (corresponds to a typical acceptance threshold setting of 100 mV of a Gain 6 sensor)
3) Lightning peak currents are assumed to be lognormal distributed with a median of 15 kA and σ_{log10} = 0.26. The peak current distribution employed in this simulation reflects the first stroke distribution found in Austria and southern Germany.
4) Peak current calibration: LLS estimate the peak current from the peak electric or magnetic field. For the DE modeling we have to assume a conversion from peak current to peak field, which could be done either based on return stroke model calculations or based on empirical results. In the model calculations 1 kA converts to 0.225 V/m at a distance of 100 km, which corresponds to a setting of I[kA] = 0.2 * RNSS (see Eq. (6.1)) at the central processor.
5) The effect of attenuation due to field propagation over ground of finite conductivity is taken into account by applying the same attenuation model as used in real time lightning processing (see Eq.(6.2)). Parameters b and L have been set to b=1.0 and L = 1000.

In the following Fig. A1 to Fig. A15 the DE contour plots are shown for a 600 km x 600 km area for the 150 km and 200 km baseline networks and for an 800 km x 800 km area for the 300 km baseline network. Sensor positions are marked by a star symbol.

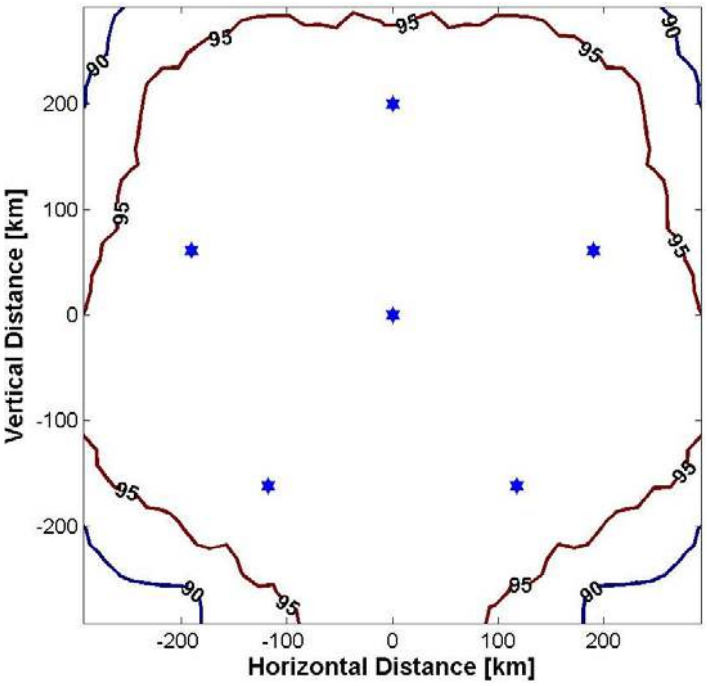

Baseline 200 km
MDF+TOA
2 sensors required
DE = 96,5%
(600 km x 600 km area)

Fig. A1 Simulation #1 for a 6 sensor network

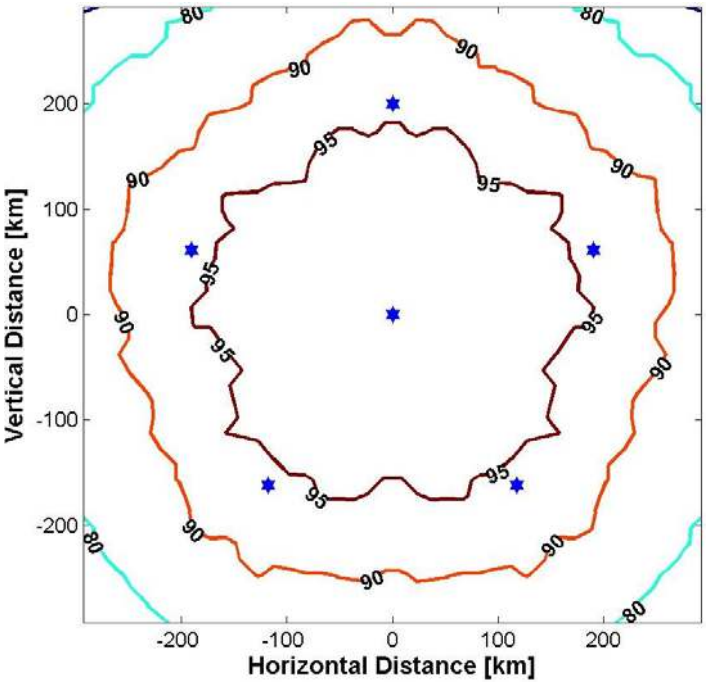

Baseline 200 km
TOA
3 sensors required
DE = 90,4%
(600 km x 600 km area)

Fig. A2 Simulation #2 for a 6 sensor network

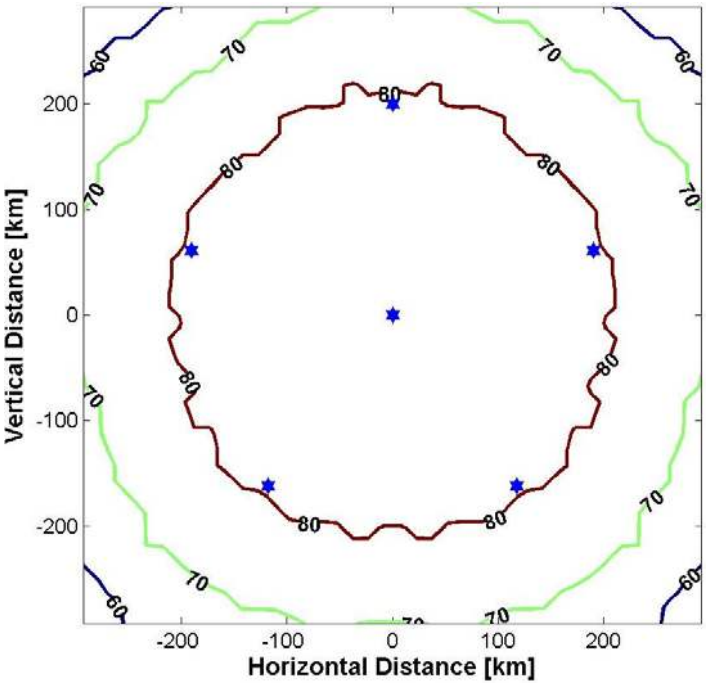

Baseline 200 km
TOA
4 sensors required
DE = 76,6%
(600 km x 600 km area)

Fig. A3 Simulation #3 for a 6 sensor network

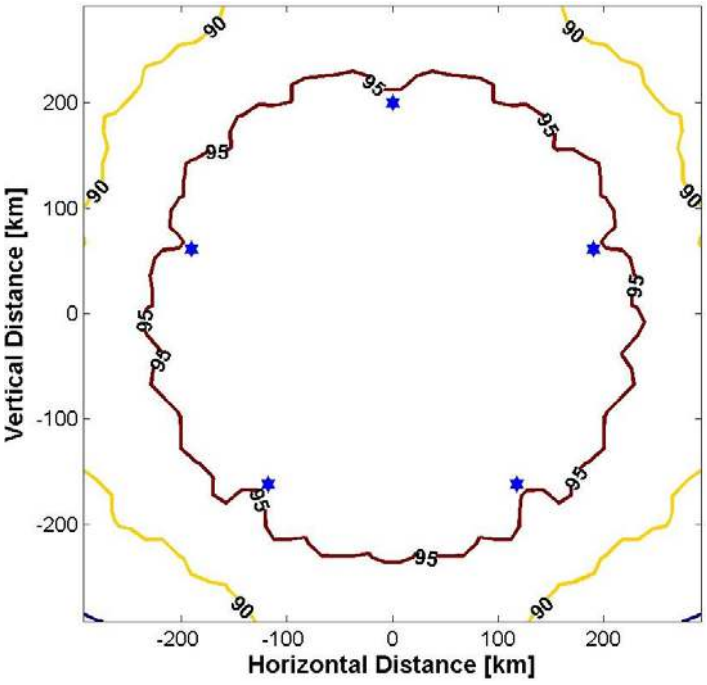

Baseline 200 km
MDF+TOA
2 sensors required
DE = 94,0%
(600 km x 600 km area)

Fig. A4 Simulation #4 for a 5 sensor network (centre sensor removed)

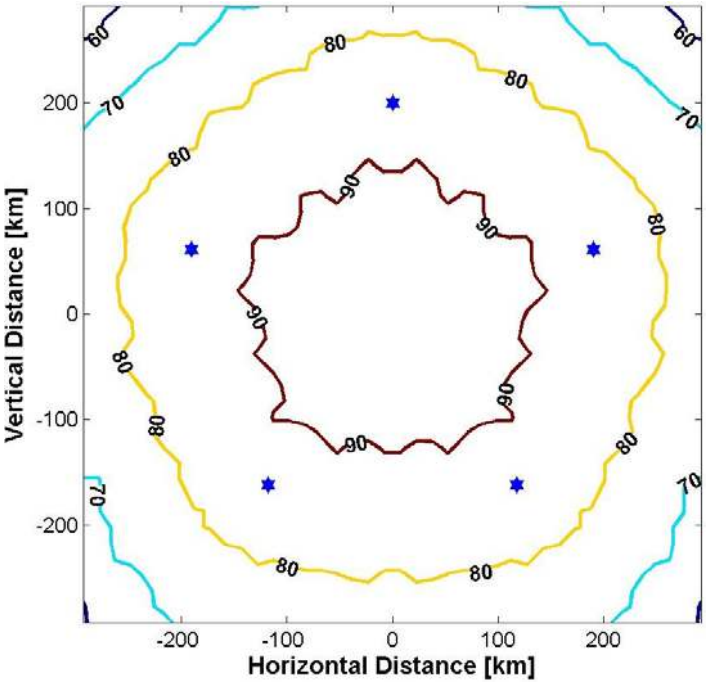

Baseline 200 km
TOA
3 sensors required
DE = 81,2%
(600 km x 600 km area)

Fig. A5 Simulation #5 for a 5 sensor network (centre sensor removed)

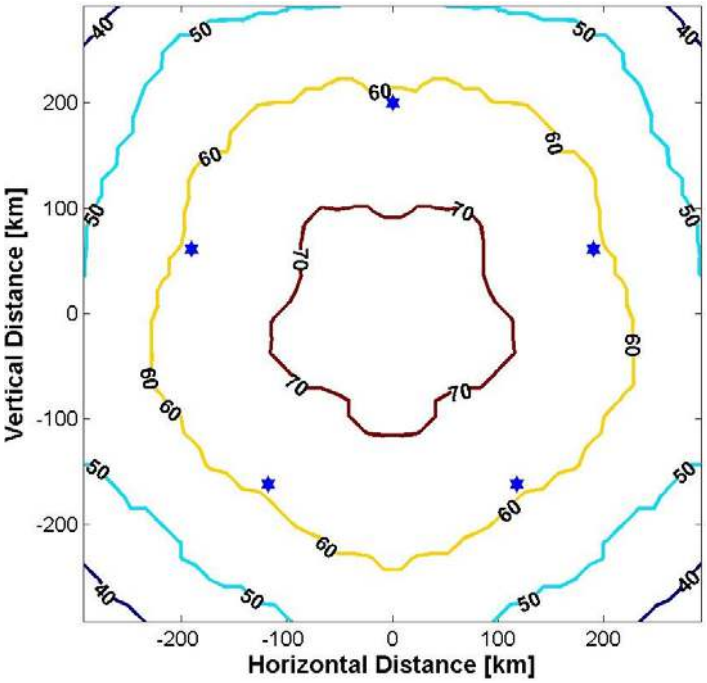

Baseline 200 km
TOA
4 sensors required
DE = 58,3%
(600 km x 600 km area)

Fig. A6 Simulation #6 for a 5 sensor network (centre sensor removed)

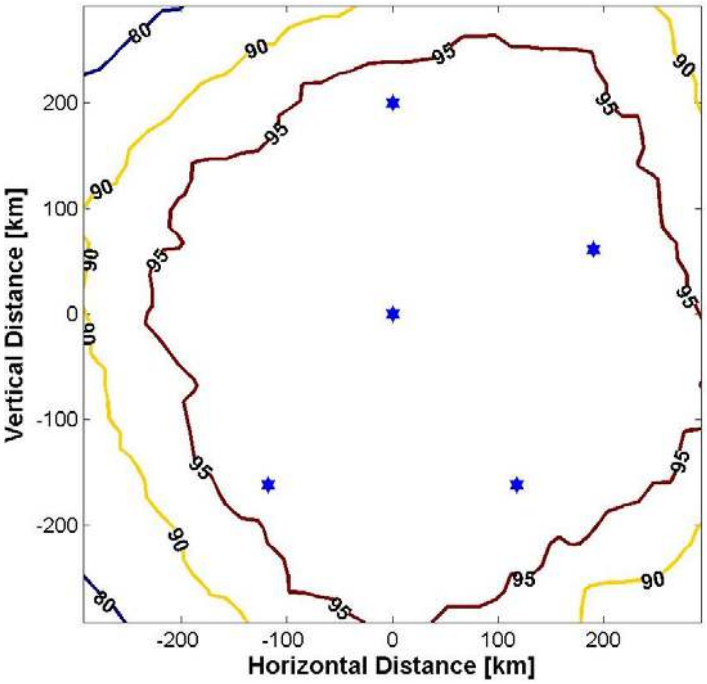

Baseline 200 km
MDF+TOA
2 sensors required
DE = 94,5%
(600 km x 600 km area)

Fig. A7 Simulation #7 for a 5 sensor network (border sensor removed)

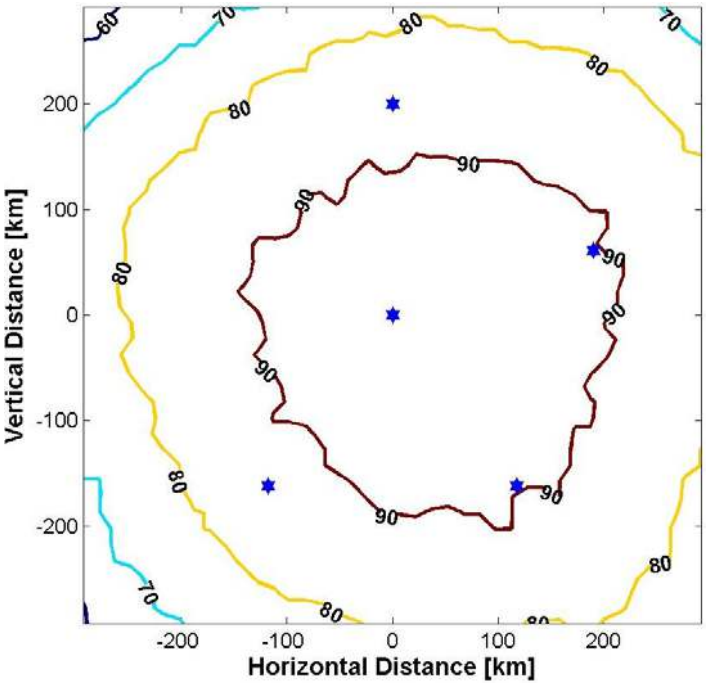

Baseline 200 km
TOA
3 sensors required
DE = 84,0%
(600 km x 600 km area)

Fig. A8 Simulation #8 for a 5 sensor network (border sensor removed)

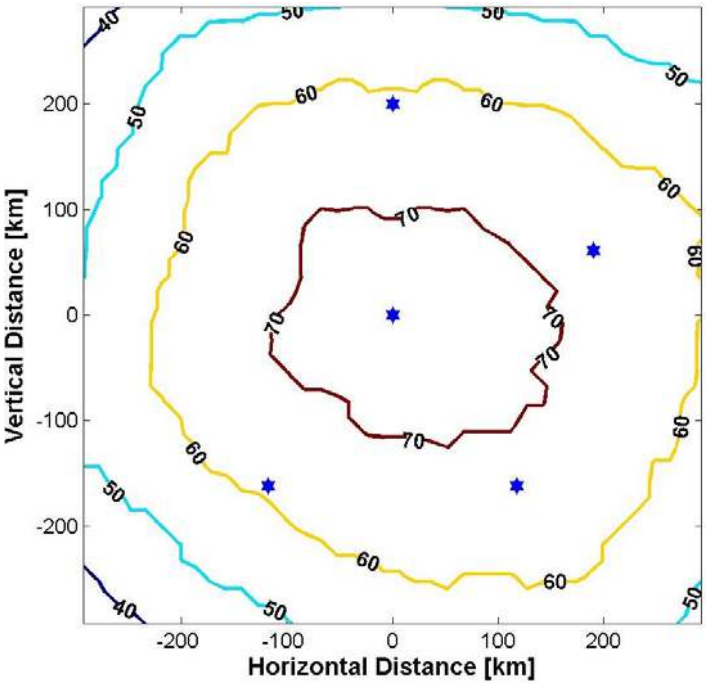

Baseline 200 km
TOA
4 sensors required
DE = 60,3%
(600 km x 600 km area)

Fig. A9 Simulation #9 for a 5 sensor network (border sensor removed)

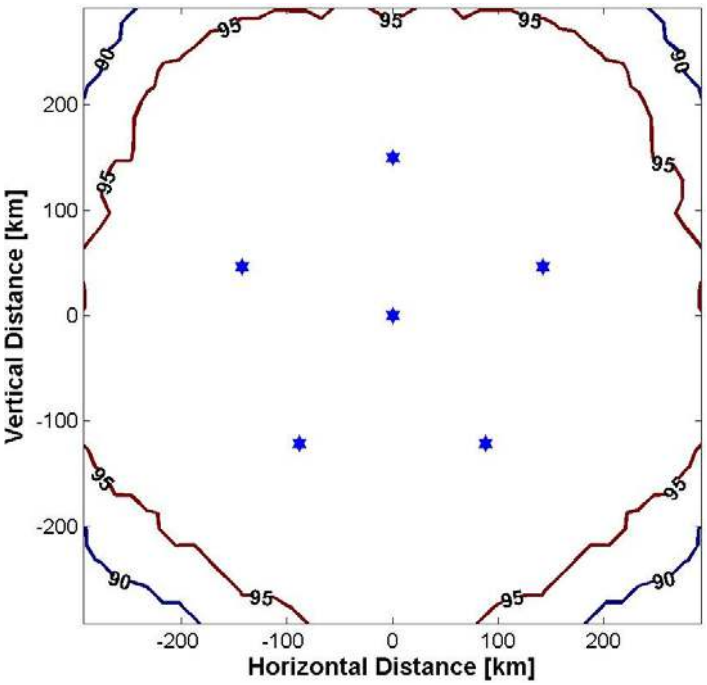

Baseline 150 km
MDF+TOA
2 sensors required
DE = 97,0%
(600 km x 600 km area)

Fig. A10 Simulation #10 for a 6 sensor network

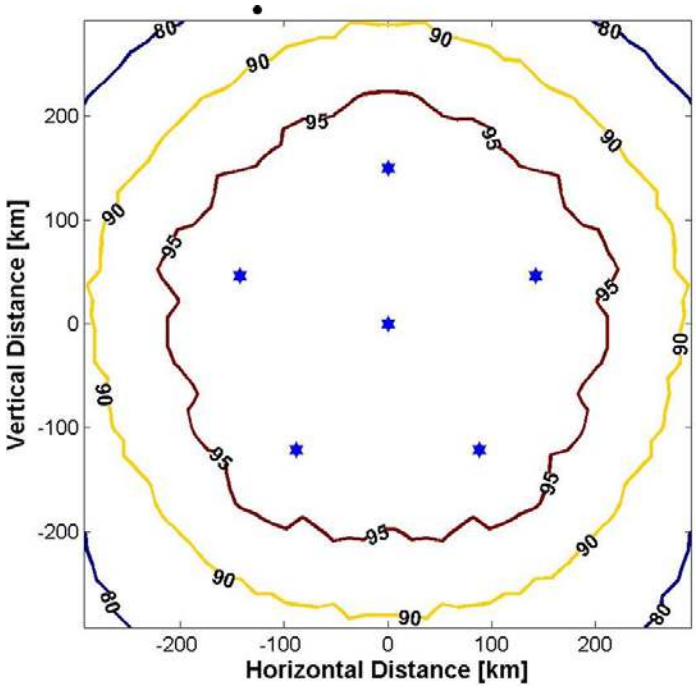

Baseline 150 km
TOA
3 sensors required
DE = 92,2%
(600 km x 600 km area)

Fig. A11 Simulation #11
for a 6 sensor network

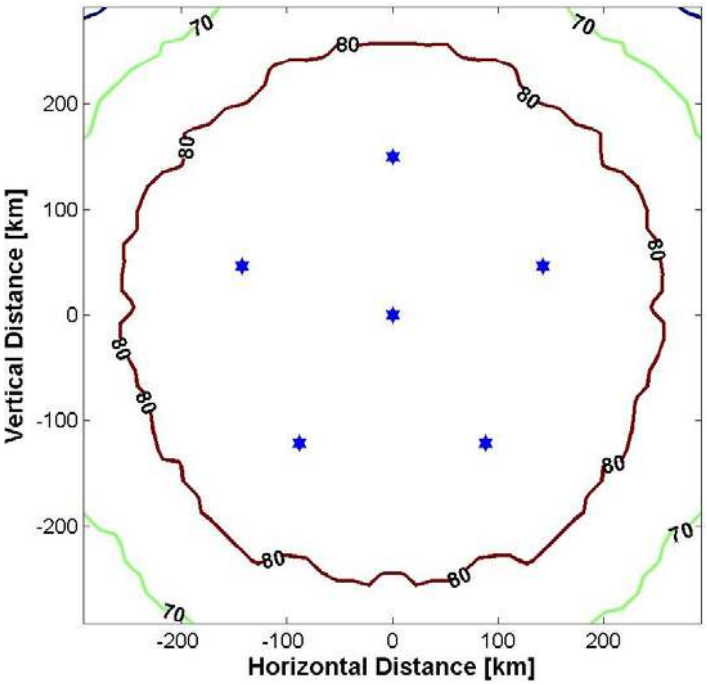

Baseline 150 km
TOA
4 sensors required
DE = 80,6%
(600 km x 600 km area)

Fig. A12 Simulation #12
for a 6 sensor network

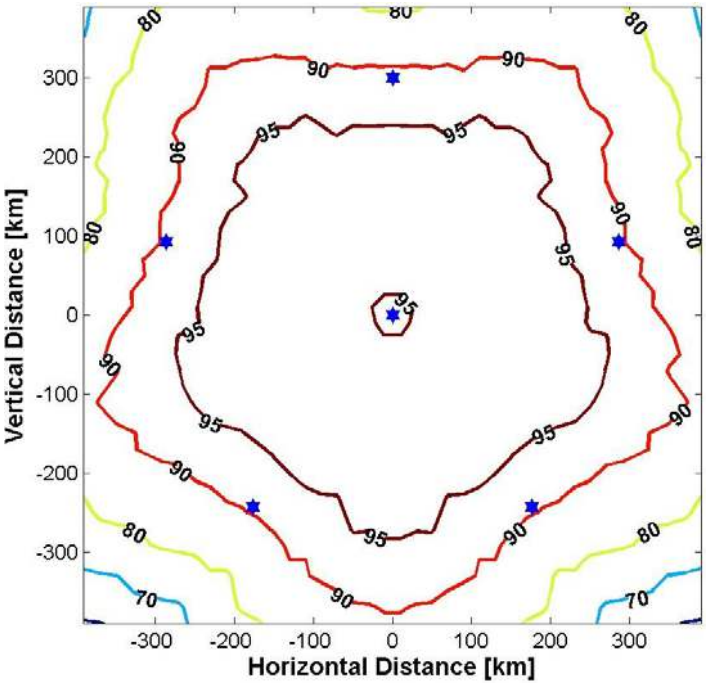

Baseline 300 km
MDF+TOA
2 sensors required
DE = 89,5%
(800 km x 800 km area)

Fig. A13 Simulation #13
for a 6 sensor network

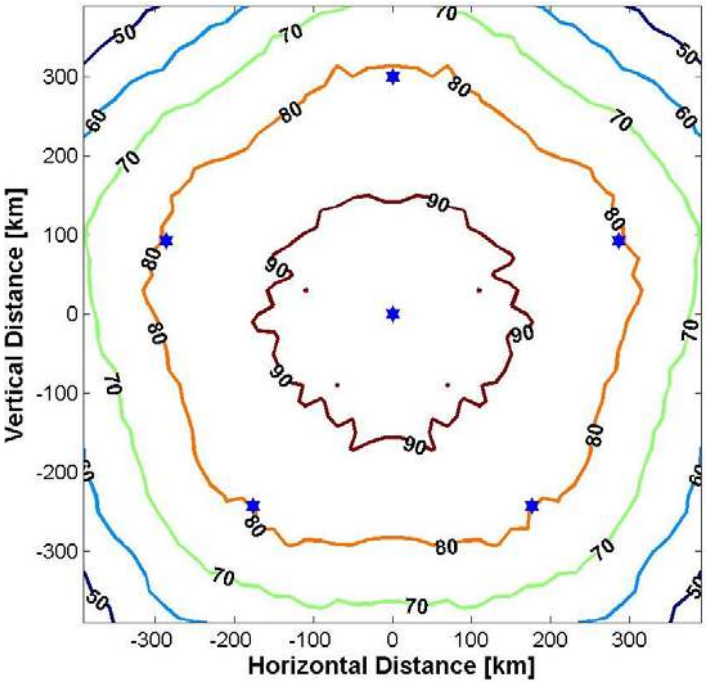

Baseline 300 km
TOA
3 sensors required
DE = 76,5%
(800 km x 800 km area)

Fig. A14 Simulation #14
for a 6 sensor network

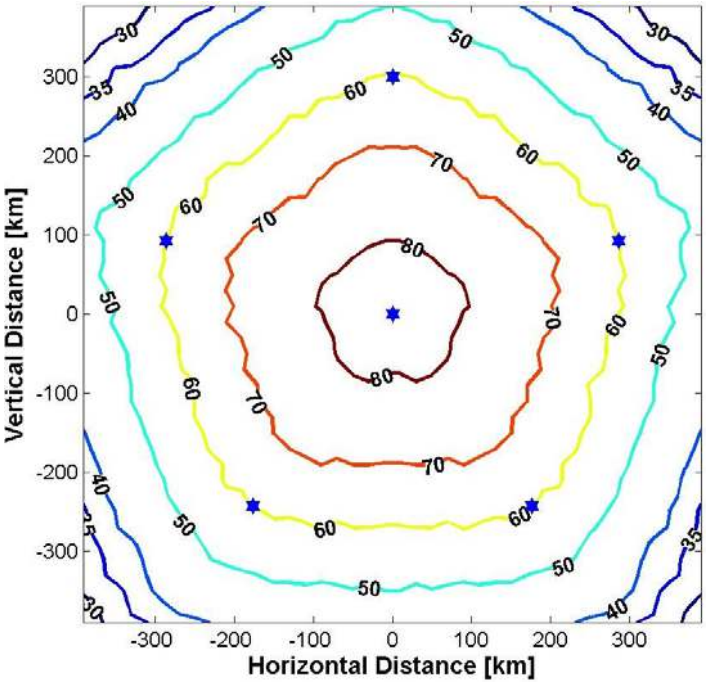

Baseline 300 km
TOA
4 sensors required
DE = 56,3%
(800 km x 800 km area)

Fig. A15 Simulation #15 for a 6 sensor network